INVESTIGATION OF INTERCOSTAL NEURONAL INTRACELLULAR PROCESSES AND CONNECTIVITY BY SIGNAL ANALYSIS AND COMPUTER SIMULATION

A thesis submitted for the Degree of
Doctor of Philosphy
in the University of London

by

David L. Tuck

March 1977

Engineering in Medicine Laboratory
Department of Electrical Engineering
Imperial College of Science and Technology
London, S.W.7.

and

Sobell Department of Neurophysiology
Institute of Neurology
Queen Square,
London, W.C.1N 3BG

ABSTRACT

The interconnections of nervous pathways to the mammalian intercostal alpha-motoneurone and the behaviour of the neurone itself are of importance in the elucidation of intercostal muscle involvement in respiration. Due to the difficulties of direct experimentation, an approach was proposed through the use of a digital computer model that simulates the important pre-synaptic and trans-membrane process of the intercostal alpha-motoneurone. A practical model to fit these specific requirements has not previously been reported, and the work described here concerns the development and use of such a model, and its assessment in comparison with its mammalian counterpart by a variety of signal processing methods. It is shown that the model produces results in good accordance with the experimental observations, and it is argued that a useful insight into the functional behaviour is offered by the study of intermediate processes in the model which are not accessable in the experimental preparation.

Evidence from animal experiments has suggested that common connectivity exists presumably due to branching in the pre-synaptic pathways of the intercostal motoneurones. The model was extended to allow further investigation of this matter by neuronal network simulation. Quantification was attempted by utilising the event cross-correlation measure, used

in the form of the Pre- and Post- Stimulus Time histogram; the simulated Average Common Excitation potentials (which agrees closely with the experimental results) also has been studied. It is shown that both techniques provide quantitative measures of common connectivity which are directly dependent on the event Input-Output probability density function. Finally, the factors contributing to this last fundamental measure are considered.

INDEX

ACKNOWLEDGEMENTS

This work was made possible by the award of a fellowship granted by the New Zealand, National Research Advisory Council which enabled me to study at Imperial College and I am grateful for their generous support.

I wish to thank Professor B. McA. Sayers and Dr. D.T. Stagg for their supervision, advice, and helpful criticism of the work reported in this thesis.

This specific work originates from the research being carried out by Professor T.A. Sears and colleagues and forms part of the on-going collaboration between the Engineering in Medicine Laboratory at Imperial College and the Sobell Department of Neurophysiology at the Institute of Neurology. My sincere thanks are due to Professor Sears and Dr. P.A. Kirkwood for performing the animal experiments which provided the neurophysiological data; I am indebted to them for their advice and help in neurophysiological matters, and encouragement.

Appreciation is expressed for support from other members of the Engineering in Medicine Laboratory through computing aid, help, advice and friendship and I especially wish to thank Dr. C. Vickory, Dr. D.M. Monro, Mr. N. Ellis, Mr. W. Cutler and all my colleagues.

This thesis was typed by Julie Savvides and I take this opportunity of thanking her for patience, care and effort.

Finally, I would like to dedicate this manuscript to my wife, Rosaline who gave me the confidence to begin and complete this work.

1.0 INTRODUCTION.

1.0 INTRODUCTION:

The investigation of the nervous control of intercostal muscles in the regulation of respiratory movement is providing both a specific understanding of breathing control mechanisms and a general insight into the nervous control of skeletal muscle in mammals. Attention is currently being concentrated on the intercostal alpha-motoneurone, which is the penultimate element of the control-effecting movement chain. This motoneurone has been demonstrated to integrate very high rates of pre-synaptically generated activity and to encode the information carried to it along the vast multitude of synaptically terminating pathways into a single, low rate sequence of motoneurone discharges. This train of nerve impulses is conducted along the axon of this motoneurone which terminates at muscle end-plate junctions and is responsible for the regulation of movement.

Analysis of the temporally-coded muscle innervating spike sequences, recorded in animals, have provided some insight into the functional neuro-anatomy of the system, particularly by offering evidence for the existence of branching in the spinal pre-synaptic pathways. Sears and Stagg (1976) produced such evidence of shared inputs to these motoneurones from an event cross-correlation analysis and suggested that it occurs both within segments and between neighbouring segmental levels, because of the significant and narrow correlation peaks observed.

The work described in this thesis follows on at this point. Its first purpose was to determine if current knowledge is adequate to account for the properties of the various neuronal signals recorded in the intercostal system and thereby clarify the origin of these properties. This work has further been aimed at establishing the amount of common pre-synaptic connectivity between the intercostal alpha-motoneurones. Because of the very fine dense synaptic structure on these neurones and the multitude of bulbo-spinal and other pathways to them, no direct estimate appeared possible. To meet this second requirement, a practical and efficient digital computer model has been developed and employed to allow investigation of the hypothesised common connectivity and to enable further interpretation of the event cross-correlation functions.

In order to achieve a realistic simulation of the motoneurone, it turned out to be necessary to develop a model which integrates high rates of very small excitatory post-synaptic potentials (see Barrett, 1975). The limitations of previous computer models would not allow practical adaptation for the present purpose and the non-stationarity due to natural breathing rhythm needed to be accommodated. Validation of the present model was achieved by a thorough comparison with its neurophysiological counterpart using a number of statistical signal and ensemble-analysis techniques.

By simulation of a pair of motoneurones with different amounts of common connectivity, levels of pre-synaptic drive, and trans-membrane mechanisms, a qualitative and quantitative evaluation of the cross-

correlation functions derived from animal experiments was undertaken. It will be argued that not only has this main aim been fulfilled, but that a more complete understanding of the information coding properties of the intercostal alpha-motoneurone has also emerged.

In addition, the model has also been successfully used to complement the recent studies of common connectivity via a new measure introduced by Kirkwood and Sears (1976).

2.0 MOTONEURONES AND THEIR MODELS.

2.1 THE NEUROPHYSIOLOGY OF THE INTERCOSTAL MOTONEURONE.

The Functional Organisation.

The Trans-membrane Processes of Motoneurones.

2.2 PREVIOUS NEURONAL MODELS.

2.3 A PROPOSED MODEL OF AN INTERCOSTAL ALPHA-MOTONEURONE.

2.0 MOTONEURONES AND THEIR MODELS

2.1 THE NEUROPHYSIOLOGY OF THE INTERCOSTAL MOTONEURONE:

The work described in this thesis deals mainly with the investigation of intercostal alpha-motoneurones and their synaptic excitation. In the first part of this section a brief description of the components which are intercoupled with these motoneurones and their functional inter-relation is presented, while the second part describes in detail the trans-membrane processes which occur in these motoneurones.

The Functional Organisation: Figure 2.1.1 displays a grossly simplified schematic representation of a mammalian intercostal motoneurone with its principal segmental and supra-segmental synaptic inputs and its axon termination in the intercostal muscle. These alpha-motoneurones are situated in the segmented grey matter of the spinal cord. They receive pre-synaptic control directly from the supra-segmental control centres along the descending bulbo-spinal pathways, and segmentally from the muscle spindles via the dorsal roots at the local and immediately neighbouring segmental levels. These pathways, numbering many thousands terminate at synapses on the motoneurone and extensively cover its dendritic and somatic surface (Barrett, 1975). The axons of these motoneurones leave the spinal cord through the ventral roots to innervate the intercostal muscles at that segmental level.

The major function of the alpha-motoneurone is to

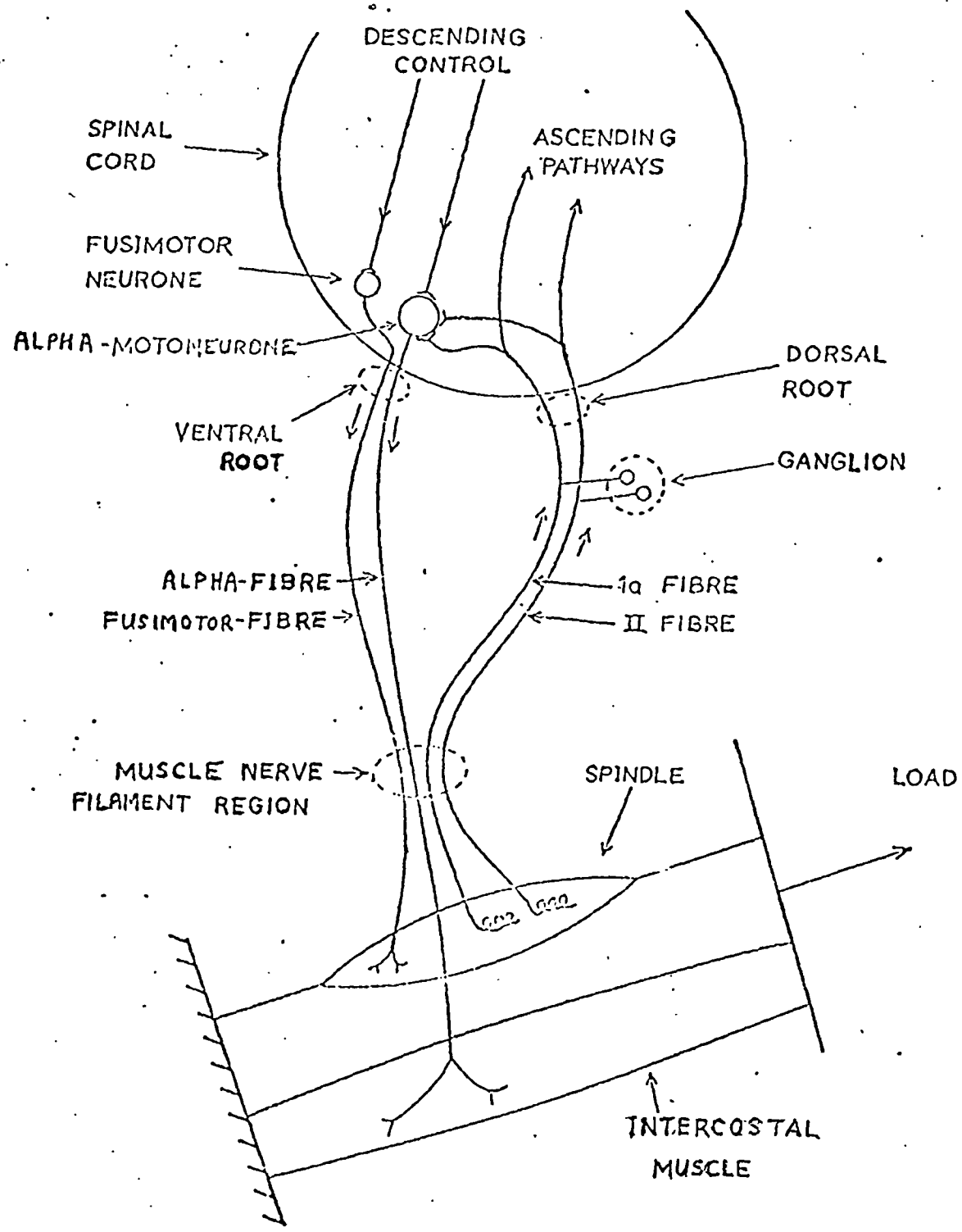

FIGURE 2.1.1:

The neuronal interconnections surrounding the intercostal alpha-motoneurone.

integrate the large amount of incoming control information, which take the form of temporally coded sequences of nerve impulses conducted along many thousands of axons (Katz, 1966). At the synaptic junctions the pre-synaptic impulses are transformed into post-synaptic potential changes across the motoneuronal membrane. The post-synaptic potentials are summated to contribute towards the generation of a new temporally coded train of nerve impulses by a non-linear, threshold voltage sensitive process. This resulting train of impulses is conducted along the motoneurone axon to inervate the intercostal muscle which responds by contracting with a force proportional to the frequency of activation.

The segmented intercostal muscles lie diagonally in one plane between, and anchored to, successive pairs of ribs (Bronk and Ferguson, 1934; Taylor, 1960). There are two layers of muscle which structurally form an internal or expiratory layer and an external or inspiratory layer, having their directions of inclination opposing. These two layers are normally activated alternately, thereby causing expansion of the rib cage and so assist with breathing.

Systematically spaced (approximately every one centimeter) lying within the continuous muscle fibre media, are the stretch sensitive muscle spindles. These muscle receptors produce two separate, rate coded impulse trains which carry information relating to the rate of change and the amount of local muscle stretch. Both these primary, Ia and secondary, II nerve plate ending responses are sensitive to length

variation while only the Ia sequence rate displays an additional significant velocity sensitive component. These Ia and II response rates are modulated or biassed by innervation of the muscle spindle by fusimotor neurones which, in turn, are under the direct control of the central nervous system (CNS).

The Ia and II fibres enter the spinal cord through the dorsal roots, via the ganglion cell bodies, and here they synapse on the local alpha-motoneurones (Kirkwood and Sears, 1974; Stauffer, Watt, Taylor, Reinking and Stuart 1976), before ascending the spinal cord together. These afferent pathways to the CNS allow the muscle spindles to play an important role in the control of more complex respiratory movement patterns. Through their mono-synaptic excitation, the fibres form a reflex which maybe viewed as being 'load compensatory', where the positioning of the intercostal spacing is maintained constant under varying tension; or as a 'length follow-up servo' mode of operation which is performed by the CNS imposing control over the muscle contraction, via the fusimotor pathway, with the spindle acting as the error detector (Matthews, 1972).

The Trans-membrane Processes of Motoneurones: The cations of sodium and potassium play an essential role in the functioning of a nerve cell. They are almost completely responsible for establishing the resting potential of the cell and in the dynamic production, and maintenance, of the propagated action potential (Eccles, 1966). The resting state potential is approximately -70 millivolts (mV. Convention: negative inside

with respect to the outside) being determined by the major ion concentration gradients measured across the resting cell membrane. Since the sodium cations and the common anions find the membrane relatively impermeable with the cell in the resting state, the main contributor to the steady state membrane current is the potassium ion diffusion. A metabolically driven pump maintains the relative cation concentration gradients consuming energy in order to transport these ions in the direction opposing their concentration gradient across the cell membrane. Because the potassium concentration is kept high inside the cell and these cations can diffuse through the membrane wall with relative ease, then the resting membrane potential is determined principally by the concentration difference of potassium cations.

However, if the membrane potential is diminished to a critical level (approximately -60mV), it exhibits a threshold phenomenon in which the permeability to sodium ions suddenly increases and an unstable state or 'localised response' is initiated across the cell membrane. This instability immediately accelerates the depolarisation so that the membrane potential becomes slightly positive with the large influx of sodium ions. After a brief period this sodium influx is counterbalanced by a rapid efflux of potassium ions and the membrane potential becomes negatively polarised again. Following this impulse the soma begins to recover its resting potential while this resultant action potential is propagated down the axon of the cell, by the same principle of a local influx of sodium and the following efflux of potassium ions, as a wave of depolarisation closely

followed by repolarisation. In motoneurones, the membrane potential is observed to hyperpolarise (i.e. become more negative than the resting potential) following the action potential. It is thought this state is due to the influence of the short-circuiting potassium channels (Eccles, 1966). As these channels close off again, to re-establish the resting potential, the cell is said to be relative refractory. During the action potential no second action potential is initiated and the cell is said to be absolute refractory, however this is observed to persist generally for a few milliseconds only. On the other hand, during the relative refractory phase action potential spikes are sometimes observed, but their probability of doing so is noticably less than while the cell is in the resting state. This relative refractoriness persists while the cell remains hyperpolarised (after-hyperpolarisation).

In motoneurones and other nerve cells, the depolarisation of the membrane leading to an action potential is initiated by synaptic excitation of impulses on pre-synaptic fibres. These impulses, after travelling along the axon of the source cell, which synaptically terminates on the cell under consideration, and reaching the synapse, causes the release of a quantity of transmitter substance for diffusion across the narrow synaptic gap. The transmitter substance, on making contact with the membrane wall of the cell, brings about a local change in the membrane ionic diffusion rates. There is a reversed current locally, opposing the potassium ion current flow, due to an instantaneous increase in the sodium permeability. This produces a temporary depolarisation of the membrane potential of

this post-synaptic cell, generating an excitatory post-synaptic potential (EPSP). Normally, within the mammalian motoneurone an individual EPSP is insufficient to depolarise the membrane potential from its resting level to the threshold level to generate an axon discharge spike (Eccles, 1966). An example of this is demonstrated by the cat intercostal alpha-motoneurone in which the threshold potential is found to be more than 10 mV above the resting potential whereas the averaged unitary EPSP amplitudes in the somatic region are approximately 0.1 mV by intracellular measurement (Kirkwood and Sears - personal communication). Instead, attainment of the threshold potential is achieved both by spatial summation of multiple synaptic excitation of the entire somatic and dendritic membrane surface of the neurone, and temporal summation due to repetitive activation of individual synapses. The site of impulse generation is generally considered to be close to the axon hillock (Eccles, 1966) which is situated at the point where the axon extends out from the soma body.

By taking into consideration the capacitance effect within the somatic and dendritic volumes, together with the cable attenuation properties of the dendritic structures and treating the transmitter substance release as analogous to the injection of charge into a leaky capacitance circuit, such a distributed capacitance network model can account for both spatial and temporal summation of EPSPs and the range of EPSP amplitudes observed (Iansek and Redman, 1973); because the dendritic diameters are considerably smaller than the somatic, then assuming a similar quantity of charge is released at the synapses on both surfaces, the evoked

dendritic EPSP will be much larger than the somatic considering capacitance alone. It is important to recognise that after electronic conduction from the dendritic synapse sites into the soma, the EPSP is reduced in amplitude and is about 50 percent as effective as somatic EPSPs (Barrett, 1975), while the EPSP shape has been markedly smoothed (Iansek and Redman, 1973). The observed phenomenon of greatly reduced EPSP amplitudes immediately following the generation of an action potential, which recovers to its normal size during refractoriness, also may be explained by considering the shunting effect of the recovery from after-hyperpolarisation. One further point is that synapses also exist which normally serve to hyperpolarise the membrane giving rise to inhibitory post-synaptic potentials (IPSP). These have been identified on intercostal alpha-motoneurones and have been shown to be dominant in the non-active phase; the inhibition effectively clamps the membrane potential low thus preventing any possible threshold crossings (Sears, 1964b). In this paper Sears demonstrates the reciprocation of the EPSP and IPSP drives to the inspiratory and expiratory thoracic respiratory motoneurones modulating their respective membrane potentials in an antagonistic manner with the slow rhythm of the 'central respiratory drive potentials'. There is, however, no evidence of IPSP presence during the active phase of a normally operating neurone and therefore the EPSP drive dictates its behaviour.

In the interest of developing a suitable model of these motoneurones the following section reviews the previous digital computer-based simulations of the trans-membrane processes just described and selectively outlines the various techniques of implementation.

2.2 PREVIOUS NEURONAL MODELS:

The history of neuronal modelling by digital computer simulation extends back some sixteen years. Even in this short period it has permitted a major advance in the understanding of neural phenomena which previously could only have been investigated by non-digital techniques; this history covering several centuries has been related in detail by Harmon and Lewis (1966).

One of the first digitally computed models of the neurone was reported by Viernstein and Grossman (1961) and is a classical example of one type of modelling approach. They described their noisy membrane potential simulation as a process in which random amplitudes were added periodically to the instantaneous membrane potential (MP). This MP was also influenced by a refractory process which, recovered exponentially from a hyperpolarised level to the resting potential, after the generation of each post-synaptic action potential. To this, after a short absolute refractory period, were summed the accumulated step amplitudes. Each representative post-synaptic potential amplitude was regularly drawn from a zero-mean, gaussian distribution with an allocated standard deviation parameter. A positive step was said to be due a dominance of EPSPs and a negative transition due to IPSP dominance. Under the combined influence of these two processes, the MP eventually attained a magnitude which was regarded as the threshold potential for spike generation, the spike event was recorded and the process reset to start again. With this minimal parameter, noisy MP model, Viernstein and Grossman were able to simulate experimentally observed

spike sequence patterns recorded from several types of sensory relay neurones. They concluded that this model had allowed them a better understanding of the synaptic mechanics associated with the transmission and coding of the sensory information in the neurones studied.

In 1966 Geisler and Goldberg published an account of their minimal parameter, noisy membrane model which extended the type of simulation described above. By employing an additional parameter, they provided for a memory process which produced a significant negative serial correlation coefficient for a single interval delay of the spike sequence generated. They achieved this by determining each new depth of hyper-polarisation as an inverse function of the length of the previous discharge interval. This allowed the simulation of many neuronal interval statistics by the appropriate selection of the controlling parameters, but it was only accurate in accounting for the gross effects observed experimentally.

A comprehensive digital model was described by Perkel (1964) which provided a more detailed representation of the trans-membrane processes observed within most neurones. His programme was developed to allow coupling between several separately simulated neurones to form networks and thereby could also allow the investigation of multiple neuronal structures and their interactions. The basis of this modelling programme was a table of queuing times to enable the 'time to the next interesting event' to be determined and thus allowed an effective continuous time simulation which was efficient and more accurate than the fixed time increment principle generally employed. Each process was allocated a time to the next important occurrence and stored in the table so that as

each event time became due, the times and the associated process variables were updated accordingly. Perkel treated the pre-synaptic junctions as resevoirs of transmitter substance, allowing each a time course of recovery and an adjustable amount released for summation with the MP in the form of a post-synaptic potential by each pre-synaptic event. In addition to an exponential time course for the relative refractory recovery and an absolute refractory period, he included exponential time decaying functions for both the threshold and the MP. The former expression allowed the threshold to approach an asymptotic level, which if it was set below the resting potential, simulated a pacemaker cell; the latter decay function simulated the cell membrane time constant which also accounted for the post-synaptic potential decay towards the cell resting potential. Finally, his programme provided for the generation of a significant first (i.e. delay-one) serial correlation between intervals of the spike sequence produced by the simulation. The modelling programme had provision for a total of 350 pre-synaptic sources, terminating axon-synapse junctions, and cell function parameters. Perkel also incorporated some simple and higher-order interval analysing options for processing at the completion of a simulation run. He concluded the report with results from a preliminary study and also proposed a modification to the programme which would allow more accurate EPSP shapes to be generated by replacing the decaying post-synaptic step function with a smoothly rising, and then decaying, potential pattern.

Segundo, Perkel, Wyman, Hegstad and Moore (1968)

gave an account of an extensive investigation of a simulated network of neurones which concentrated on synaptic properties. In this model they considered different numbers of pre-synaptic neurones converging on a final single neurone and studied the effect, on the discharge interval statistics of this final neurone, of varying the number and form of the pre-synaptic source. The overall strength of the pre-synaptic drive was held constant; this was achieved by proportionally decreasing the amplitude of the EPSPs released for summation to the MP with increase in the number of active synapses considered. They demonstrated, without exploring the matter in depth or offering an explanation, that the degree of pre-synaptic correlation was a functionally significant variable in determining the post-synaptic spike pattern; they established also that, in the absence of any input correlation, this pattern rapidly changed from a direct dependence on the pre-synaptic interval-distribution to a dependence on the average pre-synaptic rate as the number of active synapses was increased. Concluding these important findings, they argued strongly that future neuronal models should bear these fundamental factors in mind, as indeed is the case for the work described later in this thesis.

Walloe, Jansen and Nygaard (1969) also used an extensive model in their study of second order sensory neurones. Their model employed large amplitude EPSPs (e.g. 2.7-5.0 mV) which were typically half of the resting- to threshold potential. These were shown by simulation, to require about fifteen independent and gaussian distributed pre-synaptic sources to reproduce the experimentally observed interval statistics of the output train of spikes. They found it interesting

that, although the pooled pre-synaptic interval distribution was indistinguishable from that generated by a Poisson process (i.e. a negative exponential distribution), when the pre-synaptic sources were replaced by such an interval generator the observed data could not be reproduced. It demonstrated that an important time structure existed in the converging multiple source situation which could not be revealed by simple interval statistics alone and was a good example of the corresponding remark given by Segundo et al.

In his investigation into the interval variability of discharge spike sequences from neurones, Stein (1965) used a mathematical model. The simulation allowed for a randomly occurring, exponentially decaying, fixed amplitude step post-synaptic potential by the application of the gamma distributed function to achieve an analytical description. This minimal parameter model was shown adequately to simulate many of the first order interval statistics of neurones which are observed to maintain unity correspondence between the mean interval and standard deviation. He also concluded that, as the number of post-synaptic increments required to reach a fixed threshold was increased, then the resulting discharge spike sequence rapidly changes from one reflecting the pre-synaptic interval pattern to one determined only by the average input rate.

The investigation by Moore, Segundo, Perkel and Levitan (1970) into methods for identifying simple synaptic interaction in neuronal networks, by the use of spike interval sequence autocorrelation and cross-correlation techniques computed from simulations and experimental recordings, demonstrated the importance of the EPSP and IPSP function in relaying the characteristic properties of the pre-synaptic connectivity.

They suggested that the post-synaptic potential shape was an essential contributor to the Input-Output correlation functions derived between the pre-synaptic and discharge spike sequence. Knox (1974) found similar results and goes further to conclude that the correlation kernel observed was directly related to the rate of rise of the EPSPs.

One type of model not yet discussed, but which became quite popular for a period, is that involving a random walk or pseudo-Markov process. Although considered unsuitable for this current investigation, because it neglects the shape of the EPSPs and IPSPs which are important when studying the correlation between neurone discharge sequences, it has been quite successful in the simulation of quite a number of brain cell spike discharge statistics (Ekholm and Hyvärinen, 1970). Ekholm and Hyvärinen introduced a two state model with which they were able to simulate the serial correlation measured in a number of interval sequences studied. The random walk model described and used by Gerstein and Mandelbrot (1964) begins with the MP at the resting state, which was bounded by an absorbing (threshold) level a discrete number of steps above and a reflecting level (potassium ion equilibrium) below, and was moved in discrete steps with the randomly occurring input. A drift process was included to simulate the bias towards one level, indicating a predominance of EPSP or IPSP drive respectively. When the MP reached the absorbing level an axon discharge was assumed to have occurred and the simulation was reset. With this model they were unable to determine any unique solution which accounted for the phenomena observed from the auditory neurones of the cochclear nucleus but they did gain some further insight into the problem

they were investigating.

To conclude this review of digitally computed neuronal models, a particularly important report by Jack and Redman (1971) must be considered; this is a comprehensive study which employed a model of the neuronal dendrites and soma. The investigation had been previously pursued by Rall, whose work has been thoroughly discussed and referenced by them, and who has now collaborated with them. Together they treated the dendritic structure from the formal compartmental cable approach and have demonstrated, in theory and by experiment, methods for determining the various cell parameters and for estimating where along the dendrites the active synapse might be situated. Their theory showed that when measured in the soma the large dendritic EPSPs are considerably attenuated and smoothed in time, by the cable characterstics. They concluded with the suggestion that the dendritic synapses may be responsible for only the adaptive underlying control in motoneurones, whereas the faster rising somatic EPSPs are probably recruited for the more critically timed and delicate control functions.

Turning now to the immediate problem, and the modelling approach to it; the salient features of the intercostal motoneurone can be identified, and the acceptability of previously mentioned models for their description, can then be considered.

Within the intercostal motoneurone structure, there are apparently some signs of direct pre-synaptic common connectivity as evidenced by the form of the discharge-event cross-correlation functions between the spike sequence recorded from the axons of groups of the alpha-motoneurones (Stagg,

1973; Sears and Stagg, 1976). The need for a suitable model arose from the difficulty, in animal experiments, of establishing the proportion of pre-synaptic inputs to such motoneurones as could arise by branching of the stem fibres. If this strength of short-term synchronization could be determined, then the neural control of these neurones, and in turn the inter-relation between this and the motoneurone control of the intercostal muscle structure they innervate, would be better understood. An evaluation by other techniques, for example neuro-signal tracing using pre- and post-synaptic nerve spike sequence correlation methods is unlikely to be productive, although further evidence may eventually come from anatomical investigation. The difficulty stems from the fine and very dense nature of these pre-synaptic fibres within the environment of these motoneurones.

It is obvious from the preceding neuronal modelling survey that there is a very important gap left unfilled. This is due to the inadequacy of these previous models to satisfactorily simulate the normal properties and working characteristics of the mammalian motoneurone. A suitable model would be expected to experience a high pre-synaptic input rate and integrate a large number of small EPSPs, realistic in shape, over each output discharge interval.

A motoneurone model is proposed to meet these requirements. It is anticipated that this mammalian motoneurone model would be suitable for the investigation of the short-term synchronization detected between intercostal motoneurones and should provide quantitative estimates of the strength of shared pre-synaptic inputs. This thesis reports the procedure adopted for this study, the results obtained and the conclusions

reached by the use of such a digitally computed motoneurone model.

2.3 A PROPOSED MODEL OF AN INTERCOSTAL ALPHA-MOTONEURONE:

Most of the trans-membrane phenomena described earlier in this chapter have been observed in intracellular recordings taken from the intercostal alpha-motoneurones of normal breathing cats. These typical skeletal motoneurones must integrate approximately 17 thousand presynaptic spikes per second (/sec.) according to the lose formulation which considers a 10 mV resting- to threshold-potential, 0.1 mV amplitude EPSPs, and a 6 msec cell time constant (Barrett, 1975):

In the limit, the depolarisation is 10 mV $= 0.1 \frac{e^{-(t/6)}}{1-e^{-(t/6)}}$

(assuming a regular arrival rate of EPSPs)

so that the mean interval of EPSP arrival $= 6 \log_e(10.1/10)$

$= 0.0597$ msec

(or 16750/sec.)

In particular they generate an average axon discharge rate of about 10/sec. which innervates the intercostal muscle and causes it to contract during the appropriate active respiratory phase. Therefore, the proposed simulation must integrate many more and much smaller amplitude EPSPs than in previous neurone models. Since these amplitudes are typically about one percent of the resting- to threshold- potential and because a model of this detail for motoneurones has not hitherto been reported, a completely original model had to be developed. Evidently, more attention to detail is necessary to allow adequate interpretation of the complex physiological results under invest-

igation, but a risk exists in this situation of the model becoming too cumbersome. It is important then that due weight be given to the experience and techniques already reported in the literature to ensure the simulation is pratical and efficiently computed. The facilities available and the need for subsequent digital processing of the data from the simulation, dictate that it is most convenient to implement the model on a digital computer.

The outline of the programme structure used by Perkel (1964), which utilised the queuing-time table principle for interesting events allowing an effectively continuous time simulation, was extremely appealing and a similar approach was implemented. Many of the simulated trans-membrane processes he describes such as his suggested modification to include a realistic EPSP shape were also incorporated. The conclusions of Segundo et al (1968) determined from their extensive synaptic property investigation suggest that since the proposed model will normally be required to integrate many small EPSPs, the number of synaptic terminals simulated might be reduced. This is allowable if there is little or no dependence between the pre-synaptic pathways and will certainly be investigated in the interest of keeping the simulation efficient without sacrificing important detail.

Therefore, in conclusion, the proposed digital neuronal model should comprise a limited number of synaptic terminals which will elicit a high rate of well described EPSP waveforms for summation with a pseudocontinuous MP; the decaying tail of the EPSP reflecting the cell time constant. It should include an asymptotic resting potential and the refractory

process observed in respiratory alpha-motoneurones which display after-hyperpolarisation characteristics. No IPSP effects were considered initially in this stationary model because of the lack of evidence for their existence during the active phase of these neurones, to which attention is restricted in this study.

As described in the next chapter, an effort has been made to ensure that the model produces a realistic simulation before studying the properties of interacting groups of these neurones. By comparison of the discharge interval statistics from the simulated neurone, and the MP trajectories produced in it, with the results of similarly analysed neuronographic and intracellular recordings from cat intercostal alpha-motoneurones the model can be, and was, evaluated. Any obvious discrepencies can thus be corrected to allow a valid simulation of this neurone.

3.0 THE TRANS-MEMBRANE POTENTIAL MODEL.

3.1 THE MODELLING PROGRAMME PARAMETER AND PROCESS DESCRIPTION.

The Arrival Times of Pre-Synaptic Events.

Cell, EPSP and Refractory Time Constants.

EPSP MP Components.

Refractoriness.

The MP and the Axon Discharge Threshold.

Tracking and Recording Events of Interest.

3.2 SOME IMPLEMENTED COMPUTER PROGRAMMING TECHNIQUES.

3.3 PRELIMINARY METHODS OF ANALYSIS.

The Quantitative Description of Point-Event Sequences.

Investigation of Membrane Potential Mechanisms.

Event Input-Output Probability Density Function.

3.4 THE PRELIMINARY SIMULATION RESULTS.

3.5 COMPARISON OF THE MODEL AND NEUROPHYSIOLOGICAL RESULTS.

3.6 THE PROPOSAL OF FURTHER INVESTIGATION USING THE MODEL.

3.0 THE TRANS-MEMBRANE POTENTIAL MODEL:

This chapter provides first a descriptive outline of the programmed simulation of the motoneurone trans-membrane potential and then briefly relates the programme development and structure, before continuing with an evaluation of the model's accuracy in representing a real neurophysiological neurone. In this second part, the results are reported of using several preliminary techniques for analysis applied to both the simulation results and recordings made from cat intercostal alpha-motoneurones to assist in establishing, by comparison, the validity and limitations of the model. During the course of these discussions the importance of non-stationarities in the data are considered and this is shown to account for many of the discrepencies that occur. The conclusion demonstrates that a better insight now exists into the information coding properties of this type of neurone, and proposes further investigations utilising the model.

3.1 THE MODELLING PROGRAMME PARAMETER AND PROCESS DESCRIPTION:

The most essential intermediary between the mass of incoming pre-synaptic neural stimulation to the neurone and its resulting post-synaptic axon discharge sequence, is the trans-Membrane Potential (MP). In the previous chapter the proposal of a suitable model included a brief outline of the main synaptic and other trans-membrane mechanisms which constitute the means for establishing and influencing this MP in the intercostal alpha-motoneurones. These processes are implemented into the model by the use of relatively simple algorithms which simulate their approximate electrical (voltage)

analogues for the convenience of producing their additively contributing MP components, thereby allowing a direct comparison with its intracellularly recorded counterpart from physiology. This is demonstrated in Figure 3.1.1A.

Table 3.1.1 gives a list of the parameters used to initialise or generate the variables employed to simulate these processes and their function description in the programme. Also given with this table is an expression which demonstrates how the appropriate components contribute towards the instantaneous MP potential. It will be seen that the dimensions of the parameters and the variables are either time or voltage. In schematic terms the model consists of a pre-synaptic point-event signal input, producing a pseudo-continuous MP which is monitored by a threshold detector; together these generate a new point-event signal corresponding to an axon discharge sequence of action potential spikes. The following paragraphs present the parameters associated with each algorithm, with a description relating their function to their physiological counterparts, and then describe the algorithm implemented and the corresponding variables used. Each variable is updated or a new value is computed whenever the interval of the 'next event of interest' falls due; in other words, the simulation time is advanced according to the next shortest interval for a new event. By applying this approach, the MP components become effectively continuous time varying voltage expressions allowing the simulation to possess a realistic quality. Also, because this approach allows an irregular sampling of an otherwise continuous time simulation

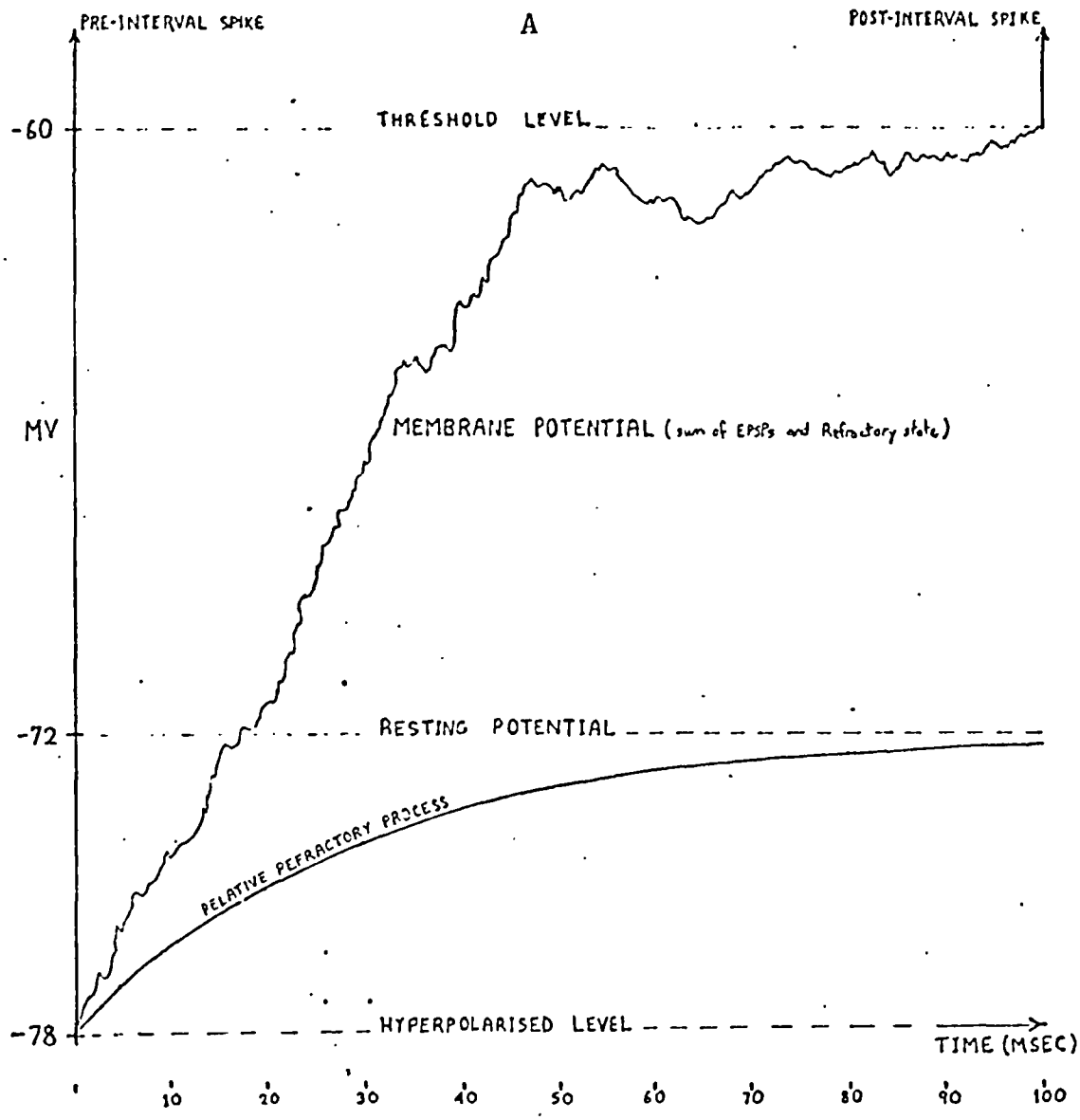

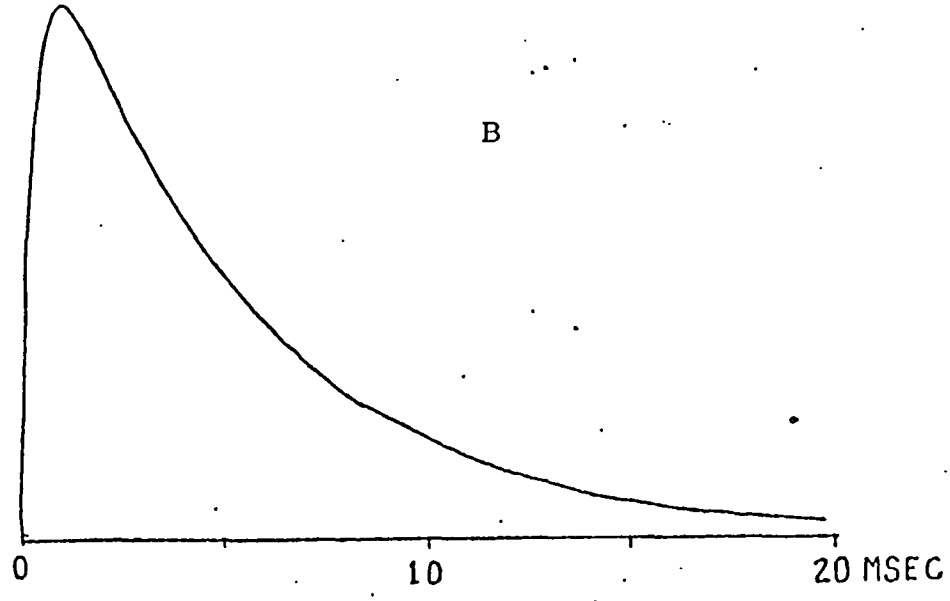

FIGURES 3.1.1:

A The trans-membrane mechanisms.

B The standard EPSP pattern.

TABLE 3.1.1:

Parameter Description and Function-

PARAMETER:	DESCRIPTION:	VARIABLE (ALGORITHM):
TDK	Cell Time Constant(TC).	-
TRT	EPSP Rise TC.	-
TRF	Refractory TC.	-
TINT(i)	Mean Pre-synaptic Arrival Intervals(i).	TIME(i)= $-TINT(i)*\log_e(RANF)$
EPSPK	Epsp Peak Amplitude Factor.	PK= $EPSPK(1.-e^{-\Sigma\Delta t/TRF})$
-	Instantaneous MP EPSP Decay Component.	ADK= $ADK*e^{-\Delta t/TDK}$ +PK (for Pre-synaptic event)
-	Instantaneous MP EPSP Rising Component.	ART= $ART*e^{-\Delta t/TRT}$ +PK (as above)
HPOT	After-Hyperpolarisation.	REF= $HPOT*e^{-\Sigma\Delta t/TRF}$
THRES	Discharge Threshold Level.	-

N.B. Variable, MP= THRES +ADK +REF -ART

(giving the instantaneous MP.)

(as opposed to regular sampling) while still retaining the chronological order of events, the simulation progresses in the most efficient way possible. An 'event of interest' can be the arrival of a pre-synaptic stimulus, which generates a post-synaptic potential for summation with the MP, or otherwise will be the production of an axon discharge spike. It was advantageous to record these events as a sequence of superimposed intervals in chronological order and therefore use the routines developed by Stagg (1973) which were written to analyse neuronal data recorded from animal experiments processed into just such a format.

The Arrival Times of Pre-synaptic Events: These are treated as the time intervals to the next release of transmitter substance at each synapse, causing the immediate generation of an EPSP shape for temporal summation with the somatic MP (the present model investigation examined only excitatory synaptic processes). Also, only two synapses are considered in this study; however, each is made to appear representative of a large multitude of synaptic terminals by stimulating them independently with rapid sequences of pre-synaptic event intervals generated according to Poisson processes. These two renewal sequences are each derived from their mean intervals, TINT(i) by computing the interval, TIME (i) before the arrival of the next pre-synaptic event of that particular sequence using the algorithm:

$$TIME(i) = -TINT(i) \times \log_e(RANF)$$

where i = the identity of the synapse concerned.

RANF = a random variable with a rectangular

distribution between 0.0 and 1.0.

The statistics of a sequence of point-events spaced by the intervals of such an algorithm are known to have the following properties; a negative exponential interval probability density distribution with an equal mean and SD of TINT(i), and a statistically flat event autocorrelation function, which is indicative of complete independence between the interval lengths of the sequence (the results in Section Three, Figure 3.4.2D demonstrate these properties for the algorithm employed).

This gross reduction in the number of active synapses has been necessary for computing efficiency and is justified in this present study despite the conclusions of Segundo et al (1968) and Walloe et al (1969). In a normally functioning vertebrate alpha-motoneurone (innervating skeletal muscle) it is estimated (Barrett, 1975) that there are some 20 - 50 thousand synaptic terminals on spinal motoneurones of the cat and up to 80 percent of these are distributed on the dendrites. Barrett finds, in his summary of results in the literature that the dendritically generated EPSPs are at least 20 - 50 percent as effective as those generated by the somatic synapses when measured in the soma and suggests that these dendritic synapses may have at least an equal or maybe greater role to play in the functioning of motoneurones. In the previous chapter (2.3) it was estimated, from the same reference, that about 17 thousand EPSPs/sec. with a typical 0.1 mV amplitude need to be summed in the soma to allow the MP to be depolarised by the 10 mV separation between the resting and threshold potentials in order to generate axon discharge spikes.

Since the motoneurones under investigation discharge typically 10/sec., this indicates the summation of at least 1700 EPSPs/discharge. This alone suggests that there must be quite a strong independence between the pre-synaptic events, otherwise why such an extravagance in the synaptic structure? Further, in view of the criteria for signs of dependence in the pre-synaptic pathways observed by Segundo et al, none of these are apparent in the physiological results of the cat intercostal alpha-motoneurone; no early mode is found in the axon discharge interval probability distributions or the spike sequence event autocorrelation functions for single units (see the results in Figure 3.5.1). Together, these arguments have been made to provide the grounds for assuming independence in the pre-synaptic pathways and therefore allow the replacement of a large population of synaptic sources by a single source with a much higher rate of stimulation, the events coming forward according to a renewal process.

Such a generator of a sequence of independent intervals can be implemented under the control of a Poisson process. In the model, two of these representative generators are incorporated (because the investigation is to be extended to study the effects of common connectivity between pairs of motoneurones, after the model has been satisfactorily evaluated). This model therefore stands in contrast to that of Walloe et al who found that a minimum of fifteen pre-synaptic sources generating large EPSPs was required to adequately simulate the second order dorsal root neurones they were investi-

'gating. It also contrasts with their model, and with that used by Segundo et al, in that the EPSP shape employed was simply a decaying step.

In the initial stage of this study the pre-synaptic rates were kept stationary, unlike the situation for respiratory alpha-motoneurones which experience a continuously varying rate of drive associated with breathing (Sears and Stagg, 1976). This restriction was due to initial computing limitations to which a satisfactory solution was found; some non-stationary results were produced for comparison with the physiological results. For the standard simulation runs the total mean pre-synaptic rate is 15150 events/sec (15.15KHz). Usually this bombardment of events is shared equally between the two synapses, so TINT(1) = TINT(2) = 0.132mSec. Under these conditions, with the standard EPSP shape and peak amplitude of 0.1mV, a mean axon discharge rate of 10/sec. is generated.

Cell, EPSP and Refractory Time Constants: From experimental work done by Iansek and Redman (1973; also Mendell and Henneman, 1971 and Jack et al, 1971), in which the size and shape of EPSPs recorded in cat alpha-motoneurones were measured, the average cell time constant was determined to be about 6mSec. This value has independent support in the case of cat intercostal alpha-motoneurones in the averaged EPSP shapes recorded by Sears and Kirkwood (personal communication) from their afferent pathway triggered-averages. These sources all also report a typical EPSP rise time (10 - 90 percent of the peak) between 0.6 and

0.7 mSec and an average half height width for this range of rise time of about 6mSec. For ease and efficiency in generating the standard EPSP shape during a simulation, the pattern is computed by taking the difference of two decaying exponentials. This expression for describing the standard EPSP allows their accumulated effect at high pre-synaptic rates to be continuously calculable and therefore lends itself very satisfactorily to the approach implemented, which works on the time of the 'next event of interest' principle. The two time constants used are TDK (= 6.0mSec) and TRT (= 0.5mSec) which generate a pattern with a rise time of 0.7mSec, a half height time of 6.03 mSec and the peak amplitude occurs after 1.355mSec. When this difference expression is scaled by a factor of 0.13674 it attains a peak value of 0.1mV. Figure 3.1.1B illustrates the shape of the standard EPSP pattern produced by the formula:

$$EPSP(t) = 0.13674 \times (e^{-t/6.0} - e^{-t/0.5}) \text{ mV} \quad \text{for } t \text{ in msec.}$$

The relative refractory process in the model motoneurone is simply implemented by another decaying exponential function which approximates the time course of recovery of the MP from a hyperpolarised state back to the resting potential. This is given a standard time constant TRF (= 30.0mSec.) and the contribution to the MP is calculated as HPOT x $e^{-t/30}$ where HPOT (mV) is the amount of hyperpolarisation incorporated in the model. No absolute refractory period is included because results in the first simulation runs with this factor included showed no significant difference in discharge sequence statistics from results with it removed. This is not very surprising: the period observed is short (typically 1.5mSec) in relation to the shortest axon discharge (usually much greater than 50

mSec). Therefore its exclusion from the simulation was upheld in the interest of computing efficiency.

EPSP MP Components: The main basis for choosing to describe the EPSP shape with two exponentials will now be clarified. There are two advantages in this choice rather than in using the more specific expressions derived for the compartmental model (Jack et al, 1971): first, the simplicity of this technique, both from the computing point of view and in allowing a reasonably accurate approximation of a typical soma-recorded EPSP; second, the efficiency it allows in computing the effect of the summed EPSPs. By dividing the contribution of the accumulated EPSPs into two components corresponding to the two decaying exponentials used, any number of EPSPs arriving at any rate can be accommodated quite conveniently. These components are simply updated by weighting each with its appropriate exponential decay value for the length of the past interval. If the 'event of interst' is an arrival at one of the synapses then, after weighting the MP components, the value EPSPK is summed to these two MP components, where EPSPK is the factor by which the original EPSP exponential difference expression was scaled in order to produce the required amplitude EPSP (EPSPK = 0.13674 for the standard 0.1mV EPSP employed). These two MP components are designated under the variable names ADK and ART for the 6.0mSec and the 0.5mSec time constants of the standard EPSP shape respectively. At any instant of time, after weighting the components for the last interval, the effect of the accumulated EPSPs is simply (ADK - ART)mV. Therefore by implementing this approach the concept of a time-

continuous MP is simply and efficiently preserved.

Refractoriness: A third MP component is added to the two described above in order to simulate the effect of refractoriness in the model neurone. This accounts for the after-hyperpolarised state of the MP immediately following an axon discharge and is implemented simply as an exponentially decaying, negative valued component, REF. After each discharge REF is initialised to the amount of hyperpolarisation, HPOT (typically -6.0mV) and decays with the time constant TRF (30mSec) in the simulated motoneurone. During this process of ionic recovery towards the balance observed for the resting state called the relative refractoriness, a further effect occurs. Initially, the amplitudes of the EPSPs are greatly reduced but as refractoriness continues and the ionic balance is recovered, the amplitudes attain their normally observed height of about 0.1mV in general. This graded EPSP amplitude effect is important in that it strongly influences the MP trajectory and variability. It is simulated by weighting the EPSPK factor by the expression $(1. - e^{-t/TRF})$. In this manner the EPSP amplitudes rise to their standard height with a time constant of the refractory process and is compatible with the time updating approach implemented. No other EPSP amplitude modulation effects, such as non-linear summation and localised spatial shunting of synaptic currents (Eccles, 1966), are considered in this present model.

The MP and the Axon Discharge Threshold: The model assumes a fixed axon discharge threshold level (typically -60mV) with the resting potential lying normally 12mV below this at -72mV. For ease in computing a threshold crossing, and the consequence of a discharge, the threshold level is translated

to allow for a test of a sign change only (i.e. the threshold potential is made zero) by incorporating the parameter THRES (normally -12mV). The expression for the membrane potential in the model is:

$$MP = THRES + REF + ADK - ART$$

Another term, -CD is included in this expression for realism when the MP trajectory is displayed, but otherwise appears to have a very limited influence on the discharge interval statistics and therefore is excluded. It is observed in intracellular recordings that, following a discharge spike, the MP does not immediately hyperpolarise (to typically -78mV) but instead smoothly decays into the after-hyperpolarised state reaching the most negative potential anywhere between 5 and 25 mSec following the discharge (see typical averaged MP trajectory in Figure 3.5.3). This characteristic, which will be referred to as 'soft-hyper-polarisation', is implemented in the model as an exponential decay (with a time constant equal to the cell, 6.0mSec) and ignores other associated phenomena such as delayed-depolarisation which has been investigated by Kernell and Sjöholm (1972).

Tracking and Recording Events of Interest: In the event of a calculated threshold crossing, the 'flag' (TDISC) is set low in value. This variable then serves a dual function not only as a 'flag' but as a temporary time storage location also. Initially it is set to a large number (10^{+100}) and remains so until a discharge event is determined to be the next of interest. At this point in time the actual interval from the next event to the instant of discharge is written into one of the pre-synaptic TIME locations while the current value of this TIME location is stored in TDISC (hence the low value of TDISC

signifying the discharge). The combination of these occurrences is detected in the simulation programme which branches to process the current TIME event as one preceding an axon discharge event. TDISC is then reset large after the pre-synaptic interval saved in this location is restored back into its TIME location again and the simulation resumes.

TOUT is a time accumulating variable which sums the intervals that have been processed between the recorded events required for data, thereby keeping a chronological account in the data recording. Generally all the axon discharge events are recorded, together with their intervals from the preceding recorded event, and in some studies, certain pre-synaptic stimulus events also. When the MP trajectories are being recorded, regular sampling at 1.0mSec (or in some cases, 0.1mSec intervals) is employed and usually under this circumstance no other events are recorded except the calculated average discharge interval.

The variable TI(NX) is the array for recording the interval and identity of the events of interest. For each event four locations are used (the indexing variable, NX, being incremented by four after each recorded event), the first contains the time of the past interval and is the current value of TOUT (TOUT is then reset to zero to keep account of the next interval), the next two locations are used to identify the spike by an amplitude value and a channel number, while the fourth is unused at present. This format is compatible with point-event processing programmes of Stagg (1973) with which he has processed the corresponding neurophysiological data; a single unit (neurone) may be selected from a grouped recording of

active units from an intercostal filament on the basis of spike amplitude. In the simulations the amplitude coding was used to identify single units, while the channel number indicated the type of event (1 = pre-synaptic, 2 = discharge).

Figure 3.1.2 displays the modelling programme flow chart and the following section outlines the programme development and some of the features incorporated.

3.2 SOME IMPLEMENTED COMPUTER PROGRAMMING TECHNIQUES:

The flow chart shown in Figure 3.1.2 was originally programmed in Fortran IV on the Imperial College CDC 6400 computer. It soon became apparent that even when a simulation was allowed to run for the maximum computing time permitted, many simulations could not generate enough data to allow statistically significant results. Several solutions for overcoming this problem were considered and the decision to incorporate a combination of these was made so that the simulation speed could be increased several-fold with little loss of the original modelled detail. This implementation still follows the flow chart structure initially employed but takes advantage of several powerful features of the large CDC 6400 and 7314 computers. First, the programme was rewritten in the CDC assembler language, COMPASS, and this was implemented as efficiently as possible, making full use of the eight arithmetic-registers and the very flexible instruction set. For example, by keeping all the variables which contribute to the membrane potential in the arithmetic-registers after updating them to the present instant of interest, the subsequent checking for, and calculation of the time to, the MP crossing of threshold

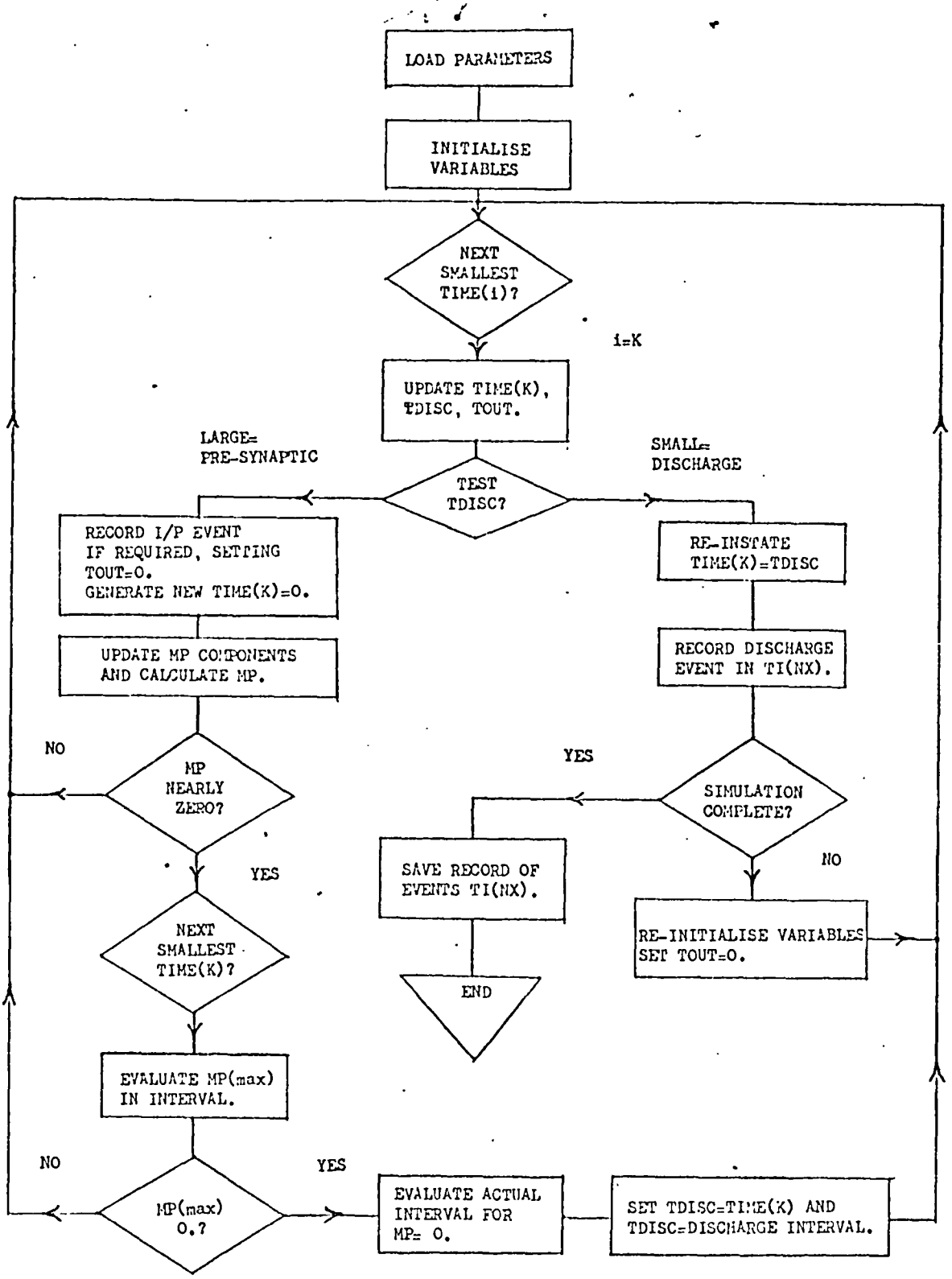

FIGURE 3.1.2:

The motoneurone modelling programme flow chart.

level can be achieved with the minimum of further memory access therefore allowing a faster execution time. These particular programming features immediately halved the time for a simulation cycle, but still did not always allow long enough runs to produce significant results, so a closer look was taken at the times for execution of the functions and algorithms employed. The exponential function used to calculate many of the time-weighting values in the simulation was found to account for approximately 30 percent of the total execution time and the calculation of the pre-synaptic arrival times using the natural logarithmic function, another 20 percent.

A useful feature of the CDC computers is their large core allocation (over 50000 words) and their efficient organisation of the core-to-register transfer of data (direct access from core to any of five registers and storage to core from another two registers), allows for a fast and easy manipulation of data. By taking advantage of this and substituting look-up tables for each of the different exponential time-constant expressions, the function call can be replaced by a short and simple index calculation followed by a core access-load instruction which takes relatively very little time. This approach is made possible by accepting one compromise: requiring a certain minimum time increment resolution. It was decided to use a resolution of 0.01mSec which is 2 percent of the shortest exponential time constant and which has been shown to provide sufficient accuracy for the typical range of simulation parameters used here. Having established the resolution, the number of values in each table can then

be determined from the longest interval expected. This upper limit factor is known and finite because the algorithm used to generate the pre-synaptic intervals will only generate intervals which are less than eight times the mean arrival selected. For the usual range of pre-synaptic rates considered the length of each exponential table is at the most a few thousand values.

In a similar manner an array table of the logarithmic values used in the generation of the pre-synaptic intervals is incorporated. Here, in place of the standard $\log_e$ (RANF) algorithm initally used, 500 natural logarithmic values calculated from the variables over the range 0.002 to 0.999 are used. Because the generation of the random variable between zero and one by the RANF function is very rapid, multiplying it by 500 and using the integer part of the result to address the table of natural logarithmic provides a very fast pseudo-negative exponentially distributed independent sequence of variables. Although this might appear superficially to be a gross approximation, testing the resulting interval sequence (scaled by the mean interval required) demonstrates the method to be adequate for the purpose to which it is applied. The interval-distribution is of a negative exponential form and the autocorrelation function is statistically flat (as shown by the example given in Figure 3.4.3D which results from an interval sequence with a mean of 1.0msec) and the CV is 1.0; all these properties are typical and characteristic of a Poisson source.

One final algorithm employed, which again utilises

another look-up table, does so to avoid the implementation of the $\log_e$ function and is involved in the determination of time to the peak value of the MP (i.e. of maximum depolarisation). This is calculated by differentiating the two accumulated EPSP MP components and re-organising the expression to give the time to a maximum; the time constants involved are known, as are the instantaneous magnitudes of ART and ADK, (This method makes one assumption: all other time constants and processes have negegible effect over the short period in which the maximum is reached; e.g. if only one EPSP has contributed to the MP components, then with the standard time constants of 0.5 and 6.0 msec, a maximum occurs after 1.355msec although, as more EPSPs contribute, the time to a maximum rapidly decreases). The following formulation is used in determining the time to a peak:

The EPSP contribution to the MP = $ADK.\ e^{-t/TDK} - ART.\ e^{-t/TRT}$

Differentiating, to find the expression for the maximum, and rearranging:

$$t_{max} = \frac{TDK.\ TRT}{TDK - TRT} \cdot \log_e\left(\frac{TDK.\ ART}{TRT.\ ADK}\right)$$

$$= \frac{12.\ TRT}{11.} \cdot \log_e\left(12.\frac{ART}{ADK}\right) \text{ for a standard EPSP}$$

This value, t_{max} is a variable which must be calculated after the release of each new EPSP. Now the maximum time to a peak of a unitary EPSP is less than 1.355msec and the time resolution has been set to 0.01msec for the other array tables so, in order to ensure that temporal resolution is maintained over the range of t_{max}, 200 values are computed to cover the non-linear range of this variable. These values are calculated for a linear increase in the ratio ART/ADK appropriately and

therefore the addressing index for this table of t_{max} values. only requires the ratio to be multiplied by 200, thereby resulting in a very fast determination of the time to maximum depolarisation. It only then remains for the recalculation of the MP after such an interval following the next pre-synaptic event to predict whether there has been a threshold crossing or not. If there has been a crossing in this time, the time of the crossing is found by incrementing time in 0.01msec steps, and updating ADK, ART and REF until there is a sign change in the recalculated instantaneous MP, which indicates that an axon discharge is imminent.

The inclusion of these look-up table techniques, together with the reprogramming in assembler language, produced an overall four-fold improvement in the simulation running time compared to the original Fortran programme. This now allows most of the simulations to generate sufficient data to give significant results and so further development was felt unnecessary.

When the simulations are required to produce MP trajectory plots, or are used to examine MP variability, the programme employs a third TIME(i) variable which is initialised to the sampling interval each time it falls due. At this instant the MP magnitude is recorded, after the variables have been updated for the past interval, and the simulation continues.

This concludes the outline of the programming techniques and is followed in the next section with a description of the analytical methods employed to obtain some preliminary results for evaluating this mammalian motoneurone model.

3.3 PRELIMINARY METHODS OF ANALYSIS:

It is necessary to carry out a comparative analysis of the recorded data from the computer simulation runs and that from the neurophysiological experiments so as to allow a direct comparison between the model and cat intercostal alpha-motoneurones: first, to evaluate the reality and limitations of the model; and then to gain more understanding about the properties and information-coding mechanisms of these motoneurones. Some general point-event sequence analysing techniques and membrane potential (MP) variability analysis methods are therefore now introduced. This section also offers an introduction to the specialized Input-Output (Pre- to Post-Synaptic event) cross-correlation functions. The results of all these analyses are then presented in the subsequent sections of this chapter.

(i) The Quantitative Description of Point-Event Sequences: The definitive description of a point-event sequence requires extensive statements about statistical features expressed in event, count, or interval terms. However it is quite clear that, for practical purposes in which only a limited number of statements can be made about the signal statistics, interval statistics are basic; statistical measures expressed in event or count terms turn out to be more-or-less complex transformations of interval measures. The useful interval measures are the probability density function of intervals (or its moments) and the serial correlation coefficients r_1, r_2,..., r_k, ...: very occassionally the higher-order correlation coefficients r_{ij} may be used but in view of their poor sampling statistics they are not used here (Sayers, 1970). A useful measure is the scaled interval

probability density function (PDF) distribution $p_k(t)$ where the k-scaled interval ${}_kT$ is defined by:

$$ {}_kT_i = \sum_{j=1}^{k} T_{i+j-1} \quad ; \; i = 1, k+1, 2k+1, 3k+1, \ldots $$

another useful transformation offers a convenient means for estimating the event autocorrelation function $n_c(\tau)$ when $n_c(\tau)dT$ is the probability of an event in the interval to t_o+T , t_o+T+dT given an event at t_o. This function $n_c(\tau)$ can also be found from the sum of the scaled interval PDFs:

$$ n_c(\tau) = \sum_{k=1} p_k(\tau) $$

Most statistical measures are only useful in the presence of stationary data, but it is recognised that non-stationarity is of the essence in the present problem because of the respiratory rate-modulation (Sears, 1964b). In these circumstances the correct approach (at least as far as moments and correlation coefficients are concerned) is through the use of ensemble statistics, in which the point sequence of events during each breath is treated as a member of the ensemble. Certain difficulties do arise in this case because the individual breath starts at an arbitrary instant within a current interval of the on-going point sequence but, as will be shown, this difficulty can be turned to advantage. Hence the main measures used in comparing real with simulated data should be the general form and the first few moments of the interval PDF as estimated by the sample histogram of intervals, the first few (non-stationary) ensemble correlation coefficients of the interval sequence and the event autocorrelation function.

The interval PDF embodies several pieces of information which are used in generally classifying the generating process

and its variability in a few terms. From it can be found the common statistics of mean (M) and variance (or standard deviation, SD) of the sequential intervals between axon discharges treated as point-events; the measure of the spread of the distribution about the mean is given by the coefficient of variation (defined as CV = SD/M) which is often not a really useful index except for approximately Gaussian distributions. In the past, attempts were made to classify the interval-distributions which were generally non-gaussian and skewed towards longer intervals, by describing them with fitted Binomial or Gamma distribution functions (Stein, 1965) although occassionally the Negative Exponential distribution of a Poisson process (Ten Hoopen, 1966) was relevant. Although these classifications have some utility, especially in comparing one type of neurone with another, the present work deals with non-stationary neural interval sequences and therefore no such classification has been attempted (a broad similarity of the PDFs of the actual and the simulated data was confirmed). Instead, in view of (breathing) non-stationarity in the data, the statistics of interval delay serial correlation coefficients treated from a breath ensemble approach (Frize, 1970) have been used, together with event autocorrelation functions.

By calculating the serial correlation coefficients for a number of interval delays into the breath cycle, as described by Frize, the effect of the non-stationary process underlying the generation of the interval sequence can be observed. Further, if the serial correlation coefficients for a single interval delay are significant then the event autocorrelation function should prove worth investigating.

The autocorrelation function $n_c(\tau)$ or expectation density function of a sequence of N point-events displays the superposition of the first through to the $(N-1)^{th}$ scaled interval probability distributions (Perkel et al, 1967a, b) using the K-scaled interval distributions. The estimation of the function is best computed using a time histogram technique. It is implemented by dividing the time axis into an array of equal width bins; by locating this array with time zero placed under the first event in the sequence and accumulating the corresponding bin counts for events falling within the time-bin range, then shifting successively through the sequence, focussing on each event in a similar manner, a histogram is formed which is equivalent to the sampled autocorrelation. End effect errors are kept small if the autocorrelated sequence is many times longer than the time window of bins employed.

Perkel et al (1967a) discuss the use of the autocorrelation function (ACF) as an alternative to testing the serial dependence between intervals of a point event sequence; although, only rather insensitive, this method can have application even with non-stationary processes. The method of comparing the ACF of the original sequence with that of the same randomized series of intervals (shuffled to remove the time dependency), was used quite successfully by Stagg (1970). In their second paper (1967b), Perkel et al demonstrate how the ACF should be used in the interpretation of cross-correlation functions to signals from coupled cells and further reference will be made to this in the chapter four.

To summarize the preliminary analysis of the point-event processes studied here, attention will be concentrated on the interval sequence mean, variability, serial dependence, and

non-stationarity.

(ii) Investigation of Membrane Potential Mechanisms - In this investigational approach each membrane potential (MP) trajectory is treated as a separate member of an ensemble. Two different sets of information can be obtained by aligning the trajectories: exploring the after-hyperpolarisations phase of their MP functions immediately following the preceding discharge spike (by forming the average post-discharge MP profile) or exploring the End-tragectory average MP preceding the discharge. Both of these analyses produce results which enable a comparison between the simulated MP and the intracellular recordings from physiology and therefore allow a critical analysis of the model.

In the first method in which the MP Profile is found the MP trajectories are sampled at 1 msec intervals until a discharge occurs, thus completing an interval that was initially synchronised by the negative falling edge of the previous discharge (Calvin and Schwindt, 1972; Schwindt and Calvin, 1972), each contributing as an ensemble member of the profile. This average trajectory is found from (usually) 200 simulated trajectories, or at least 100 physiological recordings, and is terminated when only 30 contributing ensembles remain (i.e. the others stop contributing to the average at the point of a discharge spike generation). In addition to the ensemble mean value of each sample, a measure of the ensemble variability is calculated (presented on the plots of the MP profile as the fainter lines $\pm$ 2.58 standard deviations above and below the, heavy-lined, mean profile). Associated with the MP profile is the membrane potential probability density function (MPDF) which indicates the

probability of finding the MP at any particular voltage level. Levitan, Segundo, Moore and Perkel (1968) give a detailed account of this important probability density function which is estimated by a voltage bin histogram technique. The histogram is calculated by setting up a series of equal width (subthreshold) voltage-bins and incrementing the appropriate bin count for successive MP sample values over all trajectories. Finally, the area under the histogram is normalized to unity by dividing the bin counts by the total number of contributing samples. For the resulting MPDF as presented here, the bin width is 0.2mV; the variability of this density function is calculated and presented as the faint line, 2.58 standard deviations above the MPDF (heavy-lined) estimate.

The format for the presentation of the average MP End-trajectory is much the same as that for the MP profile except only the final 10 msec prior to the discharge are displayed and the sampling interval is much shorter, 0.1 msec. Again the ensemble variability is shown as $\pm$ 2.58 standard deviations around about the mean End-trajectory. This method should allow a closer investigation into how the MP, under the direct influence of the pre-synaptic drive via the EPSP pattern, finally attains the spike initiating threshold level. As a reference, the asymptotic level of regularly generated EPSPs (at the pre-synaptic rate selected for the simulation run) taking into account the influence of the recovery hyperpolarised state (after an equivalent mean discharge interval for that run) is superimposed on the end-trajectory result as a dashed line.

(iii) Event Input-Output Probability Density Function - This Input-Output PDF $P_{io}(\tau)dt$ is defined as the probability that

a pre-synaptic event (releasing an EPSP for summation with the MP) at time t_o is associated with an axon discharge in the interval $t_o + dt$. It can be found by appropriately scaling the event cross-correlation function, known as the Pre-and Post-Stimulus Time (PPST) histogram method (Stagg, 1970 and 1973), which in this case treats the pre-synaptic events as stimuli and the axon discharge events as the responses. An array of equal width time bins are set up and the histogram is then formed by accumulating bin counts for response events falling within the histogram range (both Pre-and Post-Stimulus) with the centre of the histogram bin array (designated zero time) shifted successively from one stimulus event to the next for the full length of the event sequences. End effects are again minimised by using a time window which is small relative to the sequence length and by making allowance for the starting up and termination of the process, such as starting and finishing at half the time window interval from the ends of the event sequence. Because the PPST is constructed from a process generating an independent sequence of events, then statistical variability limits such as $\pm$ 2.58 SD may be determined for the resulting function for regions well away from any obvious signs of correlation. These 1% confidence limits (Stagg, 1970) are superimposed above and below the mean probability level of the resulting PPST histogram to help aid its interpretation. The importance of the Input-Output probability density function will become apparent later in this thesis, so is introduced here without further discussion. As there is no way at present for deriving this function for the neurophysiological situation under investigation, it cannot be used to help evaluate the validity of the model. Nevertheless it offers a useful insight

into mechanism and so some typical simulation results are presented in the next section and some reference to these is made during the concluding part of this chapter.

3.4 THE PRELIMINARY SIMULATION RESULTS:

A preliminary study of the model was undertaken to determine its characteristics when driven with a stationary pre-synaptic excitation. Some of the initial results are presented here to demonstrate these. It will be argued that these results allow a better understanding of the roles played by trans-membrane mechanisms in the information coding operation of a typical moto-neurone. The parameters of the model for these trials were chosen so that the model simulated, essentially, an intercostal alpha-motoneurone (of the cat) under a random stationary pre-synaptic drive (which therefore has, effectively, a steady mean level). Random, in this context means that each pre-synaptic event is independent of all others, although of course all pre-synaptic intervals will be drawn from a source with a constant distribution.

Figure 3.1.1 displays the trans-membrane effect of a stepped mean pre-synaptic rate increase. In figure A the drive is sub-threshold; this implies that the rate at which the EPSPs are summated is insufficient to lift the MP from the resting potential at -72mV to above the discharge initiating threshold level at -60mV. Each burst of pre-synaptic excitation lasts for 200 mSec and the mean rates in KHz (1000 events/sec) are indicated above the plot. The neurone, under these sub-threshold drive rates, does not display refractoriness as this is a property of the dynamic situation and directly related to the mechanisms

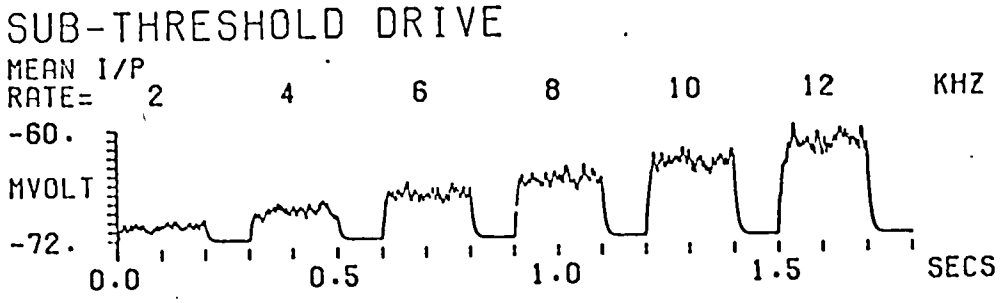

A: The response of the Membrane Potential (MP) to sub-threshold pre-synaptic rates (I/P= Input).

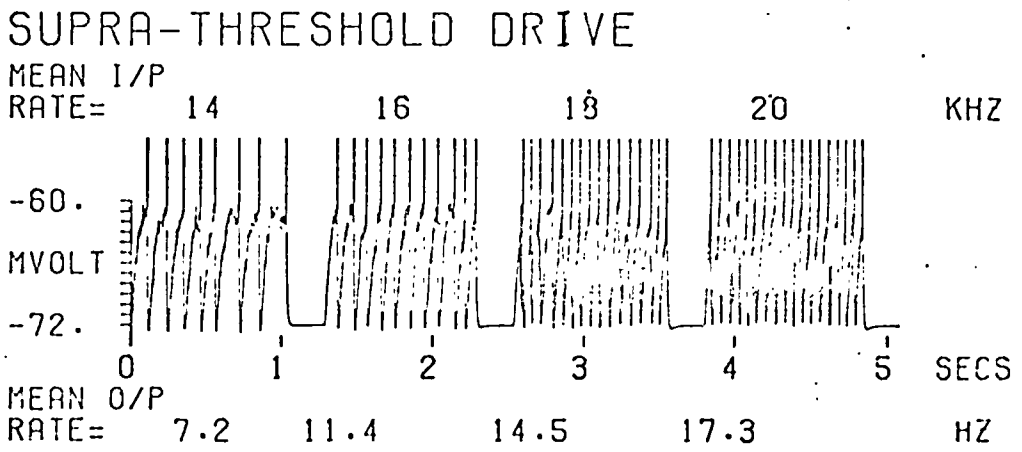

B: The response of the MP to supra-threshold pre-synaptic rates (O/P= Output).

FIGURES 3.4.1.

involved in the production of a post-synaptic discharge (action potential) spike. Instead it demonstrates, through the MP, the characteristics resulting from the summating of EPSPs (in this case, all of standard shape and amplitude i.e. TRT = 0.5 mSec. TDK = 6 mSec and peak = 0.1 mV) and the variability of pre-synaptic drive. The effect of this latter phenomenon is observed to be quite pronounced despite the filtering effects of the time constants describing the EPSP shape, (TDK being the cell time constant); this filtering effect is responsible for the MP decay back to the resting potential at the termination of each burst of stimulation. Also the initial rise to the inherently noisy asymptotic MP level is rapid, in the absence of graded EPSP contributions which only come into effect during the refractory phase (taking about 30mSec for the 12KHz drive rate which is only a third of the typical interval times observed). The results in figure B are in complete contrast to those of A, displaying the dynamic properties of this neurone under supra-threshold pre-synaptic rates as indicated above the plot. Here the threshold is attained a number of times during each burst of presynaptic drive (approximately one second in length) allowing both the non-linear threshold characteristic (the point-event discharge spike is indicated by a short vertical line above the -60mV threshold level) of any active neurone, and the refractory process specific to most alpha-motoneurones, to be observed. Also, these results demonstrate the typical variabilities of post-synaptic axon discharge intervals that occurs at various levels of stimulation. Strictly speaking, both the 14 and 16 KHz rates are still

essentially sub-threshold, as shown by the way the MP hovers just below the threshold before being driven across it by a random increase of short-period pre-synaptic activity due to its variability; even so these crossings occur quite readily, as indicated by the mean output (O/P) rates given below the plot. The rate division characteristic of such neurones can be seen to be highly non-linear, indicating an information compression property. This is evident within their typical operating regions (as shown in B), where a high sensitivity-displayed to pre-synaptic rate changes particularly in terms of output rate and variability.

These changes in output characteristics are better illustrated by the interval-histogram results presented on the right in Figures 3.4.2A, B and C. In A with a 14KHz pre-synaptic drive rate, the interval distribution is somewhat skewed towards longer intervals with a mean of 137.1 mSec (7.3Hz) and is considerably more spread (CV = 0.227) compared with that for the higher drive-rate results shown in B and C. The skew and spread of these latter interval-histograms are much reduced as shown by the 15.2KHz stimulation which has a mean O/P interval of 101 mSec (10 Hz) and CV = 0.152 and at 18KHz, a mean O/P of 68.7 mSec (13Hz), CV = 0.103. To the left of the interval-histograms are the corresponding event autocorrelation functions which show marked differences, from highly-to slightly-damped oscillatory form, for the results demonstrated. These, when considered together with the serial correlation coefficients presented in Table 3.4.1 (all very small) calculated from the same discharge event sequences, indicate a strong independence of intervals; these also

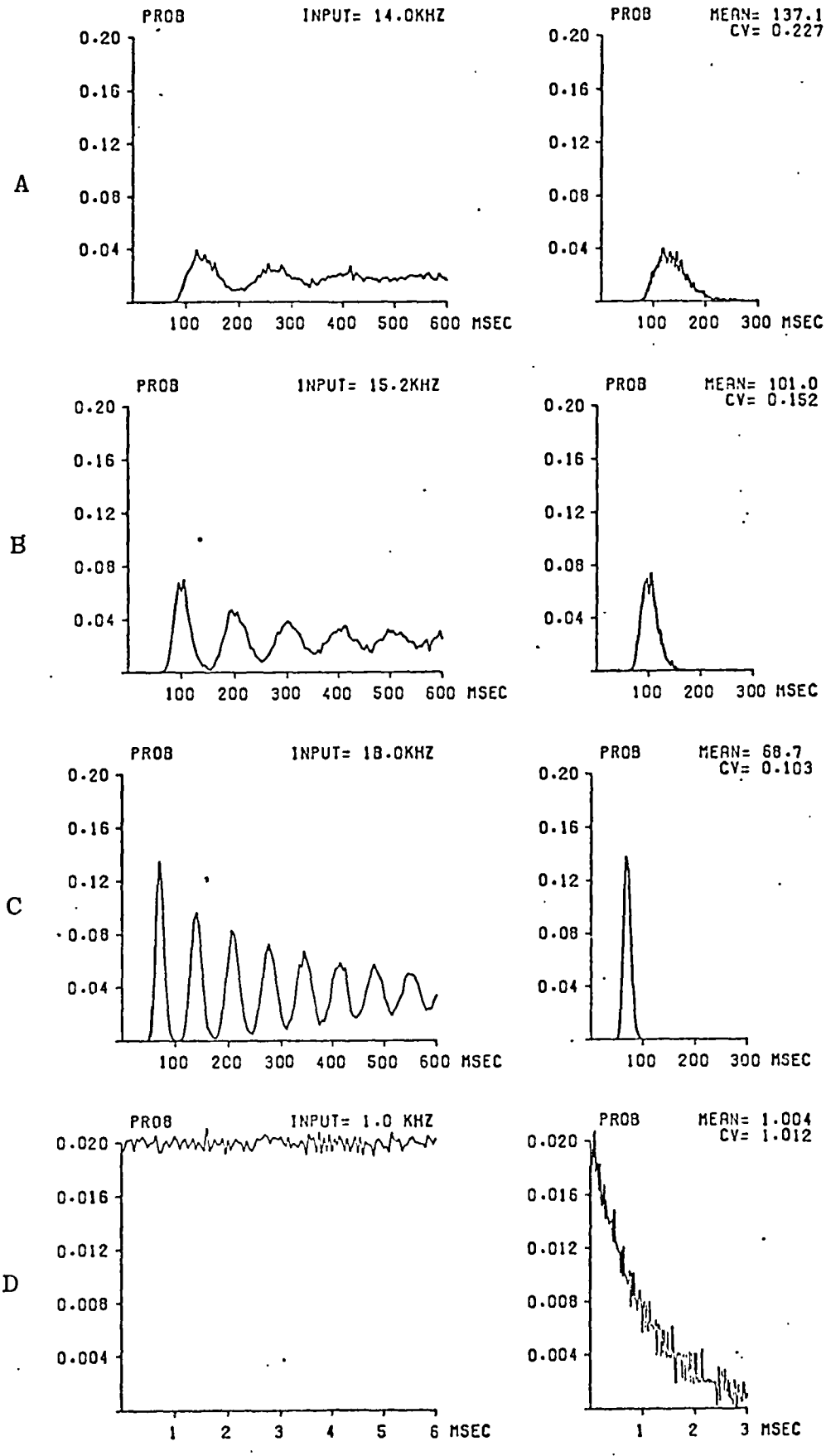

FIGURES 3.4.2:

Some discharge event autocorrelation functions and interval probability distributions determined from the stationary model (refer to text for details).

TABLE 3.4.1:

The Stationary Simulation Serial Correlation Coefficients-

Pre-synaptic Rate:	Serial Correlation (Delays): 1	2	3	4	5
14 kHz (N= 2838)	0.001	0.000	0.008	-0.030	0.001
15.2 kHz (N= 3604)	-0.020	0.000	-0.024	-0.008	0.011
18 kHz (N= 3999)	-0.009	0.031	0.000	0.028	0.006

N= The Total Number of Discharges in the Interval Sequence.

highlight the rapid change from irregular to quite periodic interval sequences when the pre-synaptic drive is altered over the limited range of rate from 14-18KHz. For comparison the results in D display the interval histogram and ACF of a truly independent sequence from a Poisson-generated interval sequence (using the psuedo-Poisson algorithm incorporated in the modelling programme). They demonstrate all the essential characteristics of such a renewal process; negative exponential interval-distribution, unitary CV, and a statistically flat ACF as expected for completely independent intervals. It is interesting to note the effect of slight quantization in the interval PDF distribution tail due to the limitation of the look-up table approach used to generate the pre-synaptic event arrival times.

The pre-synaptic to post-synaptic rate transfer characteristic of the model shown in Figure 3.4.3A clearly demonstrates the non-linearity within the normal operating region (0 to about 25Hz) of intercostal alpha-motoneurones, but however, fails to show the secondary break point (with a gradient increase) around 35 discharges/sec observed by Calvin and Schwindt (1972). Calvin and Schwindt in their study of cat spinal motoneurones, used excitatory current injection methods and plotted axon discharge rate against injected current which showed two distinct linear regions: primary from 10 to 30/sec and secondary from 40 to above 100/sec. Although these observations indicate an obvious inadequacy in the model, the secondary effect does occur outside the typical operating region of the motoneurones under investigation and therefore is not regarded as a serious limitation. At the lower end of the transfer characteristic in Figure 3.4.3A, for pre-synaptic

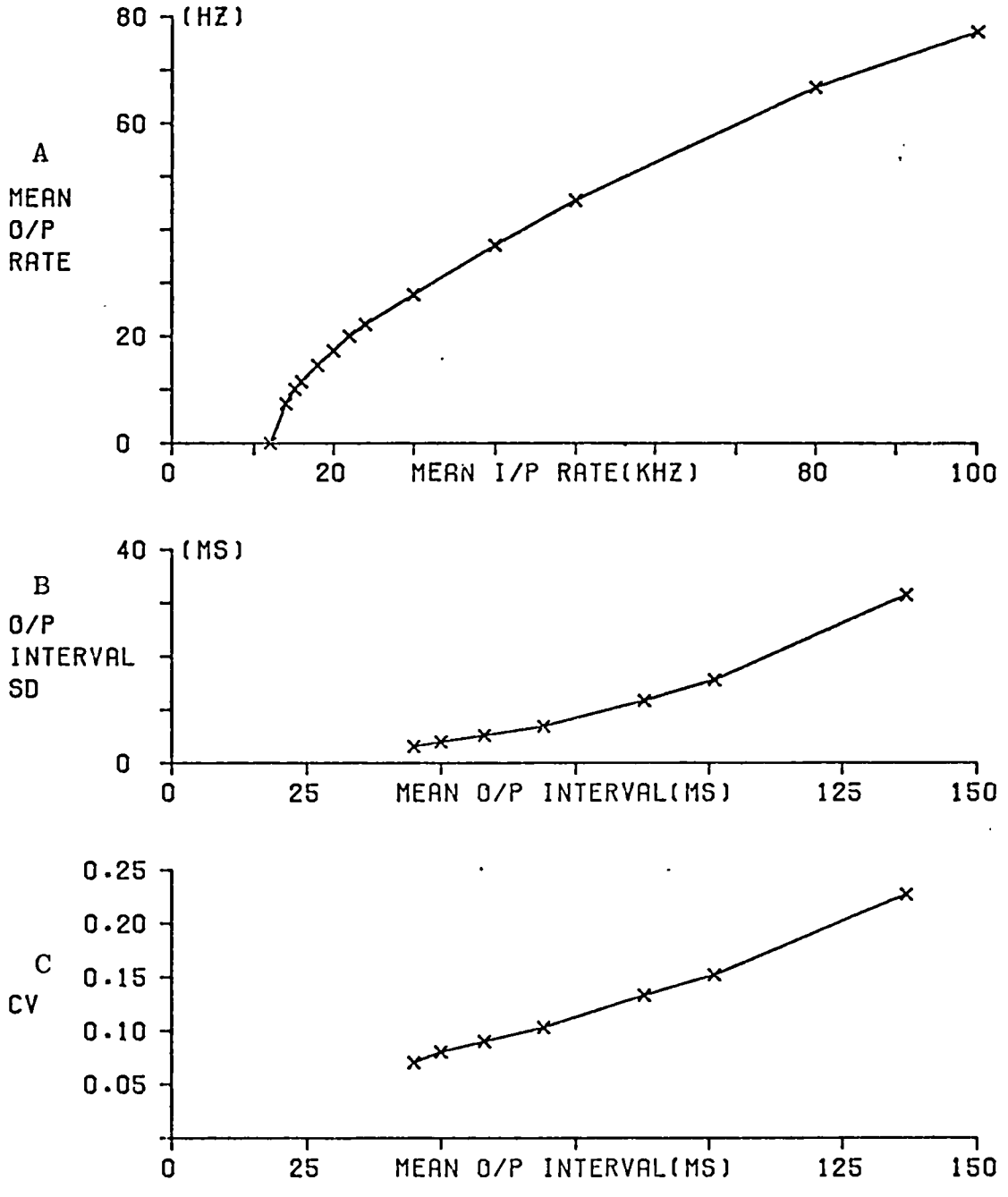

FIGURES 3.4.3:
Some interval characteristics of the discharge sequence of the stationary model.

A The rate transfer graph.

B The standard deviation graph.

C The coefficient of variation plot.

rates below about 12KHz, a dead space exists as was described at the beginning of this section being due to the MP remaining sub-threshold. Drive rates between 12 and 14KHz produce a very erratic discharge interval sequence with an abrupt increase in discharge rate. Above 14KHz the rate of increase of discharges smoothly rolls off through the remainder of the normal operating region to become quite linear. This type of compression characteristic will obviously play an important role in both the coarse and fine control properties of alpha-motoneurones.

On the same page, the Figures 3.4.3B and C show the typical axon discharge sequence statistics reported in the literature (Geisler and Goldberg, 1966; Clamann 1969; Walloe et al, 1969) - specifically, the discharge interval SD and CV for the model. The result in B is in close agreement with that found by Clamann who studied single motor unit firing patterns recorded from the human brachial biceps muscle. Both in the model and in Clamann results, the curve of SD against mean interval lies well below the line of unity relationship occasionally observed by the others. It is also interesting to note that Clamann demonstrates evidence for a gaussian distribution of intervals (sometimes with a slight skew towards longer intervals), an underlying renewal process as indicated from his successive interval scatter diagrams, and ACFs which appear very similar in form to those derived for the stationary motoneurone model with 14 or 15.2 KHz pre-synaptic drive.

Considering how the intracellular variability studies Figure 3.4.4 demonstrates the average MP Profile and the

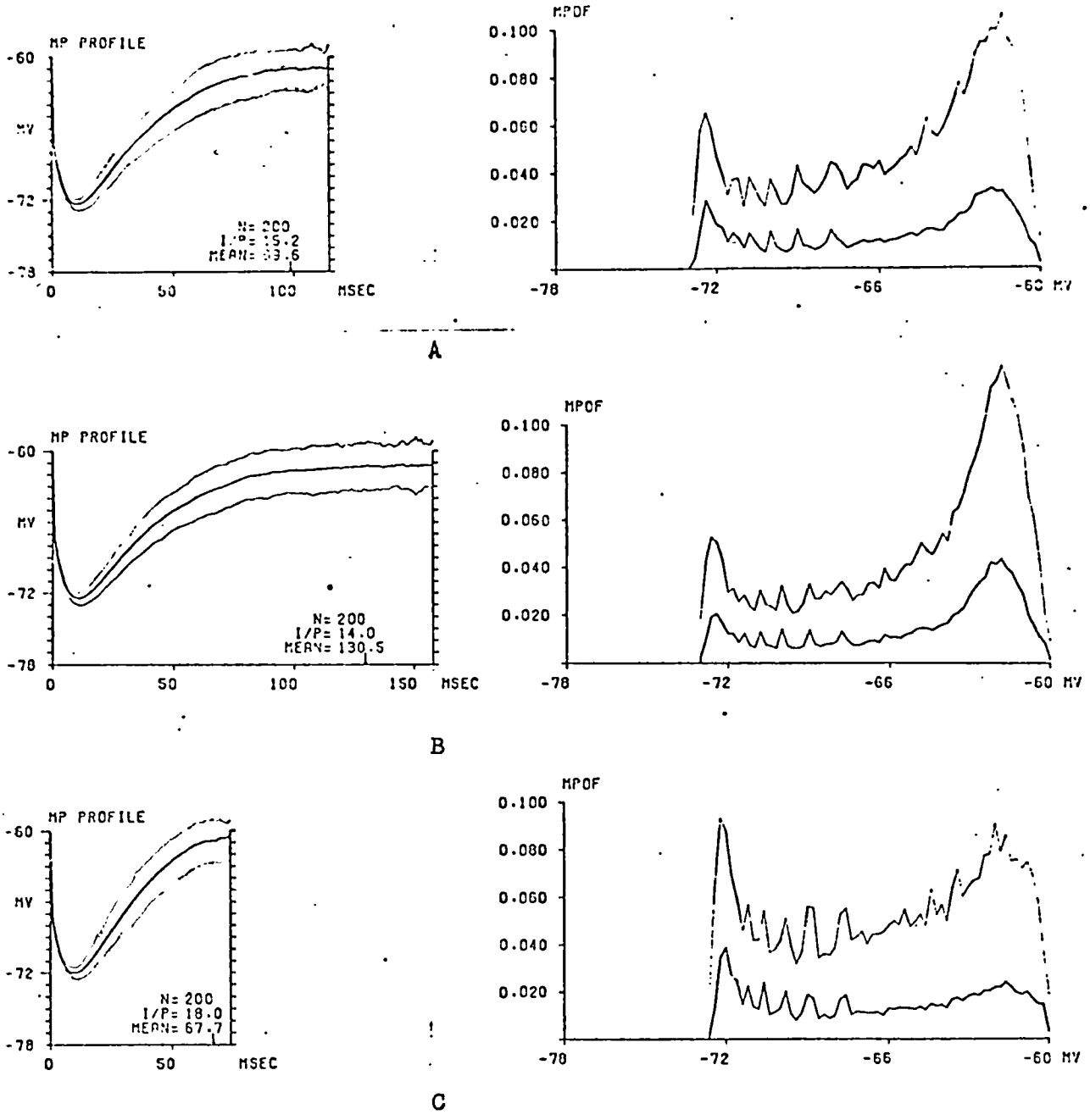

FIGURES 3.4.4:

On the left are the average MP Profiles and on the right are the MP Probability Density Functions (MPDF) from standard (stationary) simulations with pre-synaptic rates (I/P) of 15.2 (A), 14 (B) and 18 (C) kHz. MEAN indicates the average discharge intervals in mSec (for further explanation refer to the text).

estimated MP probability density function for three pre-synaptic drive rates: 15.2KHz(A) 14KHz(B) and 18KHz(C).

Shown on the left is the profile of the average membrane potential time fluctuation, while the right hand plot indicates the probability of finding the MP at any particular voltage level. The fainter lines above and below the MP Profile and the faint line above the MPDF give the 2.58 SD limits of variability. For the MP profile results, these are representative of the one percent confidence limits as shown by the corresponding reasonably gaussian distributions of the MP variability (Figure 3.4.5) sampled at 20, 40, 60 and 80 msec along the profile. These results all come from a stationary simulation (i.e. No breath modulation of the pre-synaptic rates) with a standard EPSP shape (TRT = 0.5, TDK = 6.0 mSec and peak amplitude at 0.1mV) and a refractory time constant of 30mSec. The resting potential is at -72mV with the threshold at -60mV and 6mV at hyperpolarisation is used. Also indicated on the profile is the mean discharge interval (with an arrow pointing to its time of occurrence), the pre-synaptic (I/P) rate in KHz, and the number of contributing members of the ensembles.

It is interesting to note the strong similarity of the profile plots to the results of the study performed by Calvin and Stevens (1968) on their Class 1 lumbo-sacral motoneurones in which there was no dependence between intervals (see their Figure 4). The resulting averaged MP profile of the model displays a stronger hyperpolarisation during after-hyperpolarisation but has about the same amount of synaptic noise (3mV) as

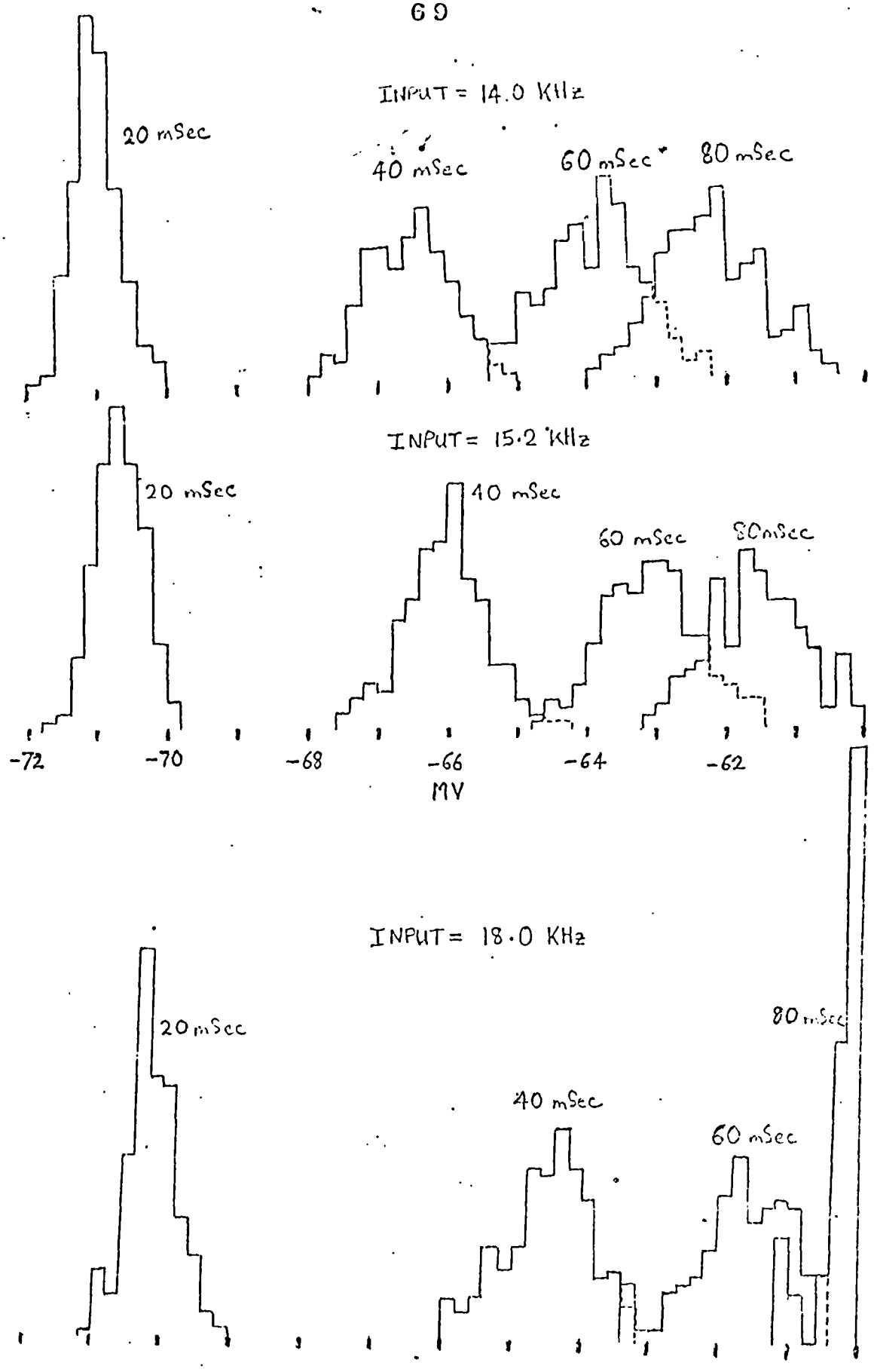

FIGURES 3.4.5:

These demonstrate the MP distributions at sampled times 20, 40, 60, and 80 mSec along the MP trajectories from the standard (stationary) simulations for the three pre-synaptic rates marked.

measured by them. This difference in the degree of refractoriness would no doubt be more apparent in a MPDF study of their motoneurones, but unfortunately this is not presented. Levitan et al (1968) gave an account of their MPDF investigation of invertebrate ganglion neurones but do not show any results for the mammalian motoneurone which might be used for comparison here. Most of the neurones studied by them have characteristically large EPSPs and exhibit little or no refractoriness and demonstrate very different probability density functions to those observed here because of these factors. In the results presented here the MPDFs show a definite change of form, from a bimodal to an essentially unimodal density function with increasing pre-synaptic drive, reflecting the changing asymptotic level for the summation of EPSPs (i.e. changing from sub-threshold to supra-threshold). The oscillatory nature of the MPDF below -66mV is due to the repetitive manner in which the MP trajectories repolarise after a discharge and the sampling rate of this profile used to generate this function. Figure 3.4.6 demonstrates the results of the averaged MP End-trajectory analysis covering the large 10mSec prior to a threshold crossing and the subsequent generation of an axon spike in the model for the same simulation runs considered above. These demonstrate that the average MP trajectory trends (heavy lined plot) for the three pre-synaptic rates used, are practically identical over the last 4mSec when superimposed. Further, the inward tapering of the 2.38 SD limits of variation about the final 10mSec MP trajectory

FINAL 10 MSEC MP TRAJECTORY

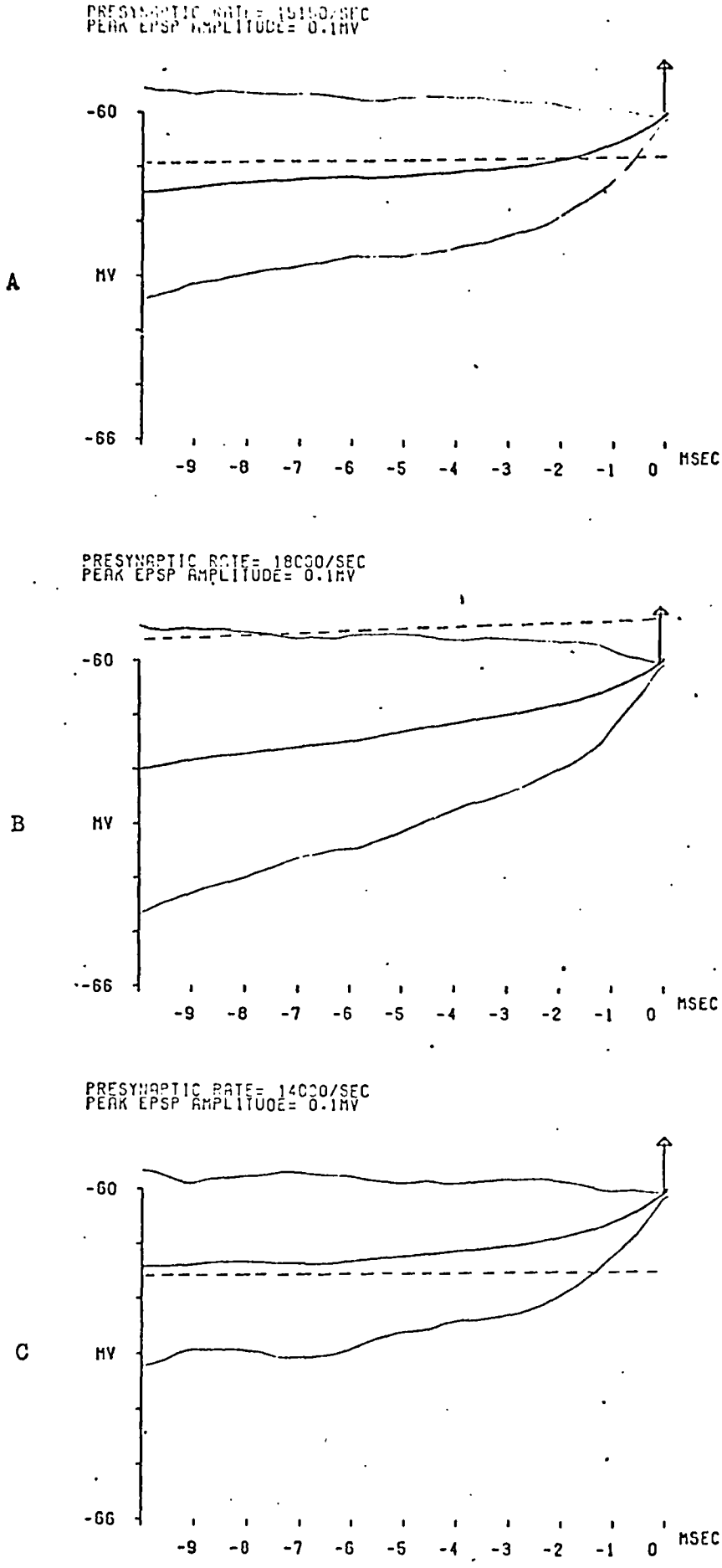

FIGURES 3.4.6:

The average MP End-trajectories (details in the text).

(fainter bording lines) indicates the presence of a selective process which places a constraint on the pre-synaptic arrival in order that the MP might cross the threshold. The averaged MP end-trajectory displays this conformity to a fairly closely prescribed pattern as an increasing rate of rise in the MP over the last few milliseconds which requires a systematic acceleration in the pre-synaptic rate of release of EPSPs for summation with the MP to produce such an effect. Each of these results have been obtained from an ensemble of 100 consecutive trajectories. The dashed lines show the asymptotic level for the summated EPSPs released at a regular rate, equal to mean rate used for the simulation, taking into account the superimposed effect of the exponential after-hyperpolarisation recovery following a period of time equal to the mean discharge interval. It is included to emphasize the differences in the three simulations; two of these essentially have sub-threshold drive (A and B) while the third is supra-threshold, and all exhibit a matching final rise towards the threshold.

The final set of results from this preliminary analysis of the model are included in Figure 3.4.7 to introduce the use of the Input-Output (pre- and post-synaptic) event probability density function. These simulation results are derived from the same runs referred to above, namely normal runs with standard parameters and pre-synaptic rates of 15.2, 14.0 and 18.0KHz respectively. They demonstrate the average influence a single EPSP, released at time zero, can have on the probability of producing a discharge spike in the neurone

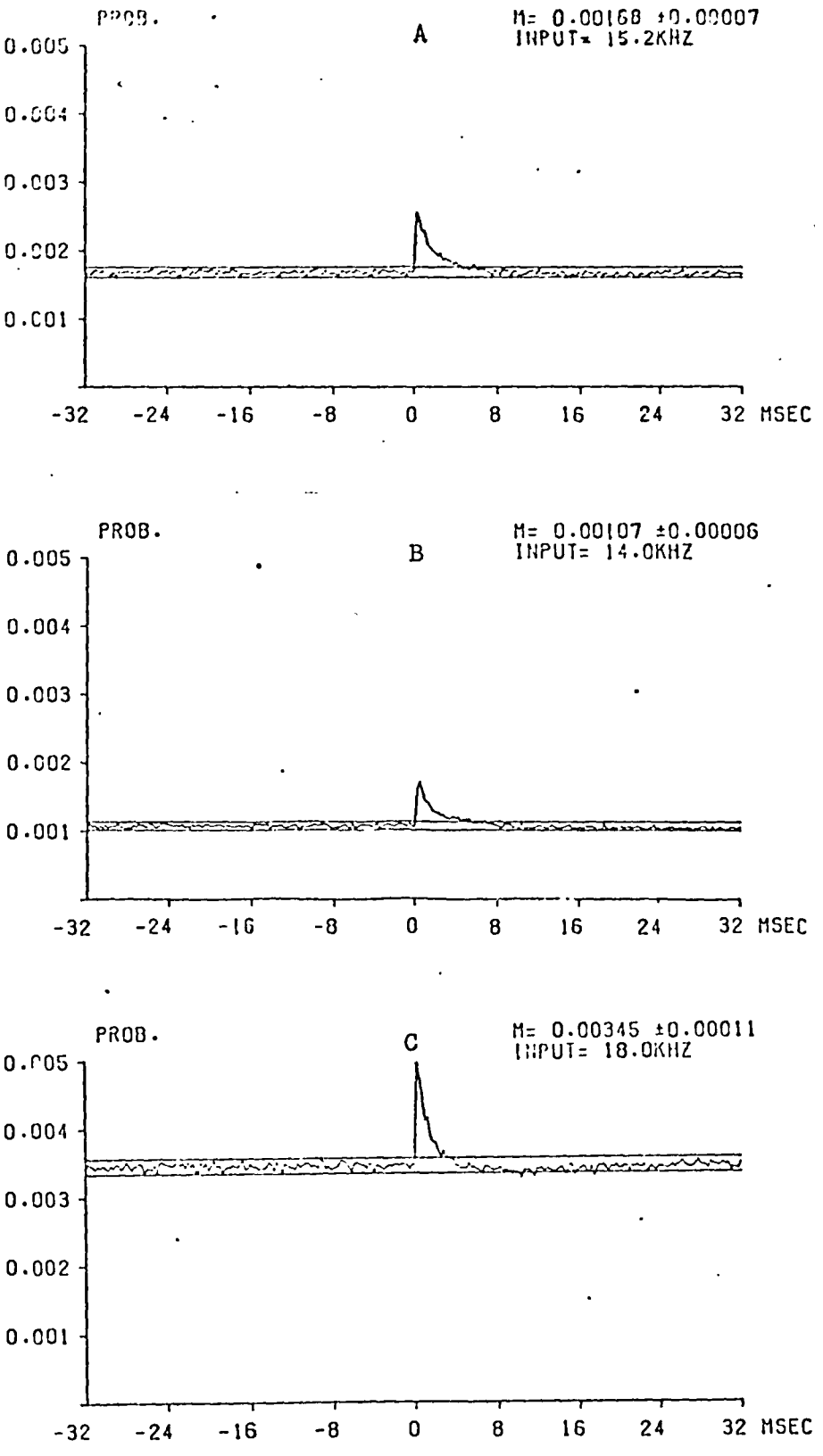

FIGURES 3.4.7:

The event Input-Output PDF from the standard (stationary) simulations with pre-synaptic excitation of 15.2 (A), 14 (B) and 18 (C) kHz.

when summed with the instantaneous MP. Naturally there is a constant probability that the neurone will discharge independently of the particular event focussed upon, as shown by the statistically flat probability level preceding this event (to the left hand side) due to the effect of all the other EPSPs released for summation earlier (which come forward independently of one another according to a Poisson process). Immediately after the instant of its release, this EPSP is observed to have a significantly strong transient effect on the probability of a discharge (the bin width of the PPST histogram is 0.25 mSec) which again falls below the mean level in 3 to 7mSec for the simulation rates indicated. Following this transient kernel is a phase of slightly depressed probability which gradually recovers back to the mean (not clearly obvious on the results shown because of their limited time span) as can be seen most clearly for the 18KHz pre-synaptic rates with the aid of the displayed lines indicating the upper and lower 1% confidence limits of the mean. A more critical examination of this probability density function is reported in chapter five, while its role in the derivation of the discharge event cross-correlation functions between axon events from a pair of neurones or two groups of neurones is outlined at the end of this chapter and demonstrated in chapter four.

3.5 COMPARISON OF THE MODEL AND NEUROPHYSIOLOGICAL RESULTS:

In order to obtain the neurophysiological data for analysis, two different types of recordings, neuronographic and intracellular, were made during experiments designed to

investigate the properties of cat intercostal alpha-motoneurones. For the neuronographic method the lightly anaesthetized animals were prepared according to the procedure of Sears (1964a) to expose the surfaces of the external intercostal muscles and intramuscular nerve filaments but then modified as described by Sears and Stagg (1976). The nerve filaments conducting the motor discharges to be recorded were laid across a pair of platinum hook electrodes, individually mounted in glass tubes for support and clamped above the animal. These electrode pairs were buffered by screened, high input impedance amplifiers again as described by Sears and Stagg with the details of recording and processing techniques for the data measured. By use of an amplitude technique the processing allows the isolation of a single unit spike train which is subsequently analysed as a point-process signal by the methods discussed in section 3.3.

Intracellular recordings were obtained by careful insertion of a hollow glass micropipette electrode (filled with approximately 4M potassium acetate solution and referenced to the extracellular fluid potential by a remote Ag/AgCl electrode) into the spinal cord, immediately medial to the dorsal root entry, where a suitable alpha-motoneurone was located and impaled after preparation of the lightly anaesthetized cat according to the methods of Sears (1964b); in addition the cat was paralysed and artificially ventilated. (The contents of this reference give a more extensive account of the recording procedure). The measured intracellular signal was amplified with D.C. amplifiers while the action potential spikes of the dis-

charging cells were clipped by a soft-clamping diode network, before both signals were recorded on a F.M. tape recorder, utilising the full dynamic range to minimise the signal/noise ratio. This recording was later digitised on an IBM 1800 computer and the resulting sampled membrane potential analysed by the methods described in section 3.3.

Consider first the neurongraphic data analysis. Shown in Figure 3.5.1 are the resulting spike sequence interval-histogram and their corresponding event autocorrelation functions for three essentially separate single units, recorded during an experimental investigation on a normal cat, from segments T_4, T_{7a} and T_{7b} respectively. By comparing these with the results of the stationary model, presented in a similar manner in Figure 3.4.2, several obvious discrepancies are observed. Although the interval-histogram results for T_{7a} and T_{7b} might be considered to have arisen as under-sampled versions of 3.4.2B (standard model run with 15.2KHz pre-synaptic rate), there are several factors against this as a likelihood. For one, the coefficients of variation for the physiological intervals are much higher than that for this particular modelled case. This is certainly due to the large amount of skew observed and no doubt is a result of the underlying non-stationarity in the physiological data.

To allow a more compatible comparison, the model was given a breathing-like non-stationarity by sinusoidally modulating the pre-synaptic arrival rates about a mean

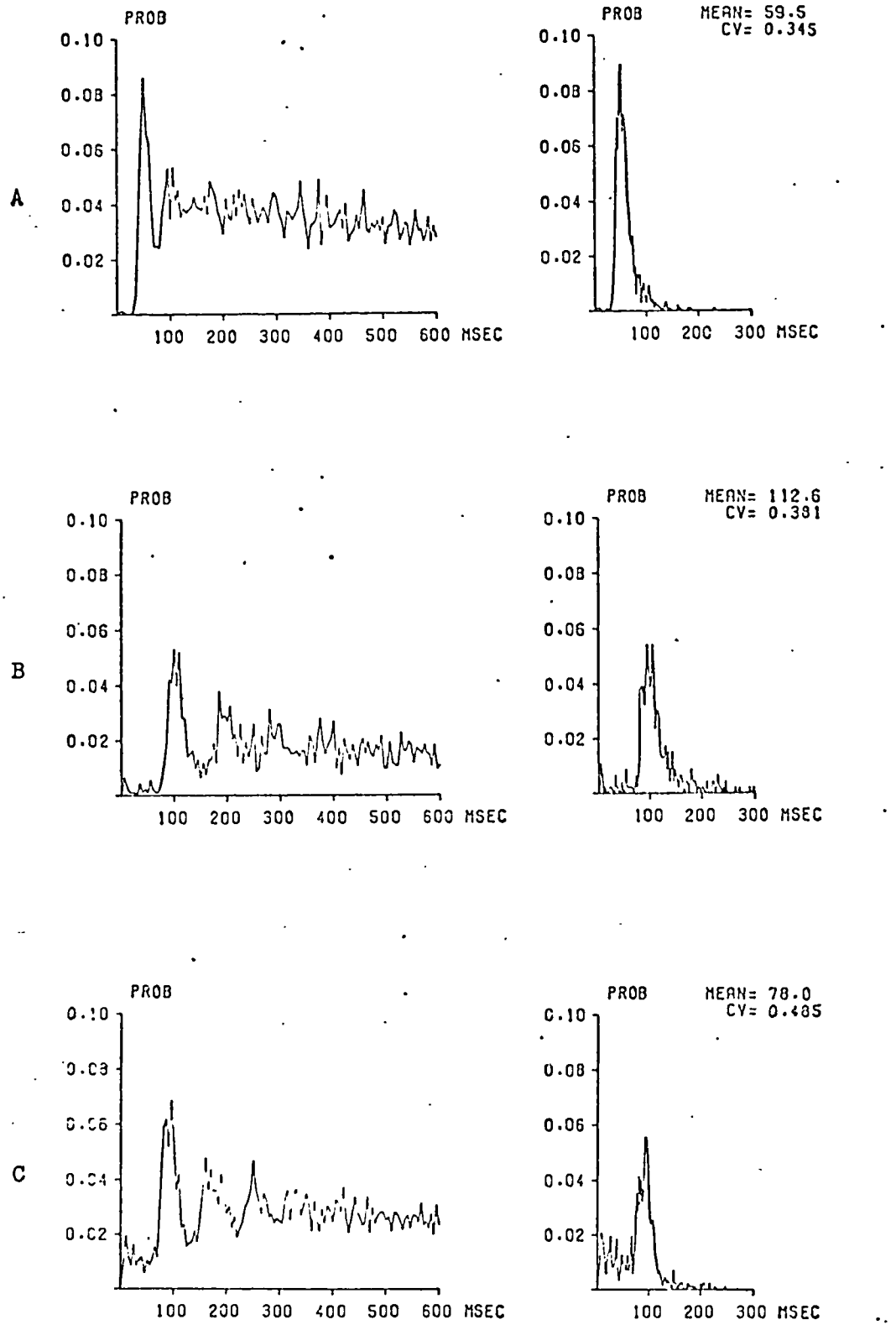

FIGURES 3.5.1:

Some Normal cat results of single unit discharge event auto-correlation functions (left) and interval PDFs (right). Refer to the discussion in the text on the problems of non-stationarity.

total input rate of 15.2KHz. The period of the modulation was made equal to 4 seconds while various depths of breath were investigated; the resulting event autocorrelation functions and interval-histograms for 20 percent and 40 percent modulation of the mean rate are presented in Figures 3.5.2A and B respectively. Visually, this introduction of non-stationarity into the model improves the resemblence between the simulated and recorded discharge sequence. As the number of tests available for comparison are limited to two (i.e. by the nature of the interval-histograms and by the amount of inter-relation between the intervals making up the discharge sequences), it is important that both are thoroughly investigated.

First, considering the interval-histograms: while a 'chi-sqared goodness of fit test' between the simulated distributions and these coming from the neurophysiological source might allow a critical comparison, it would not tell much more than can be seen by eye; there are obviously some similarities such as: approximate similar form, skew and probability strength, and likewise dissimilarities in mean interval length and CV. Also for the T_{7a} and T_{7b} results there is respectively some minor and quite strong contamination of the single unit recordings, as demonstrated by the significance of very short intervals. In the latter case, for example, if intervals greater than 65m Sec only are considered then the mean interval becomes 89.7mSec and the CV = 0.284. (N.B. In all cases these calculations ignore the long intervals, greater than 320mSec, between consecutive active breath phases which

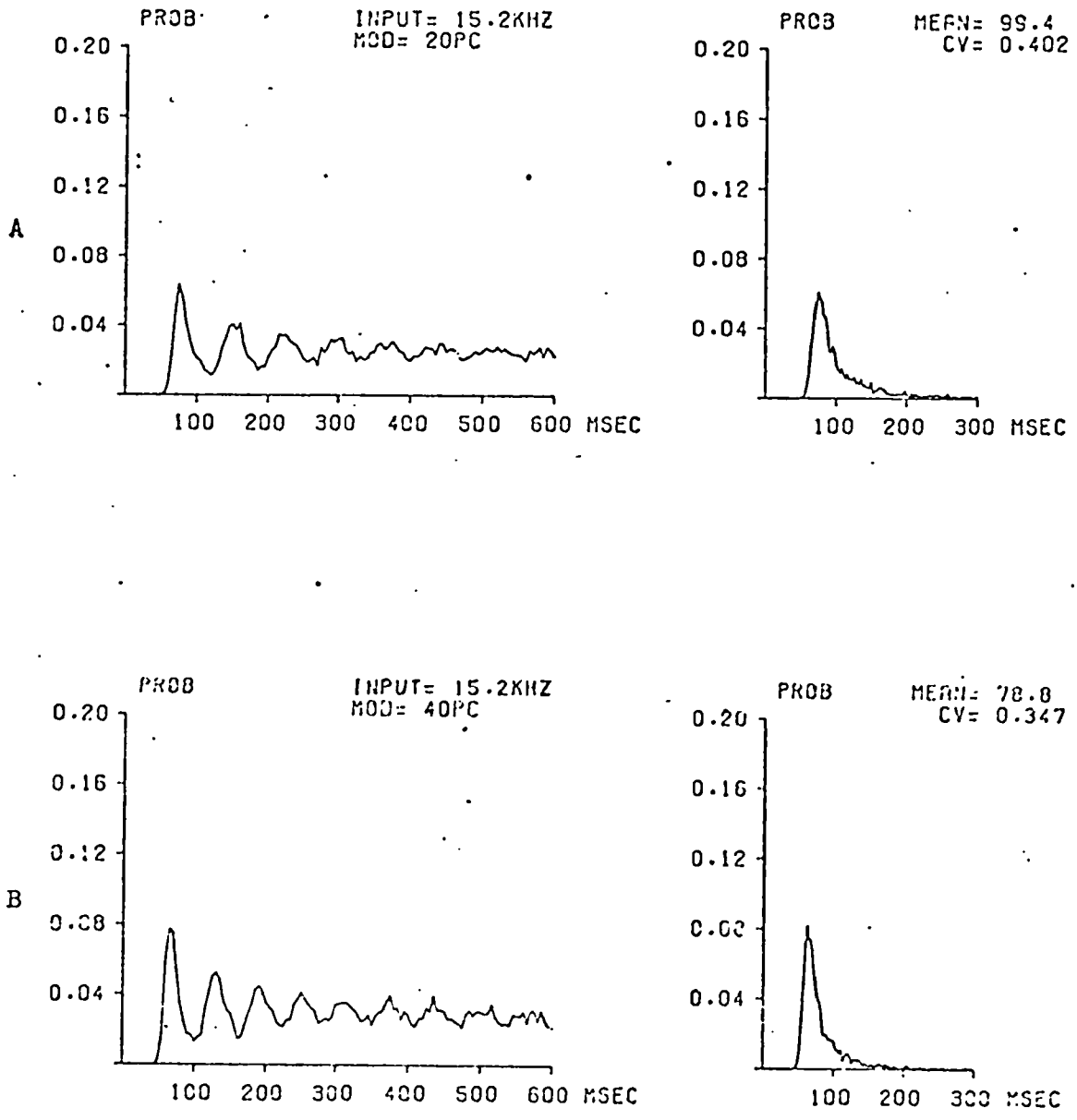

FIGURES 3.5.2:

The simulation results of the discharge event autocorrelation functions (left) and the interval PDFs (right) with non-stationarity included in the model to allow a better comparison with the neurophysiological results presented in Figure 3.5.1.

would otherwise dominate the CV and increase the mean interval). It is therefore only possible to suggest from this comparison that in general the behaviour of the model with 20 percent or less modulation is not unlike that observed from the physiological results.

The second test involves a comparison of the first order serial correlation coefficients, which calls for special treatment because of the non-stationarity involved. These values account for the linear inter-relation between intervals, so that while strong unimodality of the interval-histogram fixes the oscillatory nature of the event autocorrelation function, the first order serial correlation coefficients are important in determining the pattern of scatter of the intervals about the mean (Sayers, 1970).

Frize (1970) in her investigation of significance of neural spike patterns in the respiratory control system, has employed an ensemble approach for calculating the first order serial correlation coefficients of the breath modulated spike trains. This is achieved by effectively laying out the record of intervals for each individual breath one under the other to form an ensemble and determining a non-stationary ensemble correlation coefficient over all breaths, for each interval into the breath, and at a fixed delay between interval pairs. The following expression was used to evaluate the joint interval correlation coefficients

$$\rho(T_i, T_{i+j}) = R_i(j) = \frac{\sum_k ({}_kT_i - \bar{T}_i).({}_kT_{i+j} - \bar{T}_{i+j})}{\left\{\sum_k ({}_kT_i - \bar{T}_i)^2.({}_kT_{i+j} - \bar{T}_{i+j})^2\right\}^{\frac{1}{2}}}$$

where ${}_kT_i$ is the i^{th} interval, into the k^{th} breath; j is the delay and $\bar{T}$ the ensemble mean. Figure 3.5.3A displays the non-stationary serial correlation coefficients, as a function of interval number into the breath (sinusoidally modulated), for the delay-one and delay-two cases, at 20 percent and 40 percent modulation of the model's pre-synaptic rates. It is evident that the serial correlation coefficients are no longer near zero as was the case for the stationary model. The 20 percent modulation produces larger positive serial correlation values than the 40 percent modulation level an observation that was not altogether expected. Further investigation, however, clarifies the reason for this and an explanation follows.

The choice of reference instant at which respiratory modulation begins: at the start of the breath: may occur early or late in the current discharge interval. In one case the n^{th} following interval, T_n say (and also the $n+1^{th}$ interval T_{n+1}), would tend to occur later in real time within the modulating cycle and in the other case, earlier. The effective modulation level for T_n, and T_{n+1} would be greater in the former case than in the latter. Correspondingly, both T_n and T_{n+1} would tend to be less than their ensemble mean values in the former case, and both greater than their ensemble mean values in the latter case. Therefore large positive values of delay-one serial correlation coefficients would be expected for this reason, in respect of the n^{th} and $n+1^{th}$ intervals.

However, for increaed modulation depth, non-linear effects must be expected and will come from several causes. The matter can be explored by a study of the relevant interval scatter diagrams (Gerstein and Perkel, 1972). Some examples

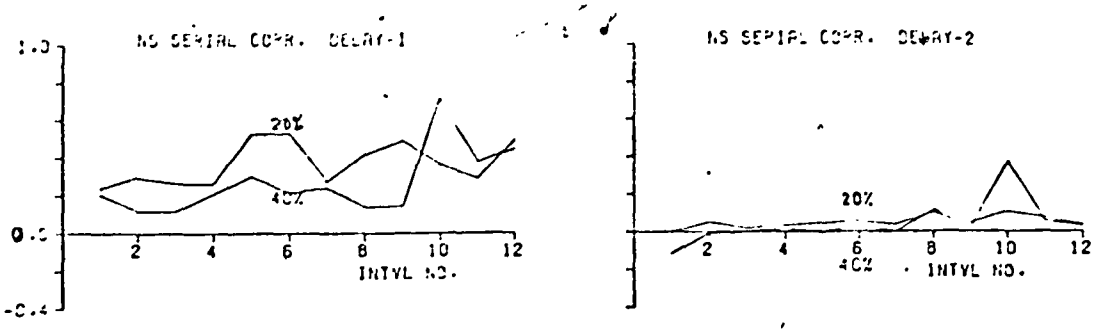

A

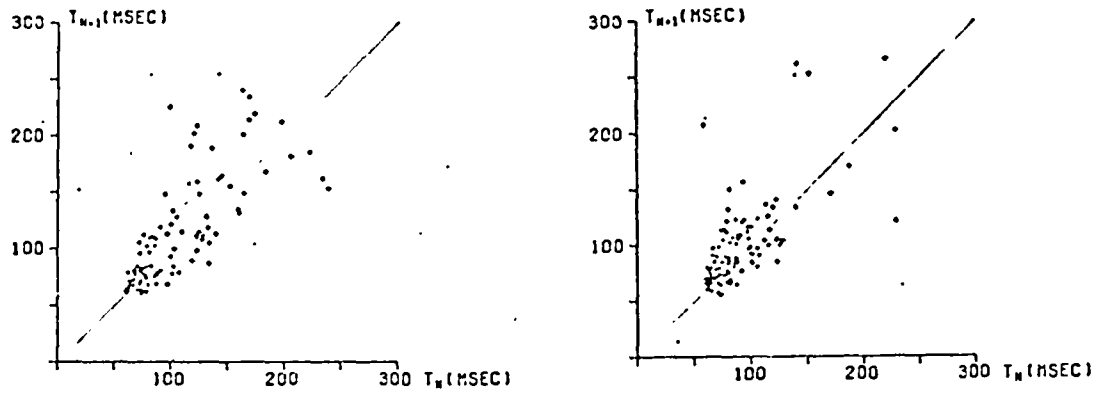

B

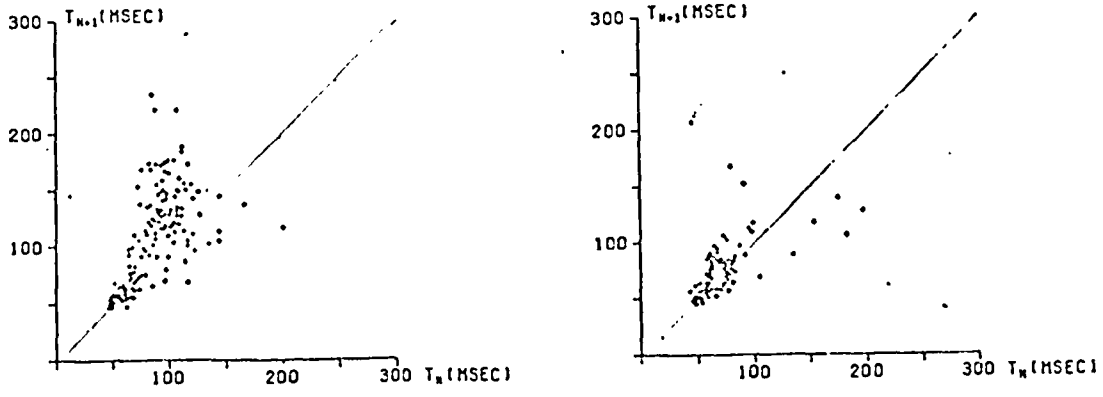

C

FIGURES 3.5.3:

A Non-stationary (NS) serial correlation analysis for the simulation and Delay-1 scatter diagrams for current-first and eighth-ninth intervals into the breath with 20 (A) and 40 (B) percent breathing modulation.

of these are presented in Figures 3.5.3B for a single delay, with current interval at the start of a breath against the first on the left and the 8th interval against the 9th on the right, for 20 percent modulation and in Figure 3.5.3C for the same interval pairs but a 40 percent modulation. These scatter diagram results indicate that there are two separate components contributing towards the distribution of interval pairs. Primarily, there is a fairly strong cluster near the line of unity relation which is very obvious for the 8th and 9th intervals (40 percent case) into the breath, while the second component is seen to be more widely scattered about an approximately vertical line indicating that some medium length intervals tend to be followed by (largely uncorrelated) longer intervals. Had there not been this second component the 40 percent modulation ensemble serial correlation coefficients would be very much larger, and in general greater, than the 20 percent case, as demonstrated by their tighter-clustering about the line of unity relation. The vertically oriented, uncorrelated, scatter is barely present at 20 percent modulation but quite noticeable in the 40 percent case and it is argued that this destroys the effect of any strong correlation between consecutive intervals. It is most likely accounted for by the fact that for the 40 percent modulation and in the less-active phase of the breath, the pre-synaptic drive rate becomes very much sub-threshold (below 12KHz) for more than 1.3 seconds. Once the pre-synaptic rate increases above 12KHz again, under the modulation, the motoneurone will almost certainly discharge in a very short time after because it will have

completely recovered from the effects of refractoriness. This suggests that the first axon spike after the dead-time period will be fairly rigidly constrained in the breath cycle-time. In the 20 percent modulation case the depth of modulation (about the mean rate of 15.2KHz) is not sufficient to drive the motoneurone into a strong sub-threshold state and therefore it is less likely that such a time of breath-locked interval will occur. It is probable then that the 40 percent modulated result demonstrates a non-linear peculiarity of the discharge mechanism occurring at the start of a new breath as only one or two intervals can occur following this time-locked marker before the selected reference time is encountered (zero modulation at the start of a breath).

A comparison of the non-stationary serial correlation coefficient (Figure 3.5.3A) with those typical of intercostal motoneurones, reproduced in Figure 3.5.4 from a study performed by Frize (1970) indicate some resemblance although the correlations are not as strong. The three neurophysiolocial studies presented all produce correlations that rise to a maximum about the 5th to 7th interval into the breath which is some what earlier than found for the model results. This may be due to the fact that a sinusoidal modulation is not wholly representative of the actual pre-synaptic drive and certainly neglects the effect of any slow metabolic influencing trends which could account for the resulting high values of correlation coefficients observed. (Only the results of Frize's experiments OCT-2, OCT-3 and OCT-4 were selected for comparison

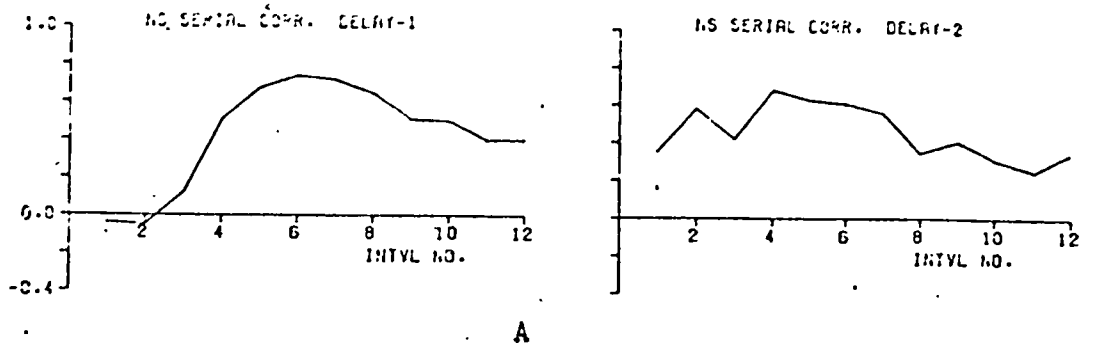

A

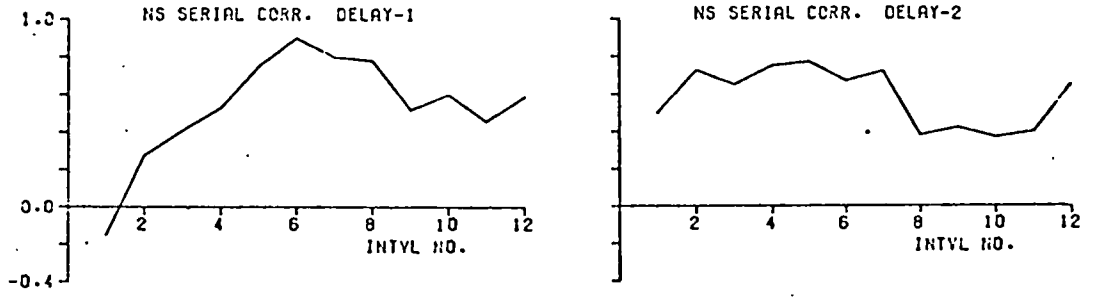

B

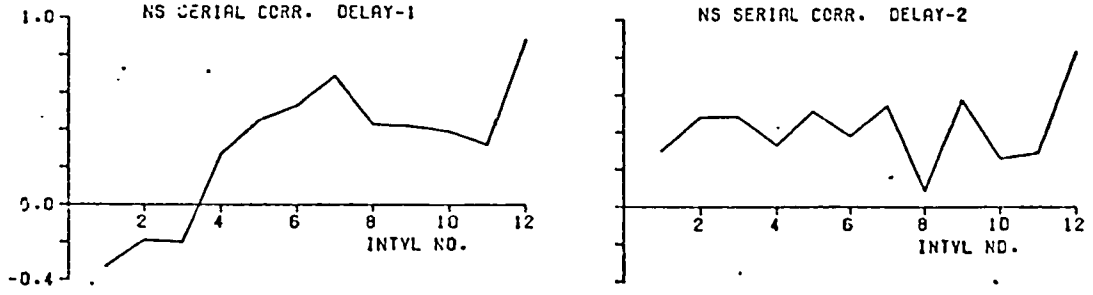

C

FIGURES 3.5.4:

Some neurophysiologically determined non-stationary serial correlation coefficients as measured by Frize (1970) from her experiments (A) OCT-2 (B) OCT-3 and (C) OCT-4.

as the double firing phenomenon observed, as indicated by the bimodal interval-histogram, are atypical of these alpha-motoneurones).

Considering now the results from the MP trajectory analysis; the average MP profiles determined from two intracellular recordings from two separate motoneurones identified as 69/13 (inspiratory) and 52/19A (expiratory), are presented in Figure 3.5.5A and B respectively. Once again the problem of dealing with the non-stationarity of the underlying breathing rhythm is met. It would have been convenient if an ensemble approach, similar to the treatment for the serial correlations could have been implemented by splitting the breath into four or five active phases, averaging separately the trajectories, but this was not practicable due to the rather short intracellular recordings available (only 7 to 15 breaths). Such a procedure would have removed most of the non-stationarity and allowed a direct comparison with the stationary model. The other alternative then, was to introduce non-stationarity into the model and compare the non-stationary MP profiles which unfortunately means that much of the MP trajectory detail would be lost. However, this was carried out and the resulting MP profile for the non-stationary model is shown in Figure 3.5.5C in which the pre-synaptic rate modulation was approximately 20 percent about a mean input rate of 15.2 kHz as used earlier. Even with this inclusion in the model to account for the effect of the breathing pattern, it is evident that some discrepancies still remain.

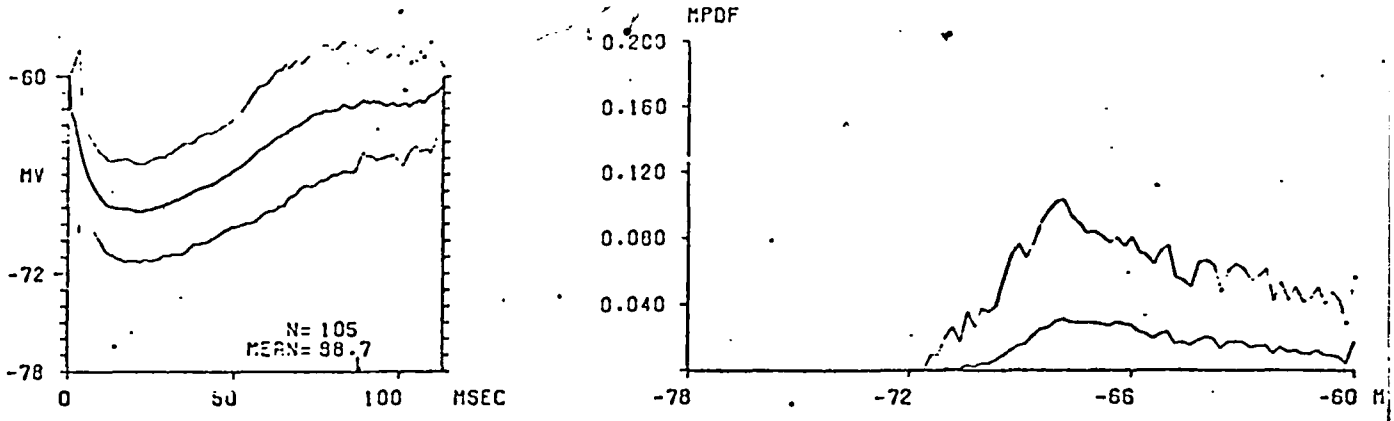

A

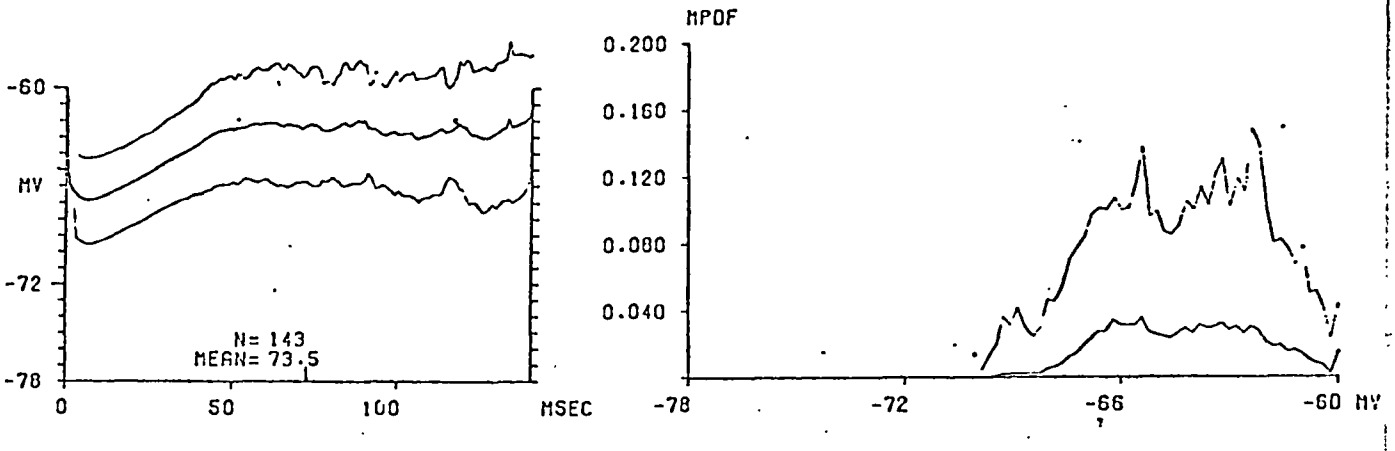

B

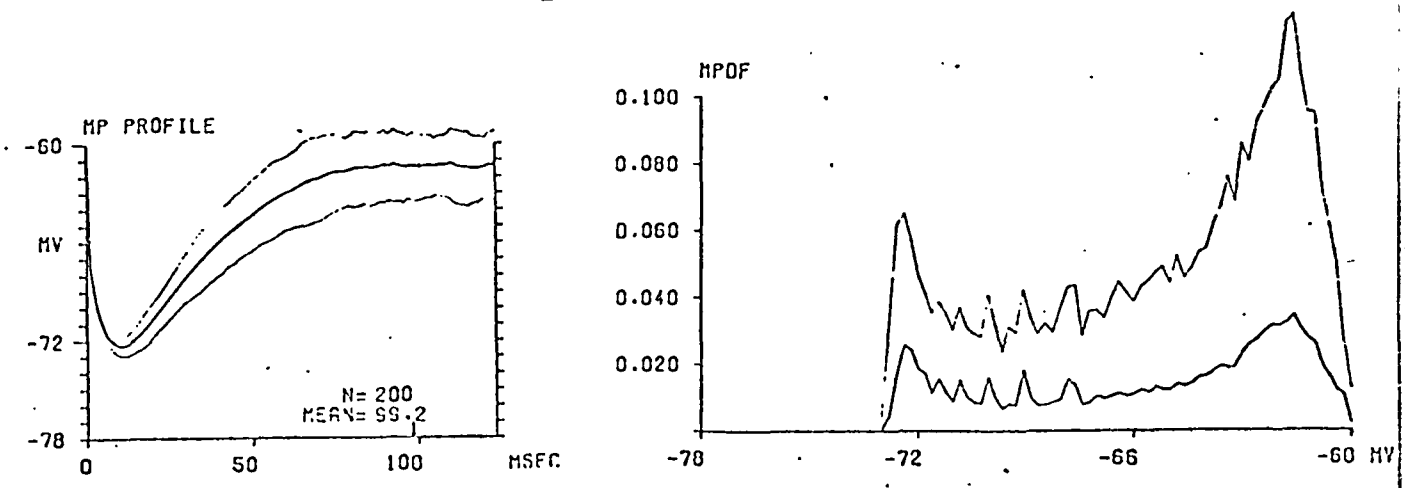

C

FIGURES 3.5.5:

A An example of an averaged MP Profile and MPDF from an intracellular recording of a cat inspiratory alpha-motoneurone (69/13).

B The same as in A but from an expiratory motoneurone (52/19A).

C A simulated result with non-stationarity for comparison (see text).

It can be seen that the depth of repolarisation is greatly reduced during after-hyperpolarisation, in the cat intercostal alpha-motoneurones investigated. This is probably explained by the known effects of non-linear EPSP summation, due to the MP depolarising towards the reversal potential (about 0mV), causing a reduction in the EPSP amplitudes coming forward, and more importantly, the reduced effectiveness of EPSPs which is due to their being released within close proximity of one another causing interactions by the shunting of their conductances (Barrett, 1975). Neither of these two mechanisms are incorporated in the model and the absence of the latter may prove to be an important limitation. However, this was intentional for the present study because its implementation would have resulted in a far more complicated and slower model. This second mechanism may also account for the much greater variability observed in the early part of the MP trajectory, which is lacking in the simulated trajectories. Because of the reduced EPSP effectiveness, a much higher pre-synaptic input rate is required to overcome the after-hyperpolarisation and a higher variability might be expected. A further limitation of the model, which could contribute to this greater variability, is that of standard EPSP shape; a fixed asymptotic amplitude is not truly representative of the physiological situation.

Consider next the MPDFs (to the right-hand side of the MP profiles in Figures 3.5.5. The MPDF of the model shows little resemblance to those determined from the

intracellular recordings. It is evident from these latter MP probability density functions that a single very flat mode exists which is not so for the simulation result. This suggests that the physiological trajectories rise in a fairly strict ramp-like manner (Levitan et al, 1968) to cross the discharge threshold: a phenomenon which has been observed very often in the intracellular recordings made from intercostal motoneurones. Schwindt and Calvin (1972) also demonstrate this in cat spinal motoneurones and observe that, in the lower part of the primary discharge rate range, the slope of the ramp trajectory is approximately linearly related to the stimulating current. They state that their injected current mimics a strong continuous pre-synaptic drive (which can only reinforce what has been said before: that is, the reduced EPSP effectiveness due to interaction of neighbouring synapses must play a major role in determining the MP trajectory; otherwise, as demonstrated by the mammalian motoneurone model, the graded EPSP effect during relative refractoriness is not sufficient to linearize the MP trajectory). This lack of linearity appears as a second mode in the MPDFs of the simulations. It occurs because the MP is lying just below the threshold level, under the influence of sub-threshold drive, for some time before random variations produce a crossing. If the pre-synaptic rate is increased this second mode is observed to diminish as shown by the stationary simulation results in Figure 3.4.4 but even at the supra-threshold drive rate of 18KHz it is still significant. This has the consequence that the model,

in its present form, will always tend to underestimate the pre-synaptic rate at least at the peak of a breath cycle and indicates that such effects should not be ignored in future models.

Finally now, the average MP end-trajectory results from the animal experiments will be compared with those found for the simulation runs. Figure 3.5.6 displays two such results (motoneurones 69/13 and 52/19A respectively) which show a strong resemblance to the stationary model results given in Figure 3.4.5. In both these results there is definite evidence of a final constraint of the MP trajectory, as indicated by the upward acceleration of the averaged trajectory, and the inward taper of the one percent confidence estimate lines. Once again, the effects of non-stationarity are apparent, as shown by the wider spread in the confidence estimates about the averaged trajectory determined from the intracellular recordings. This arises due to the differing slopes at which the ramp-like trajectories approach the point of threshold crossing.

This concludes the preliminary investigation in which the comparison between a simulated mammalian motoneurone and one of its physiological counterparts namely the intercostal alpha-motoneurone, which has allowed an intensive evaluation of the model. Despite the few limitations discussed the results have demonstrated generally that the model is very capable of simulating these types of motoneurones. It adequately displays the major characteristics and properties of such intercostal alpha-motoneurones with which it has been compared and has allowed some further

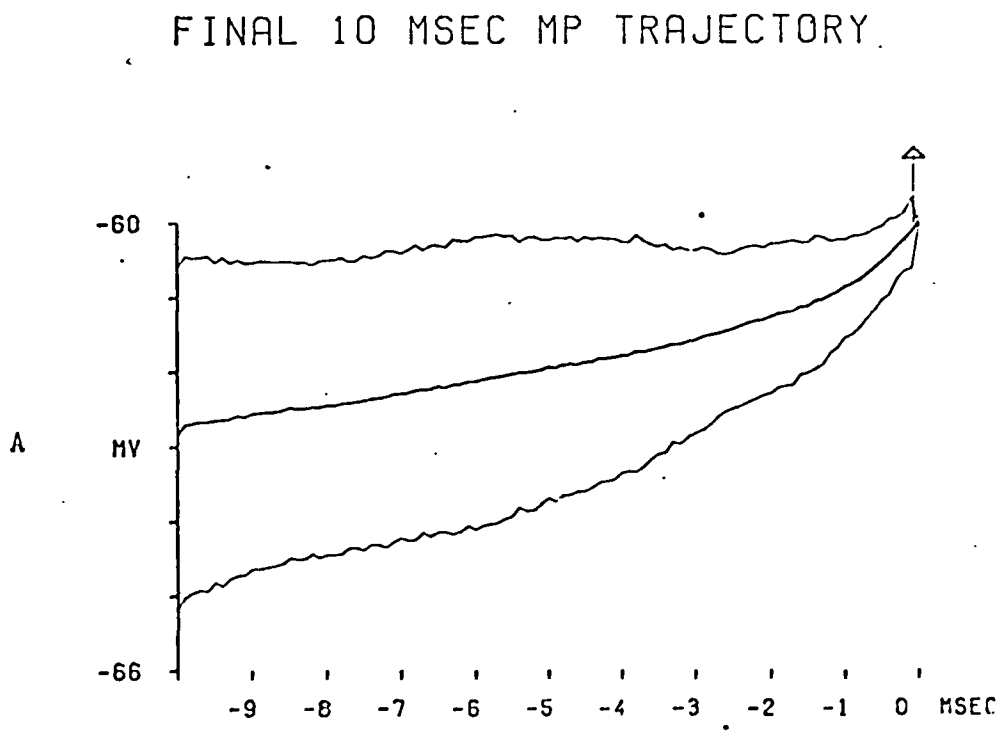

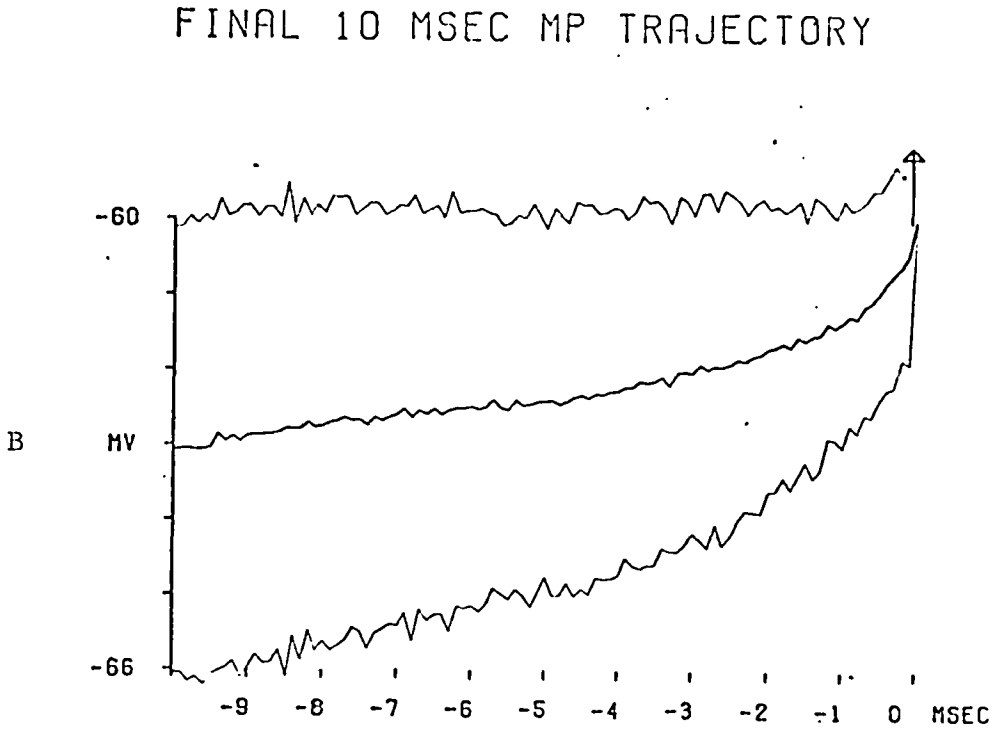

FIGURES 3.5.6:

The average MP End-trajectory from the same recordings used in Figure 3.5.5 A (motoneurone 69/13) and B (52/19A)-see discussion.

insight into the nature of the pre-synaptic drive mechanisms; therefore it should form a sound basis for further investigations.

3.6 THE PROPOSAL OF FURTHER INVESTIGATION USING THE MODEL:

This chapter has described the development and evaluation of a digitally computed mammalian motoneurone model which, not withstanding its explicit deficiencies, has most of the attributes for allowing a reasonably valid simulation of the intercostal alpha-motoneurone. Although the model lacks in accommodative and adaptive mechanisms, local responses effects (having a fixed threshold), an inhibition process (being essentially a stationary model representative of the active discharging phase only), and reduced EPSP effectiveness (due to interaction between neighbouring synapses and non-linear summation), it does include a comprehensive simulation of the excitatory and refractory processes observed to occur. It also allows a study of the pre-synaptic input to post-synaptic axon discharge impulse train inter-relation which has never before been possible for the intercostal alpha-motoneurones, and never been reported for the mammalian motoneurone in general. This relationship can be determined from the event Input-Output probability density function which gives the average measure, in probability terms, of the influence a pre-synaptic event (together with preceding events) can exert towards the generation of an axon discharge event. Some examples of these functions were given in Figure 3.4.7 for the stationary motoneurone model experiencing three

levels of pre-synaptic excitation. (15.2KHz, 14KHz and 18KHz respectively). The importance of this function in determining the pre-synaptic structure between pairs of neurone groups having common connectivity will be demonstrated early in the next chapter.

It was therefore proposed that the model should be extended to a simple neuronal network with a pair of motoneurones experiencing a known amount of shared pre-synaptic drive and as well as each experiencing an equal amount of independent pre-synaptic activity. In this manner, the stationary simulation of common connectivity between a pair of typical neighbouring intercostal alpha-motoneurones could be used to investigate and interprete the Pre- and Post- Stimulus Time (PPST) Histograms determinded for the physiological experiments being performed at The National Hospital, Queen Square, by Professor T.A. Sears, Dr. P.A. Kirkwood and others. The proportion of common-to-independent drive could be used to simulate, at different levels of input drive, the amount of pre-synaptic common connectivity while the resultant PPST histograms formed from the discharge event sequences of the neurones give the shape and strength of the output cross-correlations. Although only two gross population synapses are simulated, it should be remembered that these are each representative of a large number (because of their high rate of Poisson event generation) of synaptically terminating pathways, and therefore could be used to estimate the actual number of active synapses with common connectivity. The results of this

proposed simulated network study and other associated investigations are presented in the following chapter following a short introduction to the computer programme modifications to allow an extension to such a pair of motoneurones, and an outline of the exploratory techniques employed.

4.0 INVESTIGATION OF NEURONAL CONNECTIVITY WITH THE EXTENDED MODEL.

4.1 THE NEURONE PAIR SIMULATIONS.

4.2 NEURONAL NETWORK PROCESSING AND ANALYSING TECHNIQUES.

The Method of Studying Discharge Sequences by Event Correlation.

An Investigatory Technique Utilising the ACE Potential.

4.3 THE PPST HISTOGRAM RESULTS FROM THE STATIONARY NEURONE PAIR SIMULATIONS.

4.4 INVESTIGATION OF THE EXPERIMENTAL PPST HISTOGRAM RESULTS BY THE NEURONE PAIR MODEL.

4.5 INVESTIGATION OF COMMON CONNECTIVITY BY THE ACE POTENTIAL.

4.6 CONCLUSION.

4.0 INVESTIGATION OF NEURONAL CONNECTIVITY WITH THE EXTENDED MODEL:

In the previous chapter a suitable model of the intercostal alpha-motoneurone was established and justified. Its validity and limitations were critically evaluated and, within the bounds of these findings, a proposal was made to extend the model to study the effects of common pre-synaptic connectivity between a pair of these motoneurones. This study should provide a means for testing a number of hypotheses which have been proposed regarding the pre-synaptic inputs to intercostal motoneurones and may allow a quantitative estimate of the proportion of common connectivity. This chapter first outlines the necessary modifications to the simulation programme, and then describes the relevant processing and analysing techniques applied to the simulated and physiological data under investigation, before presenting the results of these analyses and discussing their interpretation.

4.1. THE NEURONE PAIR SIMULATION PROGRAMME:

Having developed and evaluated an efficient, versatile and valid modelling programme, the extension from a simulated single motoneurone to a pair of neurones experiencing some shared pre-synaptic drive (with the remainder of the input being independent) is relatively simple. Basically, it only involves a duplication of the parameters and process variables already incorporated (and allowing for the common drive). This is achieved by increasing the dimensional size of the variables and of some parameters (e.g. TIME (2) becomes TIME (4); ART, ART(2); ADK, ADK(2); REF, REF(2); etc) and

making some small changes and additions to the programme sequence. To implement the requirement of common connectivity, it is merely necessary to set TIME(1) and TIME(3) both equal to the time of each newly generated common pre-synaptic arrival immediately after both previous 'events of interest' have been accounted for. The programme organisation now is such that for this and all other duplicated variables, and the few parameters, the designated 'Neurone One' takes up the first location(s) in these variables and parameter arrays and 'Neurone Two' take the remaining location(s). In this manner the model could be extended further, say to two groups of motoneurones with several neurones in each, all with some shared pre-synaptic drive, but for the present study only a pair of motoneurones will be considered (i.e. TIME(1) and TIME(2) give the arrival times of the two pre-synaptic inputs to 'Neurone One' and TIME(3) and TIME(4) for 'Neurone Two'; TIME(1) and TIME(3) are equal and represent the arrival times of simultaneous events simulating the pre-synaptic pathways common to these neurones, while TIME(2) and TIME(4) are completely independent). By this arrangement the proportion of common connectivity may be adjusted by changing the ratio of the common-to-independent arrival rates. As will have been observed, three Poisson-generated interval sequences are thus required and so three expected-arrival interval parameters TINT(i) (i = 1, 2 or 3) are incorporated. Therefore, for a given common drive rate, the overall input rate to each neurone could be set separately, although in this present study both independent rates are kept equal (TINT(2) = TINT(3)). TINT(1) gives the common

drive mean interval. It should be noted that if TINT(2) is not equal to TINT(3), then apart from the fact that the neurones experience different levels of pre-synaptic drive, there is no longer a similar proportion of common connectivity to the neurones, which would greatly complicate the interpretation of such a study and make it difficult to relate back to the neurophysiological situation. For these reasons the present investigation always employed an equal overall level of pre-synaptic drive to the pair of motoneurones.

The main required change to the programme was simply to allow an identification as to which neurone was associated with the current 'event of interest' so that the appropriate course of action could be taken. For example, a pre-synaptic arrival requires an EPSP to be summed to the appropriate MP and if the event is a discharge, it must be recorded with the correct identification while the appropriate neurone variables must be re-initialised so that an after-hyperpolarisation phase occurs. One further programme modification was to include a new variable TLAST(i), one for each neurone, which allows a significant reduction in the simulation time by keeping account of the total period of time that has passed since the last 'event of interest' for that particular neurone. This allows the updating processing in the programme to be approximately halved because now only the MP variables of the neurone experiencing the current event, together with all the time variables, need be updated. TLAST(N) is reset to zero whenever 'Neurone N' has just been processed for an

'event of interest' and is then incremented again by each interval for 'events of interest' which occur in the other neurone.

This concludes the outline of programme changes that allow the simulation of a motoneuronal pair network; effectively, these changes have not altered the flow diagram in Figure 3.1.2. Now follows a brief description of the processing and analysing techniques used later in this chapter, that allow an evaluation of the intercostal alpha-motoneuronal pre-synaptic connectivity by use of the present computer network model.

4.2 NEURONAL NETWORK PROCESSING AND ANALYSING TECHNIQUES:

The main purpose of this part of the investigation is to use the extended model to attempt an interpretation of what is observed in the event cross-correlation functions derived from neuronographically recorded multiunit axon discharge sequences. These cross-correlation functions demonstrate signs of common pre-synaptic pathway connectivity between the two groups of intercostal alpha-motoneurones contributing to the multiunit recordings . Typically each group sequence comprises the superposition of spike event trains from four to six neurones, this superposition has been necessary to obtain significant results from the time limited recordings; Sears and Stagg (1976). By simulating the hypothesised situations, thought to explain the changes in form and strength of the measured functions during various stages of experimental studies performed in the cat, it is expected that the degree of common connectivity could be quantified.

A second qualitative (possibly also quantitative) technique is also investigated by use of the model in which the Average Common Excitation (ACE) Potential is found; this method has been intensively investigated recently. It involves the synchronised averaging of the MP fluctuations in one motoneurone using the axon discharge sequence of events from a second active unit, usually within the same motoneuronal group, to trigger the MP averager (Kirkwood and Sears, 1976). The resulting averaged potential form, and its time occurrence, can be shown to give evidence of shared common input through branching in the pre-synaptic fibres if certain assumptions can be accepted.

This ACE potential technique is more fully described later in this section and a discussion of its application to both the physiology and the model, with some results, is presented in section 5 of this chapter.

(i) The method of studying discharge sequences by event correlation: The cross-correlation function $n_{xy}(\tau)$ between two point-event signals X and Y can be estimated by forming the PPST histogram and treating the X series of events as stimuli and the Y sequence as the response, as was previously described for the Input-Output PPST. Such a measure of the correlation between the discharge sequences from two neurones, or from two groups of neurones with superimposed spike sequences with some pre-synaptic connectivity, has been shown to produce significant central and symmetrical peaks for intercostal alpha-motoneurones (Sears and Stagg, 1976). It was therefore proposed that an investigation by simulation of two single

units with known amounts of shared pre-synaptic connectivity, using a stationary excitatory model of the neuronal units, should allow a more complete interpretation of the results observed experimentally. However, in trying to obtain significant results from the paired neurone model, the simulations were found to require a running time which was much longer than the maximum time allowed on the College CDC omputers. Now, it is known for the PPST histograms that the average number of event counts in each delay bin (width Δt) for two independent and random processes X and Y, with average event rates n_x and n_y respectively (recorded over a total duration, T) is $n_x n_y \Delta t\, T$ (Stagg, 1970). The method described here relies on independence between the three pre-synaptic sources (see Figure 4.2.1A: e_x and e_y being completely independent random excitatory inputs to the neurones X and Y, while the third e_c is also an independent random excitatory source but common to X and Y), and in addition a knowledge of the Input-Output properties of each neurone to the common source events.

When cross-correlating the two neurone output event sequences (assuming no interaction between the neurones) from this model, there are four input combinations which independently contribute towards the total random PPST histogram bin count. This bin count is the sum of the independent cross-correlated output components generated from these paired contributions of the inputs: e_x and $e_c(Y)$, e_x and e_y, $e_c(X)$ and e_y; while the fourth combination is due to the failure of $e_c(X)$ and $e_c(Y)$ to produce near

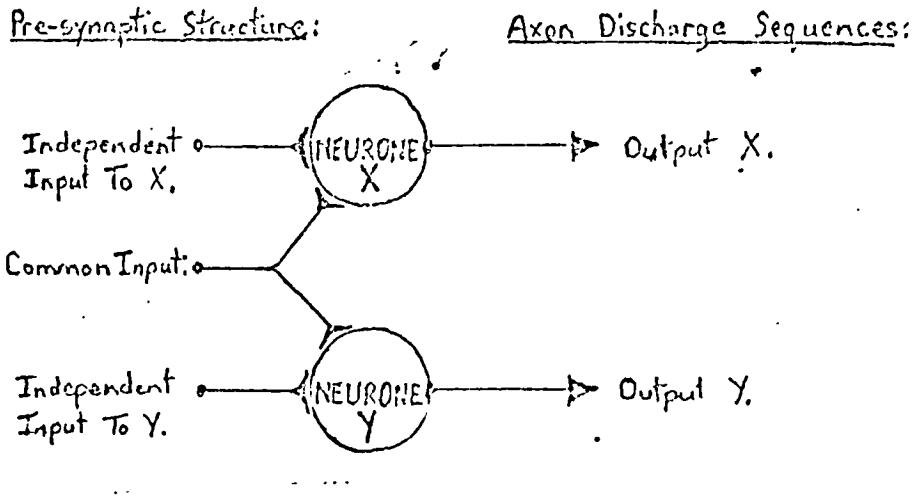

A) The neuronal pair model demonstrating common and independent connectivity.

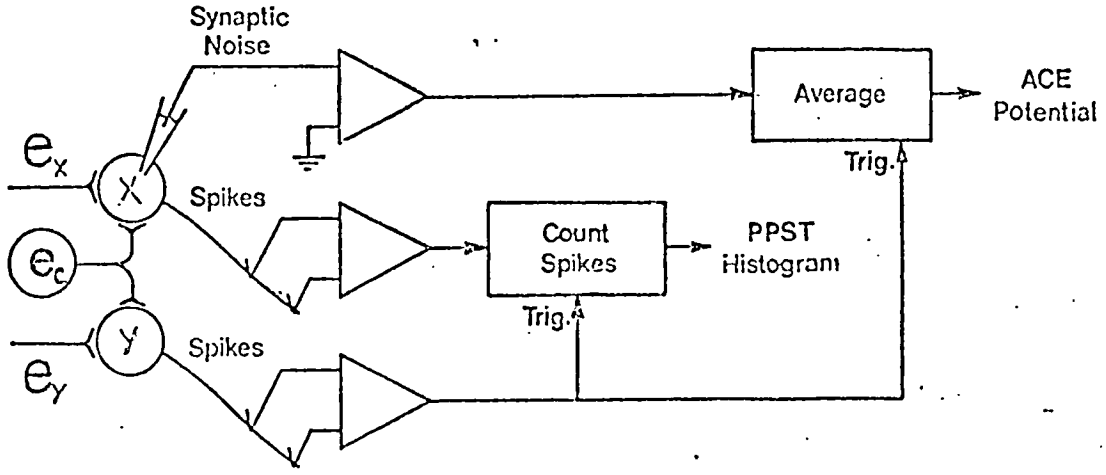

B) Schematic of the animal experiment set up for measuring the PPST Histograms and the ACE Potentials.

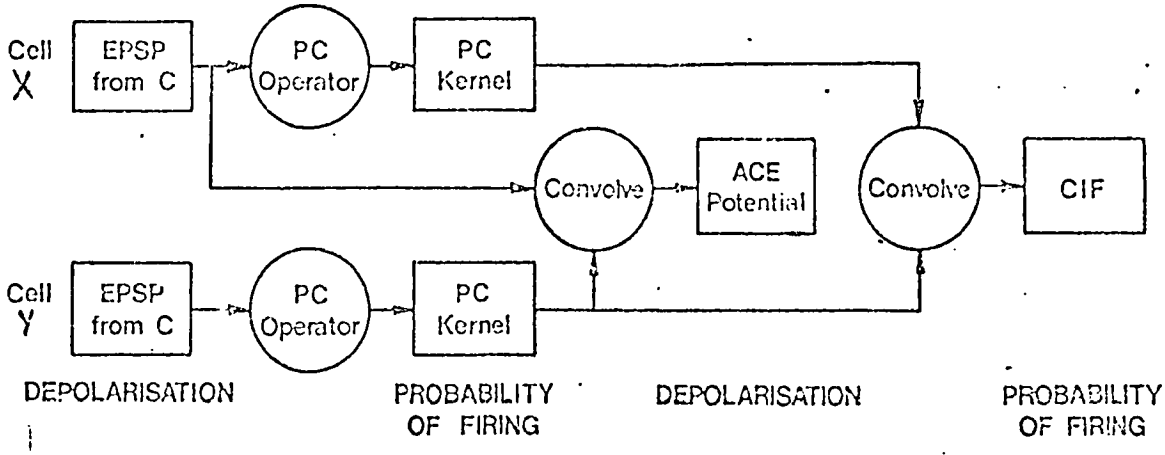

C) The mathematical model used to determine the measures in B above.

FIGURES 4.2.1:

simultaneous (correlated) outputs. This last contribution is shown below to be one of the two separate effects appearing in the correlation function of the outputs due to the common connectivity; the common input e_c also produces correlated outputs. The total random PPST histogram count can be calculated directly from the output rates; to this can be added the explicit correlation contribution to producing the total PPST. This matter is now investigated.

Consider the output joint probability of occurrence (or cross-correlation) function $r_{xy}(\tau)$ as;

$$r_{xy}(\tau)_T = \frac{1}{2T}\int_{-T}^{T} f_x(t)\ f_y(t+\tau).dt$$

Transforming into the frequency domain:

$$R_{xy}(w)_T = \int_{-\infty}^{+\infty} r_{xy}\ (\tau)_T e^{-jw\tau}.d\tau$$

or;

$$R_{xy}(w)_T = \frac{1}{2T}\cdot\int_{-T}^{+T} f_x(t).f_y(t+\tau).dt\int_{-\infty}^{+\infty} e^{-jw\tau}.d\tau$$

$$= \underset{T\to\infty}{\text{In limit}} \quad \frac{1}{2T}\int_{-\infty}^{+\infty} f_x(t)_T.e^{+jwt}.dt\int_{-\infty}^{+\infty} f_y(t+\tau)_T.e^{-jw(t+\tau)}.d(t+\tau)$$

$$= \frac{1}{2T}\ F_x^*(w)_T.F_y(w)_T \qquad F^* = \text{complex conjugate of F.}$$

Now if $f(t) = e_c(t)*g(t)$

where $e_c(t)$ = the input sequence of the common source events (i.e. coming from a Poisson Generator).

and $g(t)$ = the PDF of a common input event at t' generating

an output event at t'+t.

Hence:

$$R_{xy}(w)_T = \frac{1}{2T} .\left[E_c(w).\ G_x(w)\right]^* .\left[E_c(w).G_y(w)\right]$$

But $e_c(t)$ is defined as a sequence from a Poisson process, so $E_c^*(w).\ E_c(w) = 1$

Hence:

$$R_{xy}(w)_T = \frac{1}{2T} .\ G_x^*(w).\ G_y(w)$$

and by analogy:

$$r_{xy}(\tau)_T = \frac{1}{2T}\int_{-T}^{+T} g_x(t).\ g_y(t+\tau).\ dt$$

Two important points arise from the above derivation;

a) The PPST histogram component for the neurone pair outputs, due to the common input source, is simply the cross-correlation of the two Common Input-Output Probability Functions for the neurones for a Poisson - generated common source.

b) This component, as demonstrated by the spectral domain manipulations, may be separated into two independent sub-components; the DC mean (statistically flat correlation level) and an AC correlation component which is superimposed on the DC level. It can be seen that the mean level will represent the cross-correlation of the output excitation to each neurone, had there been no common connectivity. The AC function must therefore account for the shared input and the resulting synchronisation of trans-membrane processes in the neurones (such as refractoriness and EPSP similarities).

The PPST histograms of the stationary model pair data are presented with a time-delay axis ranging from -32 to +32 mSec (with 0.25 mSec bin widths), while those for the animal experimental measures cover a time range from -128 to +128 mSec (with 1mSec bin widths). For each histogram, the estimated probability level M and its $\pm$ 1% confidence estimate are calculated over the first and last quarter time spans (the confidence limits being derived assuming the counts in these portions of the histogram are generated by a completely random renewal process; Stagg, 1970). A strength factor R, of the correlated central peak (as defined by Sears and Stagg, 1976), given by the ratio: mean of the bin probabilities either side of zero time to the estimated mean probability M: is indicated. This correlation factor R is also assumed to have the estimated $\pm$ 1% confidence limit given by the derived variation of M. Finally, on the simulation results, the actual strength of common connectivity, is a percentage of the total input drive rate, is included.

Summarising then, an estimated PPST histogram for the output processes from the above neuronal pair model can be simply constructed from a knowledge of the mean neurone discharge rates, which determine the mean random contribution, superimposing the calculated cross-correlated contribution due to common connectivity from the two common Input-Output Probability Functions with their DC levels removed. This method is applied to most of the discharge sequences from the simulation runs to allow, by comparison with these estimated PPST histograms, a qualitative and quantitative interpretation of the experimental PPSTs and their source of origin. The

experimental PPST histograms are found by the conventional technique of accumulating time bin counts with the events in one discharge sequence designated 'stimuli' and the second, 'response' as described by Stagg (1973). During the term of research covered by this thesis, a neural spike computer acquisition interface was developed and constructed to enable faster processing of the experimental data recordings. This is described in Appendix one.

(ii) An investigatory technique utilising the ACE Potential: As outlined above, the ACE (Average Common Excitation) Potential demonstrates the average MP transient depolarisation in one motoneurone at the time of discharge from another motoneurone within the same unit group. The form of this potential is explicable if the hypothesis of the joint occurrence of unitary EPSPs evoked in the motoneurones, by branching of common stem pre-synaptic fibres alone, is accepted. This being so, then such a measure allows further insight into the mechanisms generating the short term synchronisation observed in the PPST histograms, studied by Sears and Stagg (1976), found from pairs of multiunit intercostal motoneurone discharge sequences. Kirkwood and Sears (1977) in their investigation of the ACE potential demonstrate, by theoretical analysis and experimental observations, the various measures which quantitatively predict an increase in the probability of firing due to EPSPs of various shapes and sizes. Figures 4.2.1B and C show two schematics (reproduced from their paper Figure 10) of the experimental ACE potential (and PPST histogram) measurement arrangement and the basis for their mathematical model. In Figure 4.2.1B the assumed common pre-synaptic input C to the

motoneurones X and Y will simultaneously depolarise the MP of these neurones, so that should B discharge and this event be used to trigger the recording of the MP of neurone X, then the depolarisation due to the common EPSP will be detected. Now by going a step further, and averaging many of these triggered MP fluctuations (both pre- and post- event), the Average Common Excitation Potential will be derived. If motoneurone X is also firing then the same common depolarisation mechanism is responsible for the correlated counts in the PPST histogram. These processes may be better understood by studying Figure 4.2.1C in which a Primary Correlated (PC) Operator is employed to produce a PC Kernel for each neurone. The PC Kernels used summarise the Input-Output event interaction for all common pre-synaptic events to the neurones, or in other words, give an estimate for the probability density function $P_{co}(\tau)$ that the neurone fires following a common pre-synaptic event. Therefore it can be seen that if the average Common EPSP form in neurone X is convolved with the (Common Input-Output PDF, $P_{co}(\tau)$) PC Kernel of Y, the resulting time-dependent voltage function is the ACE potential. Kirkwood and Sears have developed their theoretical predictions from this schematic outline by assuming that the probability PC Kernel can be defined in terms of summed proportions of the average Common EPSP form and its derivative which have both been shown to dictate the shape of this PC Kernel under different conditions (Moore et al, 1970 and Knox, 1974 respectively). It is anticipated that the study of the ACE Potential presented in this chapter and the investigation of the Input-Output PDF described in

chapter Five will allow a better evaluation of this last assumption made by Kirkwood and Sears.

The study of the ACE potential presented here was carried out to supplement the work already done and mainly focusses on its sensitivity to the strength of common connectivity and the pre-synaptic rate variations, in particular, the breathing non-stationarity that occurs with intercostal alpha-motoneurones. For this study only one motoneurone of the model pair, neurone Y, is firing because effectively the threshold level for neurone X is increased so that its MP can never attain the discharge threshold. This MP of the second neurone is continuously monitored and stored to allow a time window sample of the MP fluctuations (which spans from 10mSec pre-trigger to 15mSec post-trigger) to be taken whenever a discharge stimulus from neurone B occurs (the sampling resolution is kept to 0.1mSec). The model's ensemble ACE Potential is found by averaging more than 1000 of these windowed ensemble members, each comprising 251 samples of the MP fluctuation. A series of simulations covering the ranges of pre-synaptic rate of 14, 15.2 and 18KHz, and of strength of common connectivity from 50 down to 5 percent are presented, and the significance of the results discussed.

4.3 THE PPST HISTOGRAM RESULTS FROM THE STATIONARY NEURONE PAIR SIMULATIONS:

The estimated event cross-correlation functions were derived from the discharge sequences of the stationary neurone pair 'standard' simulations with prescribed percent-

ages of common pre-synaptic connectivity and total pre-synaptic rates. The standard parameters are as described in the previous chapter; a 0.1mV graded amplitude EPSP with TRT = 0.5 mSec and cell time constant TDK = 6 mSec, an after-hyperpolarisation recovery time constant TREF = 30 mSec, a resting-to-threshold level potential of 12mV, and a 6mV depth of after-hyperpolarisation.

In the last section 4.2(i), the event cross-correlation function was shown to be the superposition of two components, a DC mean probability and an AC function. The former component is the result of the cross-correlation between the output event sequences from the two neurones with the same total pre-synaptic rate of stimulation but no inputs in common. This mean probability M can therefore, be estimated and is determined by the product of the mean 'response neurone' discharge rate and the bin width selected as demonstrated below:

$$\text{Mean bin count} = n_x . n_y . d . T$$
$$= (N_x/T) . n_y . d . T$$
$$= N_x n_y d$$

where n_x = firing rate of neurone X

n_y = firing rate of neurone Y

d = bin width

T = time lengths of record

N_x = total events from X

$$\text{but calculated bin mean probability} = N_x . n_y . d/N_x$$

$$\text{so } M_{calc.} = n_y . d \text{ or } n_x . d$$
(for identical neurones)

Three sets of simulation runs were made and their resulting PPST histograms are presented in Figures 4.3-1, -2 and -3. Each set comes from the neuronal model pair excited by a constant total pre-synaptic rate; 18, 15.2 and 14KHz respectively. Within each set the percentages of common pre-synaptic connectivity is set to 50 in result A, 20 in B and 10 in C.

Regarding the form of the estimated cross-correlation function, other than this strength variation, a strong similarity exists in the shape of the peaks and the mean probability level M remains fairly constant for each total pre-synaptic drive rate considered. The central peak, in all cases, is sharp and well defined with symmetrical skirts dropping away to quite broad shoulders (symmetrical because of the convolution method of construction). These shoulders can be seen to vary somewhat with input rate being about $\pm$ 4mSec wide at 18KHz, $\pm$ 7mSec at 15.2KHz and $\pm$ 9mSec at 14KHz. Knowing the mean discharge rates for the three sets are 14.5, 10 and 7.3/Sec respectively, the formulation above for M_{calc} shows M_{est} is reliably predictable (Figure 4.3.4A).

Considering now the effect of selected amounts of common pre-synaptic connectivity. Figure 4.3.4B shows a summary of the variation in the strength of correlation (R-1) as a function of common connectivity and total pre-synaptic rate (strength of correlation is measured here as the ratio of peak probability above the mean level to the mean level, M). A very good proportionality is observed with the percentage shared input throughout the range of pre-synaptic drive studied. As the rate of excitation increases the magnitude of (R-1) is seen to

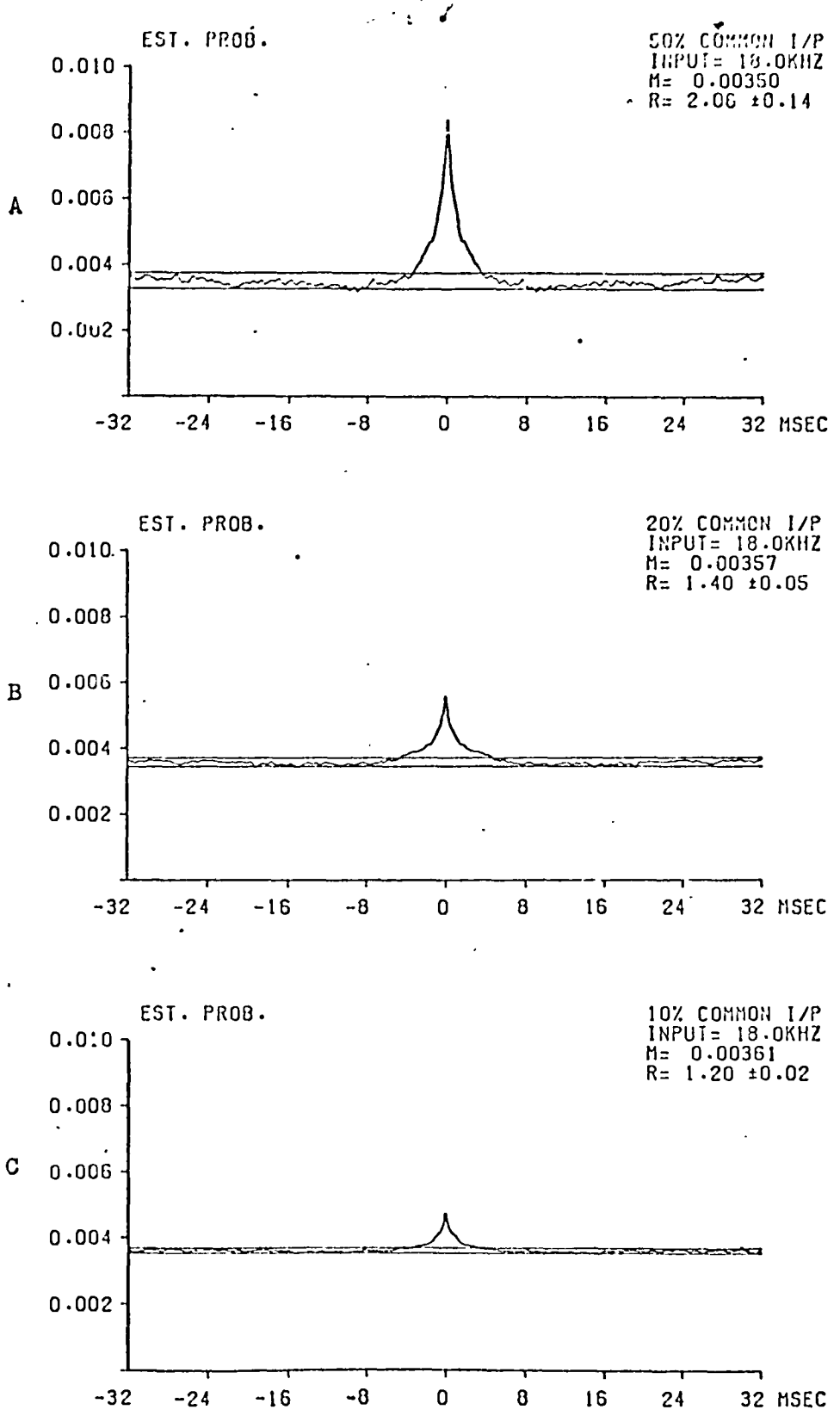

FIGURES 4.3.1:

The PPST Histogram results from standard (stationary) simulations with 0.1 mV EPSP amplitudes, 18kHz total presynaptic drive and 50(A), 20(B) and 10(C) percent common connectivity.

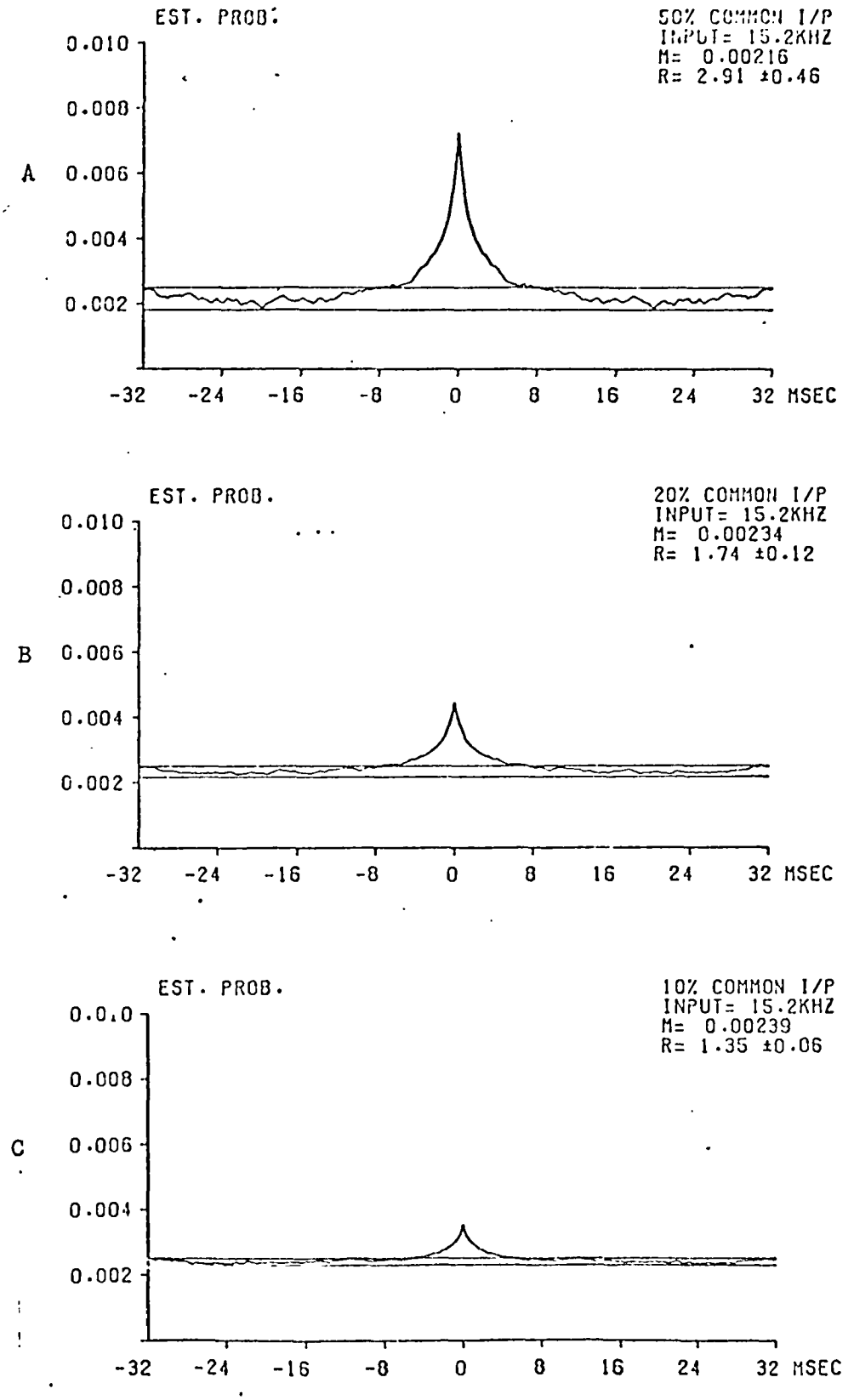

FIGURES 4.3.2:

The PPST Histogram results from standard (stationary) simulations as in Figures 4.3.1 but with 15.2kHz total pre-synaptic drive.

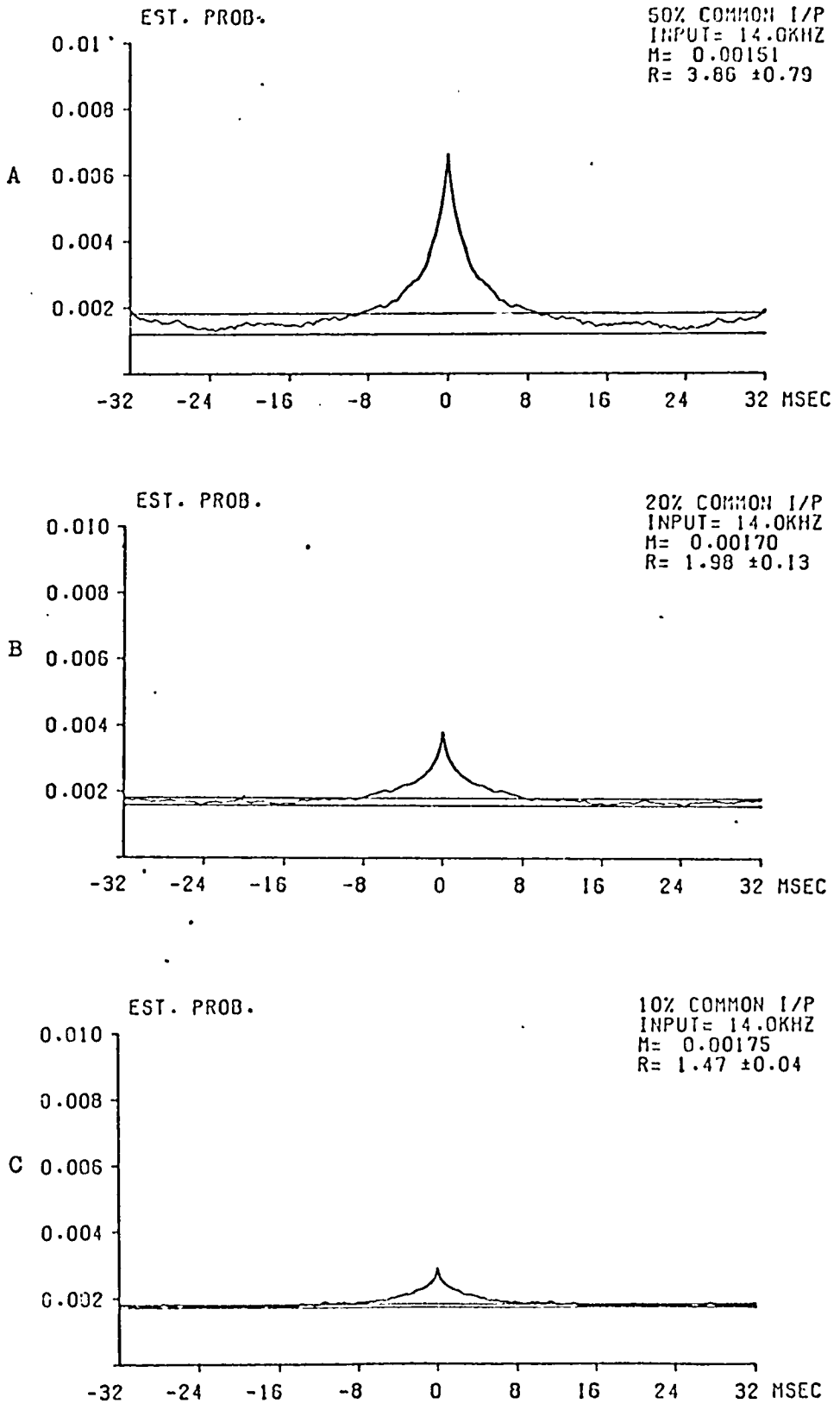

FIGURES 4.3.3:

The PPST Histogram results from standard (stationary) simulations as in Figures 4.3.1 but with 14kHz total pre-synaptic drive.

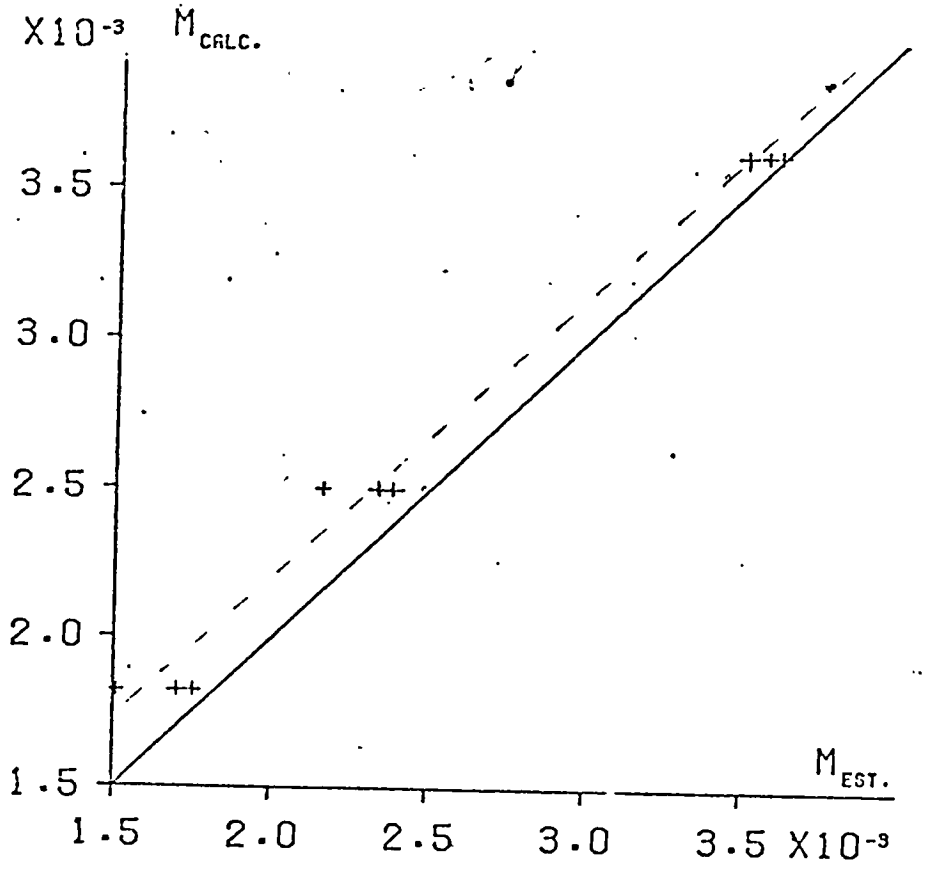

A) A good correspondence is demonstrated between the PPST histogram mean levels (M) measured (EST) and calculated (CALC). See text formula.

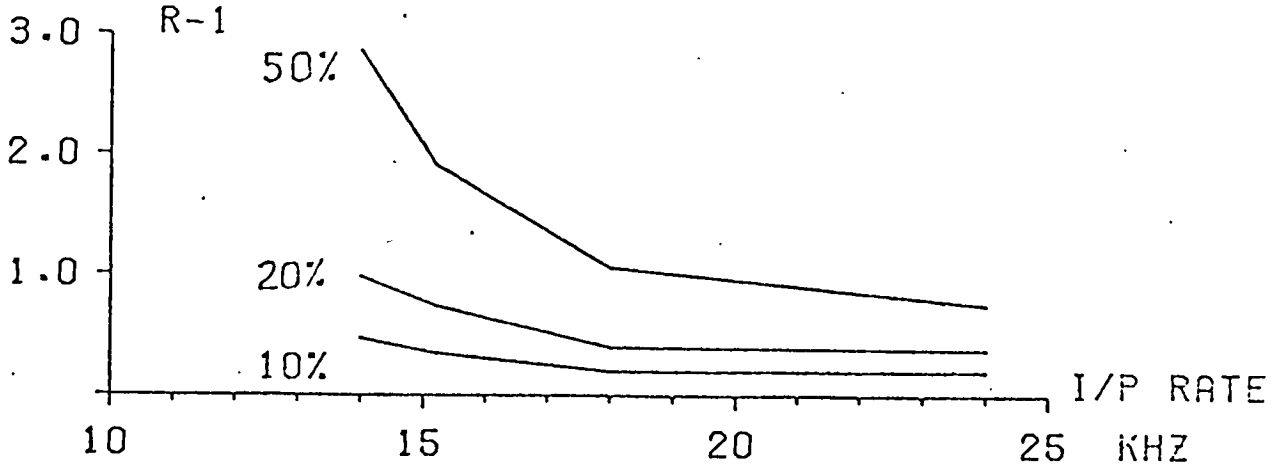

B) Summary of the PPST histogram strength of correlation measure (R-1) against total pre-synaptic rate for 50,20 and 10 percent actual common connectivity.

FIGURES 4.3.4:

decrease in an inversely proportional manner. This last relation will be confirmed later in this chapter.

Some further stationary simulation results can be now presented as an extension of the 15.2KHz pre-synaptic rate study, in which the model is kept 'standard' except for an inversely proportional adjustment of the total pre-synaptic rate and the EPSP asymptotic amplitude. In this manner the effective strength of synaptic drive to the neurones remains constant because a reduction in rate, say to half, is counteracted by a corresponding increase in the EPSP amplitude to double the original. The modelled neurone pair results shown in Figure 4.3.5 are for 0.2mV EPSPs with an average rate of release of 7.6KHz and common connectivity of 50(A), 20(B) and 10 (C) percent of the total input; while Figure 4.3.6 demonstrates the results for 50 percent common connectivity and 0.05mV (A), 0.5mV(B) and 1.0mV(C) amplitude EPSPs.

In Figure 4.3.5 the results for simulations with a 0.2mV standard shape EPSP and a total pre-synaptic rate of 7.6KHz appears, when compared to the standard 15.2KHz run results given in Figure 4.3.2, to have changed very little apart from the small but significant increase in the correlation strength ratio (R-1) of 25 percent for the 50 percent common connectivity case; there is only a slight increase in the shoulders of the peak form in general from $\pm$ 7 to $\pm$ 8mSec approximately. These observations are also true for the 50 percent shared pre-synaptic drive results for 0.5 and 1.0mV EPSPs (with total input rates of 3.0 and 1.5KHz) presented in

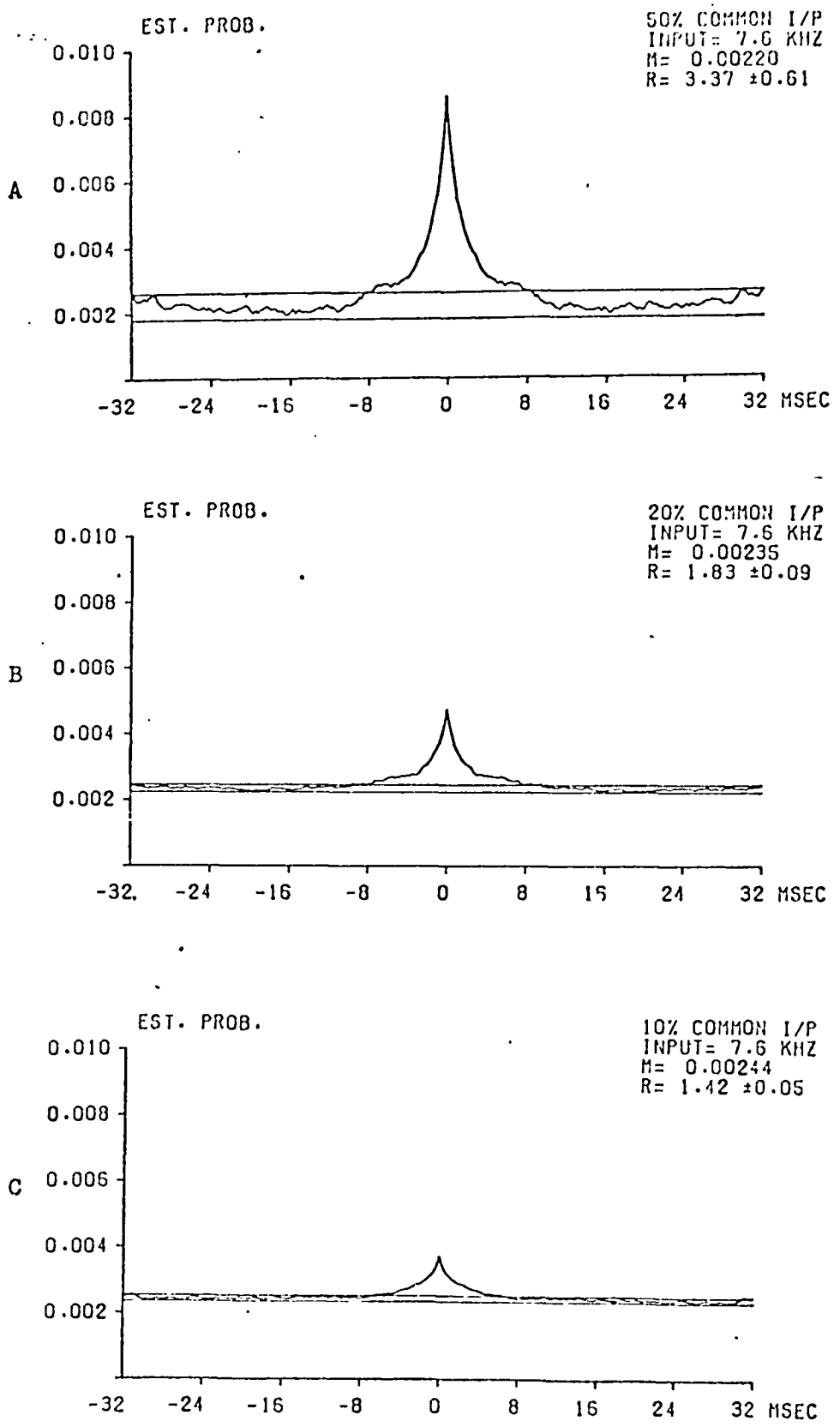

FIGURES 4.3.5:

The PPST Histogram results from stationary simulations with 0.2mV EPSP amplitudes, 7.6kHz total pre-synaptic rate and 50(A), 20(B) and 10(C) percent common connectivity.

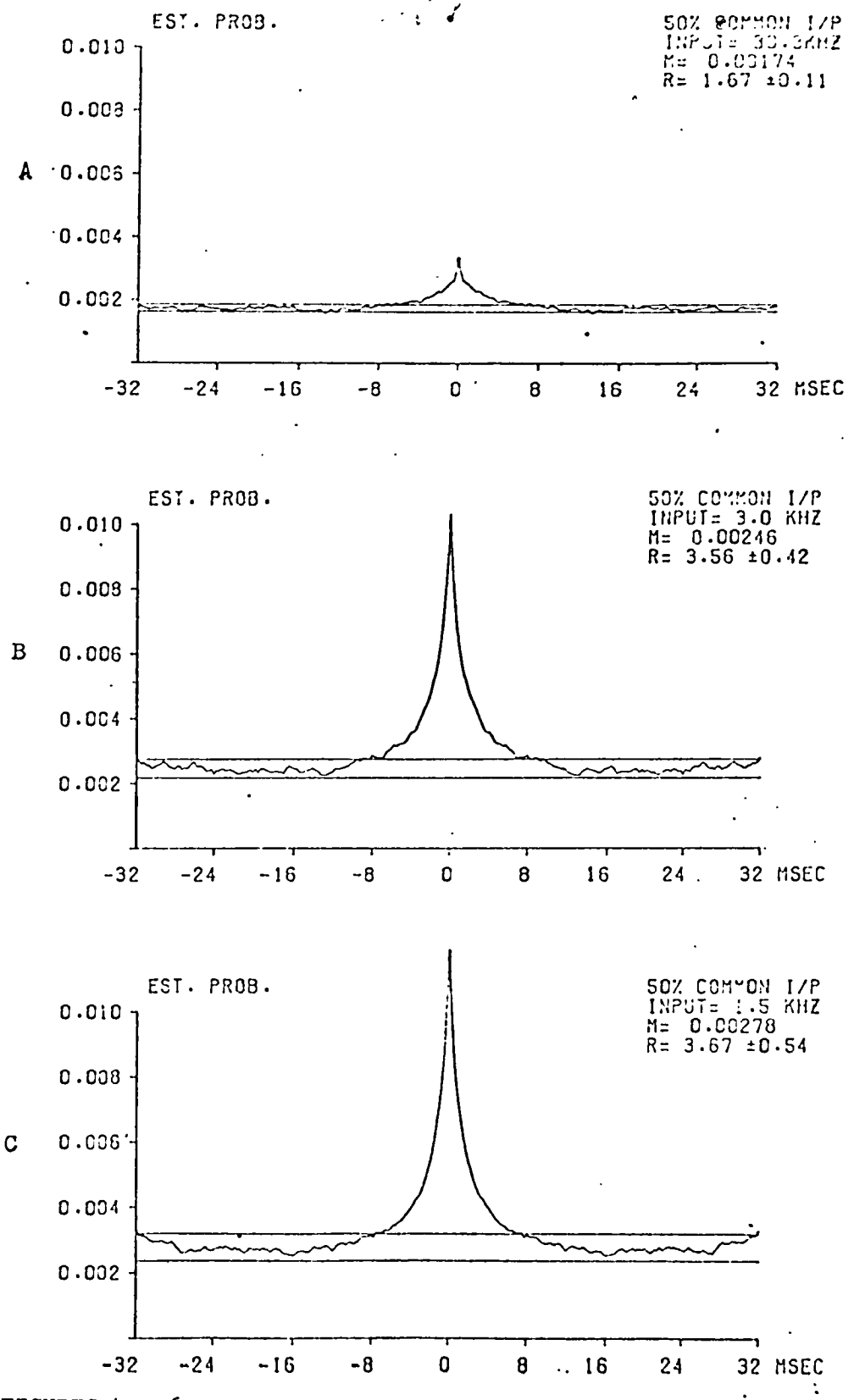

FIGURES 4.3.6:

The PPST Histogram results from stationary simulations with 50 percent common connectivity and (A) 0.05mV EPSP amplitudes/ 30.3kHz total pre-synaptic rate, (B) 0.5mV/ 3kHz and (C) 1.0mV/ 1.5kHz.

Figures 4.3.6B and C respectively, but not so for the smaller 0.05mV EPSP case in 4.3.6A. This last result shows a marked reduction in R and a decrease in the width of the shoulders of the peak (to approximately $\pm$ 6mSec). At the moment it is thought this final result must be attributed to the high pre-synaptic drive rate (30.3KHz) required. This effect has been characteristically demonstrated by the 18KHz, 0.1mV EPSP, and 50 percent common connectivity case (Figure 4.3.1A) which resulted in a narrowing of the peak shoulders and a significant reduction in (R-1)

This concludes the preliminary simulated stationary motoneurone pair PPST histogram results; now follows the presentation of some experimental correlation functions for comparison and possible interpretation.

4.4 INVESTIGATION OF THE EXPERIMENTAL PPST HISTOGRAM RESULTS BY THE NEURONE PAIR MODEL:

Two important points must be kept in mind when making a comparison between the experimental PPST histograms from discharge sequences recorded from the cat and those just presented for the model; the experimental data is from non-stationary origins while the simulated data is from a stationary process and the PPST results from the cat studies are found for superimposed multiunit trains of axon spikes as opposed to the single unit correlations of the model; the non-stationarities arise due to pre-synaptic rate

modulation and trans-membrane process variations, such as EPSP shape and size. The modulation non-stationarity effect will be investigated by the model after some of the experimental results have been demonstrated, but those of a trans-membrane origin are beyond the present model. It is expected that it will have a predominant influence on the correlated peak shape and amplitude. These characteristics will be further affected by the multiunit situation. Not only will it tend to widen the peak and reduce the amplitude, because of differing time delays in the pre-synaptic (and possibly post-synaptic) pathways, but it will increase the probability of joint-occurrence in the bins of the histogram by the product of the number of units contributing to the two sequences being correlated. This can be seen to arise from the formula given in Section 4.2 for the mean bin count for single unit sequences X and Y = $n_x n_y \Delta t T$ (as defined before), which for multiunit sequences becomes (xn_x). (yn_y). $\Delta t.T$ or (xy). $(n_x n_y \Delta t\ T)$, for x units contributing to sequence X and y units contributing to Y. Generally each multiunit sequence will have between four and eight neurones contributing so the joint-occurrence bin probability may be anywhere between 16 to 64 times as large as the single unit result of the simulations. However, although this effect directly influences the PPST mean probability level (by the product xy), it does not greatly affect the value of the estimated correlation strength R, except by the differing time delays between the units.

Another important effect, which is observed to influence the value of (R-1) and to a small extent the peak shape, is that due to using a wider histogram bin width of 1mSec. This has a low pass filtering effect on the PPST histogram form and because the correlated peaks are generally quite narrow (approximately $\pm$ 3mSec at half peak height). A change in bin width from 0.25 to 1mSec therefore significantly reduces the peak amplitude. It will be seen later, from the selected stationary simulation results which are presented with 1mSec bin widths (after the experimental PPST results), that this alone can reduce the value of (R-1) by approximately half.

Now follows some typical examples of animal PPST Histograms, derived from multiunit spike sequences recorded from filaments of intercostal alpha-motoneurones, at different stages of experimentation, and their interpretation by the stationary model results. The recordings were obtained in the cat (unpublished data from Kirkwood, Sears, Tuck and Westgaard).

Figures 4.4-1, -2, -3 and -4 show PPST histograms for five different experimental situations on the same cat between the same three paired segmental combinations T_5/T_6(A), T_6/T_7(B) and T_7/T_8(C). Each PPST histogram is derived from a pair of motoneurone efferent spike sequences selected unit populations, by amplitude window discrimination, from the segmental filaments recorded. For the first figure the data used was recorded from a 'normal' cat which was anaesthetised, paralysed and artificially ventilated to

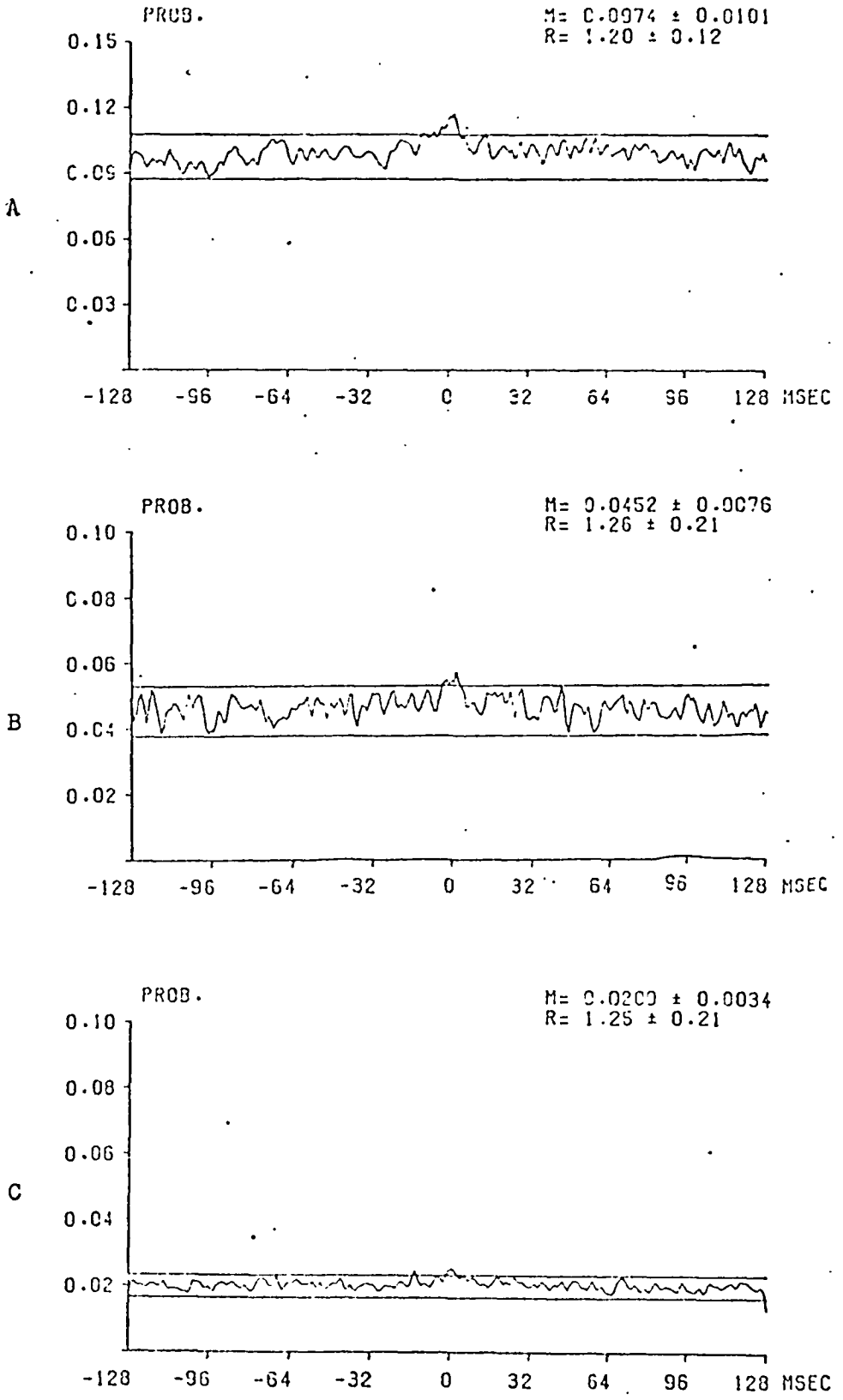

FIGURES 4.4.1:

The PPST Histogram results, from data recorded from a cat, between intercostal segments T5/T6 (A), T6/T7 (B) and T7/T8 (C)- CONTROL-1 with 4.1% CO_2.

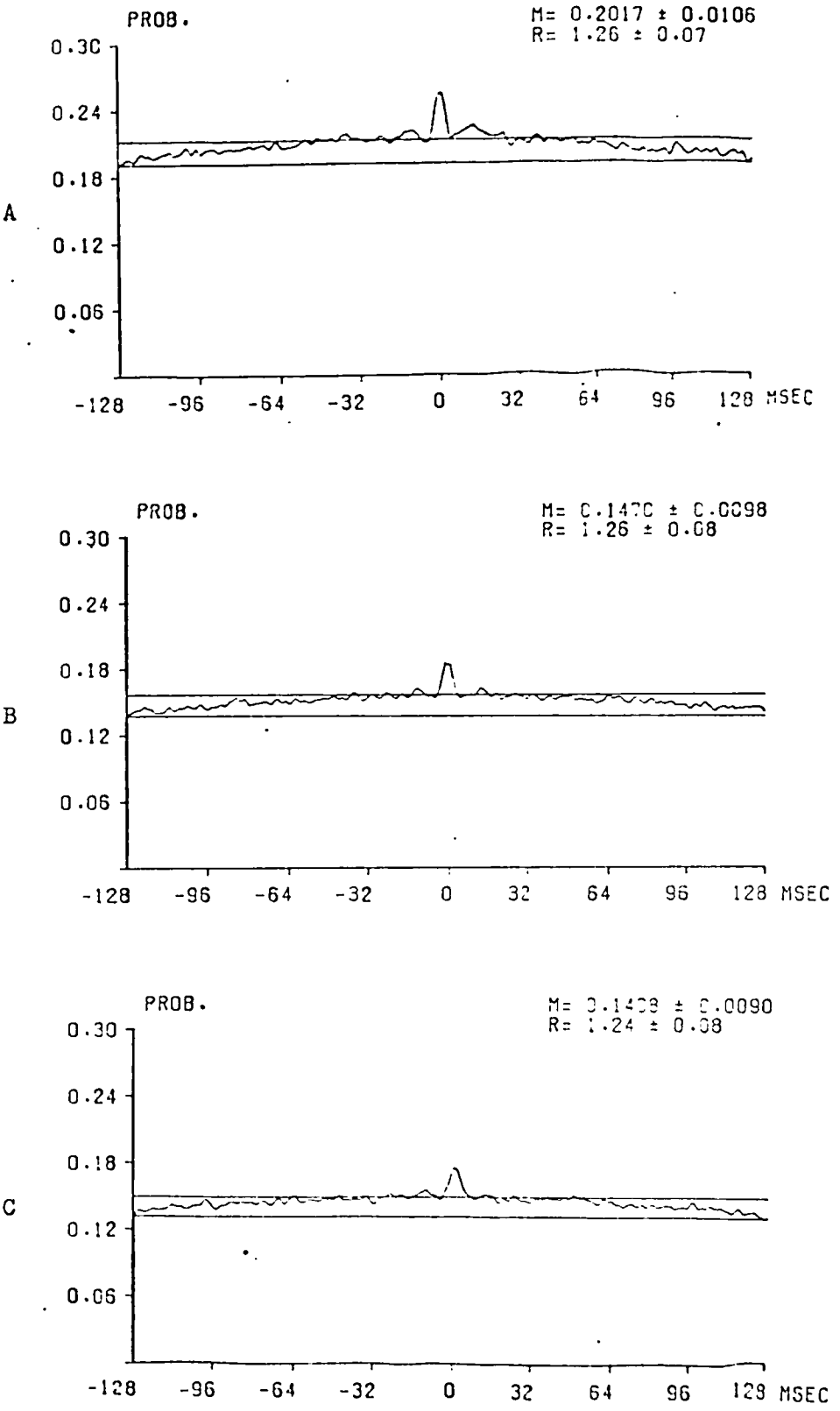

FIGURES 4.4.2:

The PPST Histogram results, from the same cat as Figure 4.4.1 and between the same segments, but with 8.1% CO_2- CONTROL-2.

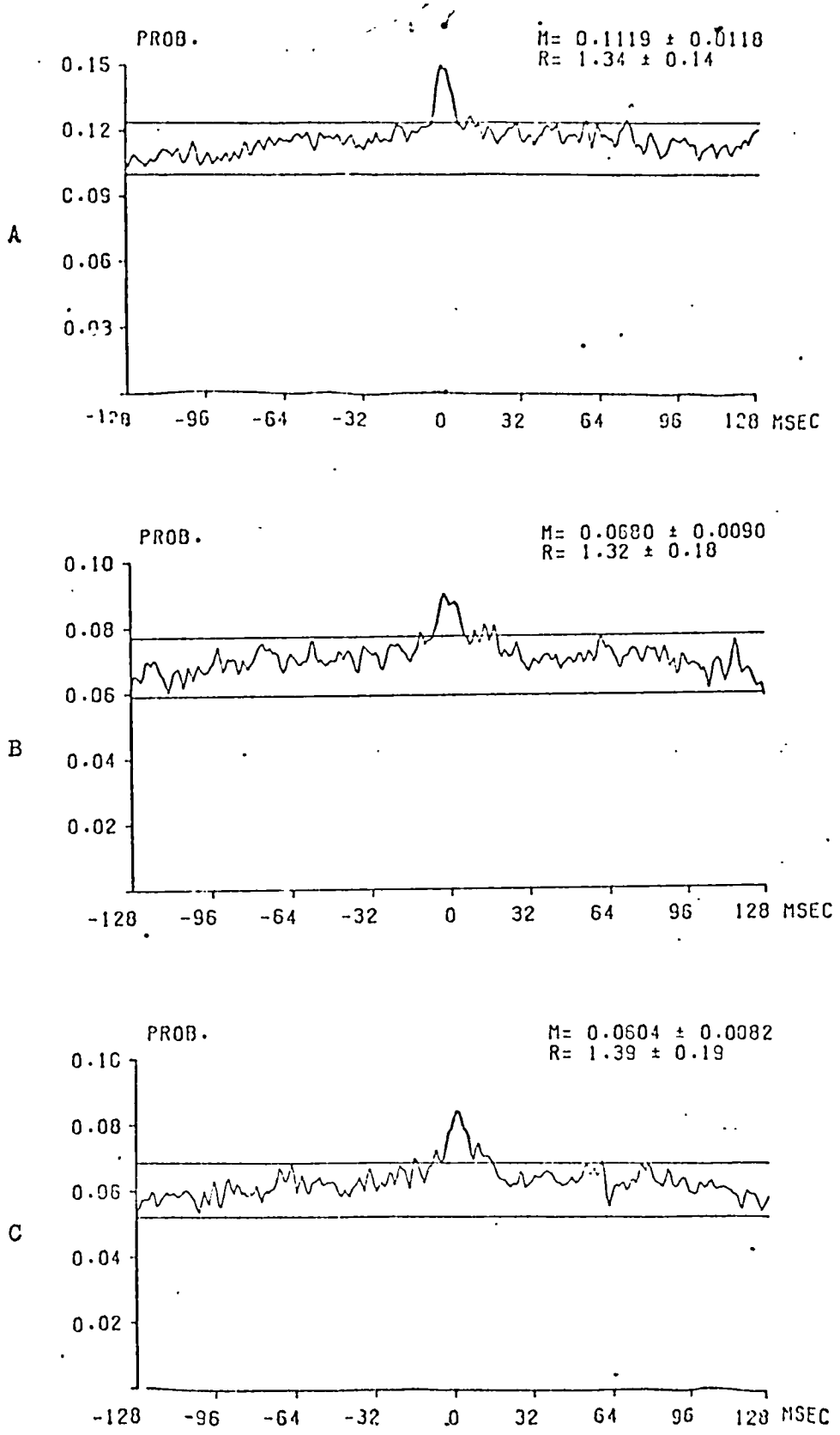

FIGURES 4.4.3:

The PPST Histogram results, from the same cat as Figure 4.4.1 and between the same segments, but after acute hemisections at T4 and T9. with 8.4% CO_2- HEMISECTION.

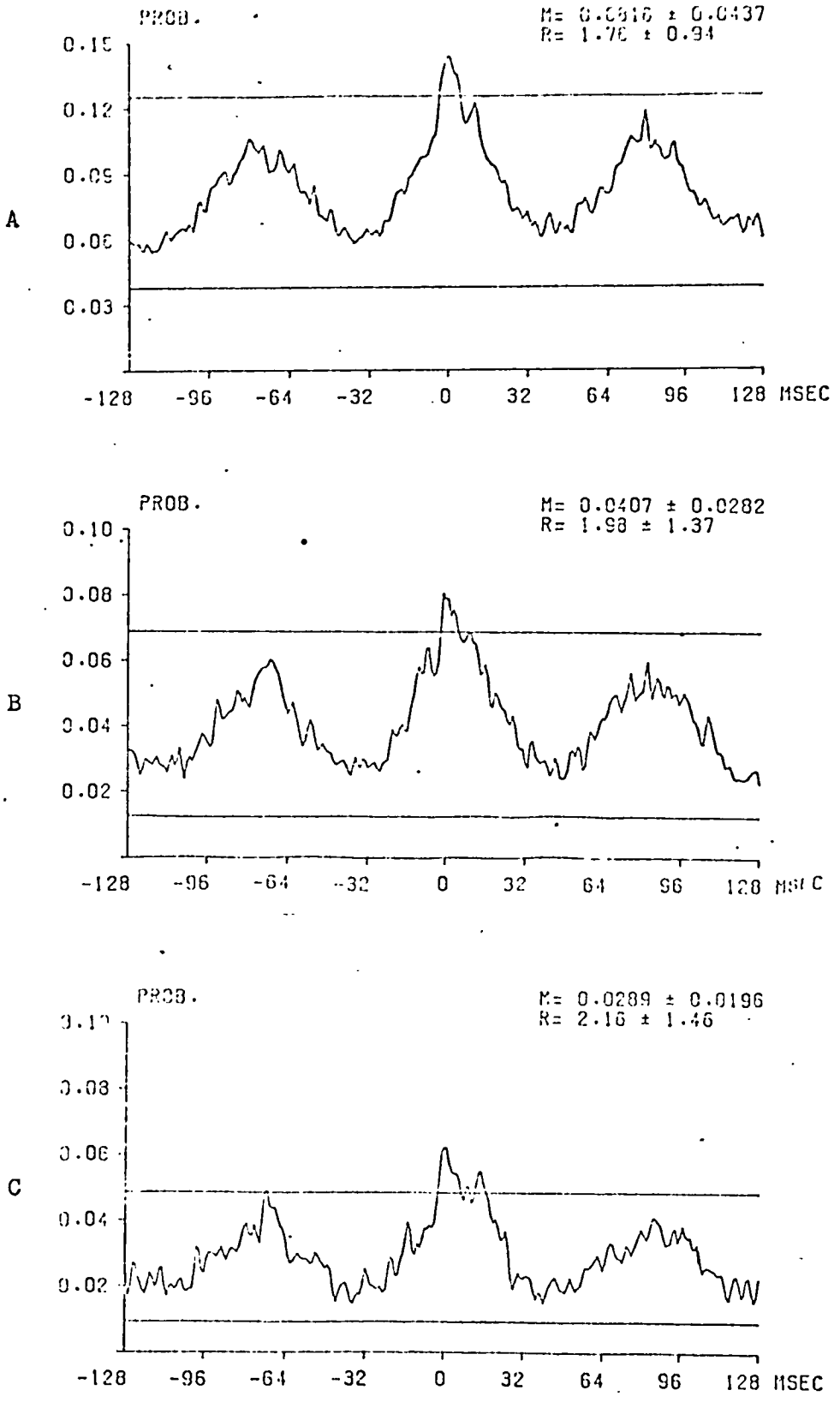

FIGURES 4.4.4:

The PPST Histogram results, for the same cat as Figure 4.4.3 and between the same segments, but following an acute 3/4 section rostrally atT9 and with 8.5% CO_2- $\frac{3}{4}$SECTION.

controlled levels of alveolar PCO_2. This set of experimental results are for 4.1 percent CO_2 and will be known as CONTROL-1. They are followed by the results of CONTROL-2 in Figure 4.4.2 which again come from the same 'normal' cat under the same conditions above except that the CO_2 level has been increased to 8.1 percent. It is interesting to note one feature held in common with all the six PPST histograms and some significant differences:

i) They all demonstrate a significant peak of activity in the centre of the PPST histogram (which can be determined by the lines of $\pm$ 1 percent confidence estimates of the mean probability level, M). Also observe the flat top of the peak which was predicted earlier.

ii) The results of CONTROL-1 show very little sign of short term synchrony (Sears and Stagg, 1976) compared to the more distinct correlation peaks found for CONTROL-2. However, the values of R demonstrate that there is a similar amount of synchronised recruitment of the neuronal groups recorded from with 4.1 percent CO_2 in the inspired air. Also, when compared to the standard stationary model results in Figure 4.4.5, the low value of M indicates that only one to three units must be active at any time in each sequence. This could be another reason why there is little significance-lack of bin counts as is discussed by Sears and Stagg. However, at the 8.1% level of inspired CO_2, the mean probability level suggests that three to five units per sequence are recruited and the better defined shape of the central peaks and the value of R, could be interpreted as being produced by at least 10 percent common connectivity

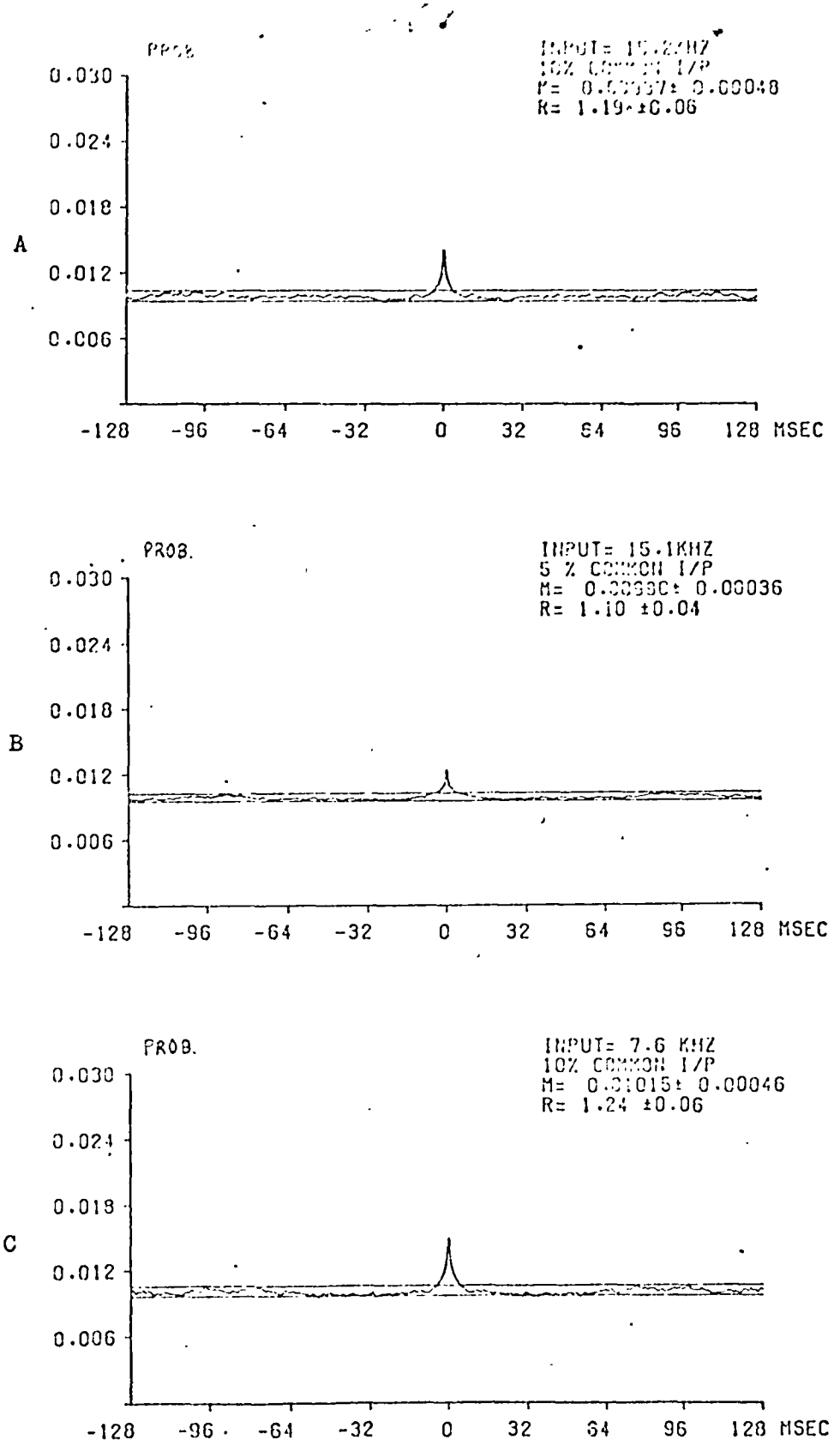

FIGURES 4.4.5:

Some PPST Histogram results from the stationary simulations for comparison with those of the cat experiments. Standard in (A) with 5% and (B) with 10% common while (C) 0.2mV and 10% common connectivity.

in the active pre-synaptic pathways of the neuronal groups considered.

Figure 4.4.3 demonstrates the PPST histogram for the same animal and segmental pairs but with 8.4 percent CO_2 and following two acute hemisections of the spinal cord at the T_4 and T_9 segmental levels (experiment HEMISECTION). An obvious decrease in M, a broadening of the central correlation peak and only a barely significant increase in R, is observed; in all three PPST the mean probability is at least halved and the peak half width increased by greater than 50 percent. Two hypothesised explanations for these characteristic changes are that the hemisections have removed the inhibition of some pre-synaptic interneurone pathways and/or some pre-synaptic inhibition of the motoneurone synapses themselves of pathways held in common by the groups of motoneurones involved. The former hypothesis is regarded as most likely. It would account for the broadening of the correlation peak in terms of the interneuronal delay. The large decrease in the value M is probably a direct consequence of the lack of sufficient drive to excite as many motoneurones of the groups as in the 'normal' case (Figure 4.4.2) at a similar alveolar CO_2 level before the partial lesions. Indeed, the high level of CO_2 (8.5%) was necessary to achieve excitation of motoneurones for PPST analysis.

A less complete explanation is that some compensatory mechanisms occur within the motoneurones themselves. Some examples of these are given as:

i) The local shunting of active synapses (lacking in

the present model), which normally tend to reduce the effectiveness of the EPSPs might be significantly decreased, as a consequence of the reduced pre-synaptic rate due to the hemisections, therefore allowing larger amplitude EPSPs to compensate for the lower pre-synaptic rate.

ii) the possiblity of a change in the cell time constant with a reduction of pre-synaptic rate which might compensate the situation by allowing for larger and longer existing EPSP shapes.

Both of these compensatory trans-membrane mechanisms are likely to occur to some degree in the normal animal, but presumably only have a small effect because otherwise they might grossly interact with the normal Central Respiratory Drive modulation and tend to cancel its effect.

One further hypothesis is put forward which suggests that the synchrony observed in the HEMISECTION case might be partly due to the muscle spindle sensitivity to mechanical vibrations, the reflex pathways having been released from inhibition by the partial lesions. This synchronisation could occur through the mechanical coupling of the spindles at neighbouring segmental levels detecting small vibrations in the inspired air, for example from the ventilating pump.

None of these hypotheses offer a complete solution to the origin of the observed correlations although a combination could account for the changes in the results that occur in the three experiments discussed. One thing is certainly clear, that as a result of the hemisections there have been basic changes in the neurophysiological state of the spinal cord. This is more apparent when the PPST histogram results, from

the same cat but with a further acute three-quarter (rostral) trans-section of T_9 and ventilation with 8.5 percent CO_2 (experiment-3/4SECTION) in Figure 4.4.4 are examined. The periodicity of the mean level suggests that a fairly regular pre-synaptic mechanism might be responsible (Moore et al, 1970). An examination of the original filament spike recordings supports this and provides a complete explanation.

In each channel only one or two alpha-units were active at any one time (if two they discharged in close succession), and then only for a very short period of the breath (each unit produced only three or four discharges per breath). The occurrence of these events were quite highly localised in time relative to the phase of the breath and fairly regular in interval thereby suggesting that the pre-synaptic rate producing the CRDP must rise sharply and maintain a near constant level before shortly dropping away again. It can be then demonstrated that the strong periodicity (with its interval of 70 to 80mSec), the low values of M, and the significant increase in R in these particular PPST histograms are to be expected from these sequence characteristics. From the periodicity, the intervals between the correlated spike events would correspond to a single unit discharge rate ranging from 12.5 to about 14.3/sec. These rates suggest that the mean probability level M, for 1mSec bin widths, would lie between 0.0125 and 0.0143 for two such single unit sequences. Because the value of M is typically two to four times larger than the calculated single unit case (and for the superimposed two unit sequences, the few pairs of events per breath occurred regularly and in close succession), their event cross-correlation function will show periodicity and

a significantly large value of R. If the multiunit case did not have the close grouping of the superimposed spikes, but still retained the same regular intervals, the PPST histogram result would have had a different periodicity or none at all.

It is thought that the discharge sequences contributing to the above phenomena must arise due to a very weak modulation of the excitatory synapses and a strong modulation of the inhibitory synapses of the motoneurones concerned. Figure 4.4.6 demonstrates a similar effect occurring in the PPST histogram derived from some simulation runs of the neuronal pair with a pre-synaptic sinusoidal modulation of 40(A), 20(B) and 10(C) percent about a mean rate of 15.2KHz. The result in C shows a strong similarity of form to the HEMISECTION results discussed above. Also these figures demonstrate a significant increase in the correlation strength, as given by R, with decreasing depth of modulation. This characteristic is directly related to the significant non-stationary serial correlation values of the discharge sequences from the simulated intercostal alpha-motoneurones which were investigated in Chapter 3.5. (N.B. At 5 percent modulation not shown, the correlation peak has narrowed and the value of R decreased to 2.8 ± 0.95).

The last set of results from the same cat, under the same conditions as above but now with an additional acute lesion in T_{10} and breathing 10.1 percent CO_2 (experiment- TRANSECTION), are presented in Figure 4.4.7. It is apparent that there has been little change from

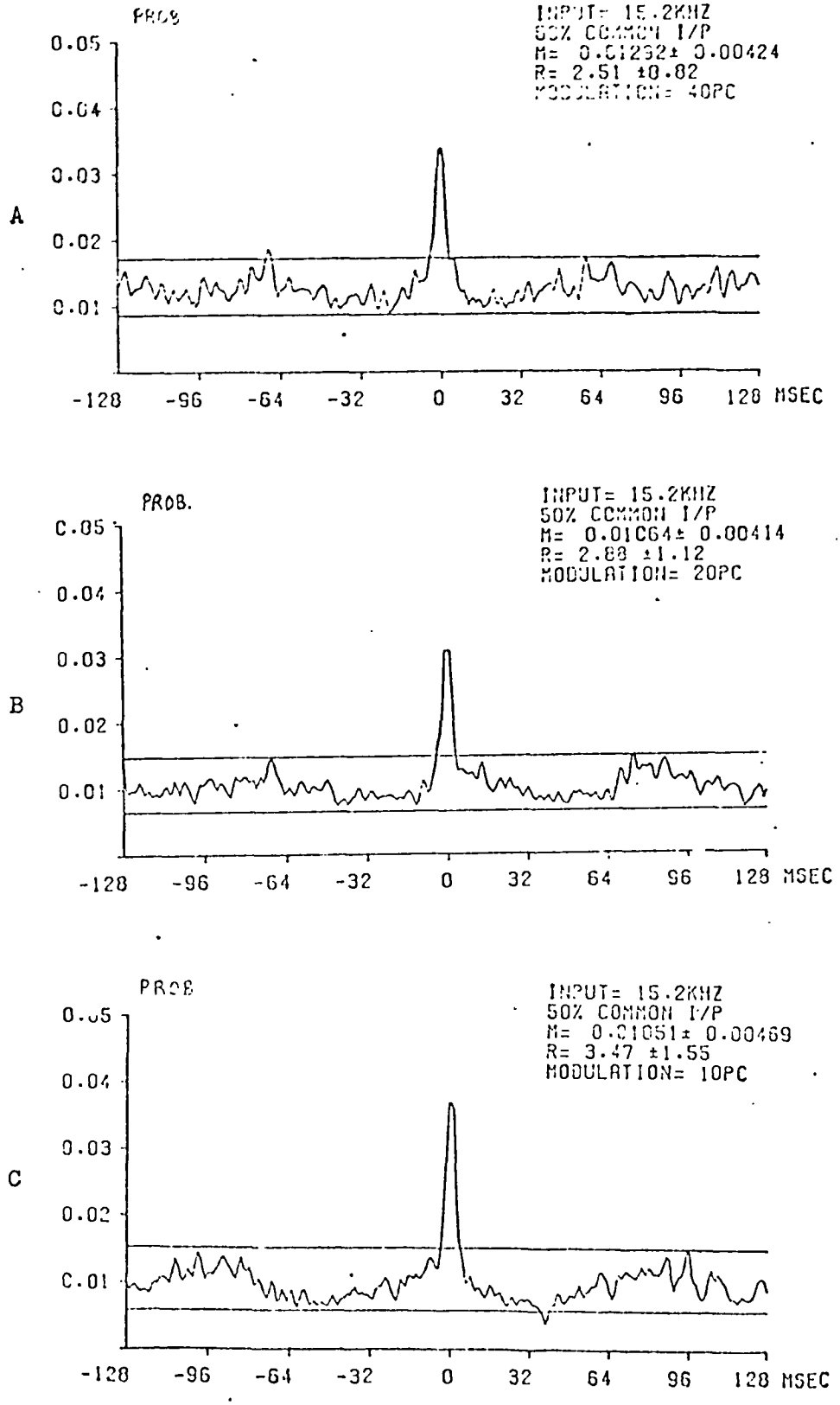

FIGURES 4.4.6:

Non-stationary simulation PPST Histogram results. All runs standard but with pre-synaptic sinusoidal modulation about the mean rate of 15.2kHz as marked (50% common connectivity).

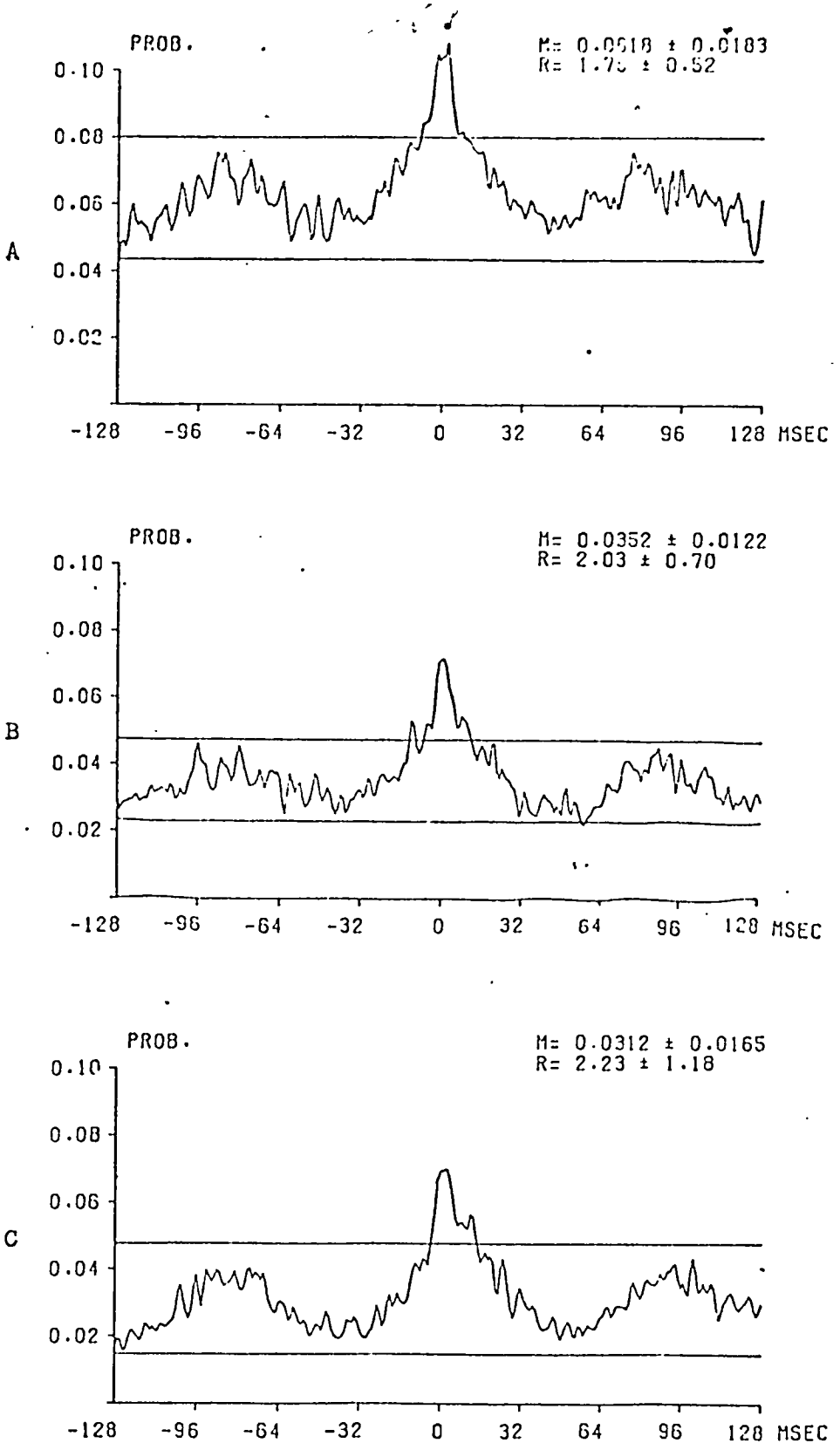

FIGURES 4.4.7:

The PPST Histogram results, for the same cat as Figure 4.4.4 and between the same segments, but following an acute trans-section at T10 and breathing 10.1% CO_2-TRANS-SECTION.

the previous 3/4SECTION experiment; perhaps a slight reduction in the mean probability level but no significant change in the strength of correlation or the periodic form of the PPST histogram. This then indicates that there is no longer any significant influence from the segments below the tenth segmental level, especially at this high alveolar CO_2 level used.

To complete this discussion of the experimental work just described, the Figures 4.4.8A and B demonstrate some typical long term changes that are observed to occur in the PPST histogram for a cat that has had a similar set of acute lesions as in the HEMISECTION experiment. The results given were derived from data recorded in T_8 and T_9 108 days after hemisections of T_6 and T_{10}. In addition the dorsal roots of T_9 had been cut. For A the anaesthetised, paralysed and artificially ventilated cat was breathing 5.6 percent CO_2, while in B the CO_2 level is raised to 8.6 percent. These correlations between the discharge event sequences recorded from T_8 and T_9 are noticeably different from those originating in the acute HEMISECTION experiment. It should be noted however that this is for a different cat and that there has been a wide variation observed in the PPST histogram peaks derived from the many long term experimental studies already performed. From this series of experiments both the width and the strength of the central peak varies, and at present, it has only been possible to loosely categorise the results. The results shown are typical of the most common category but within this group the value of R may vary from 1.5 to greater than 4, the width of the shoulders in the peak may extend out to $\pm$ 35mSec and

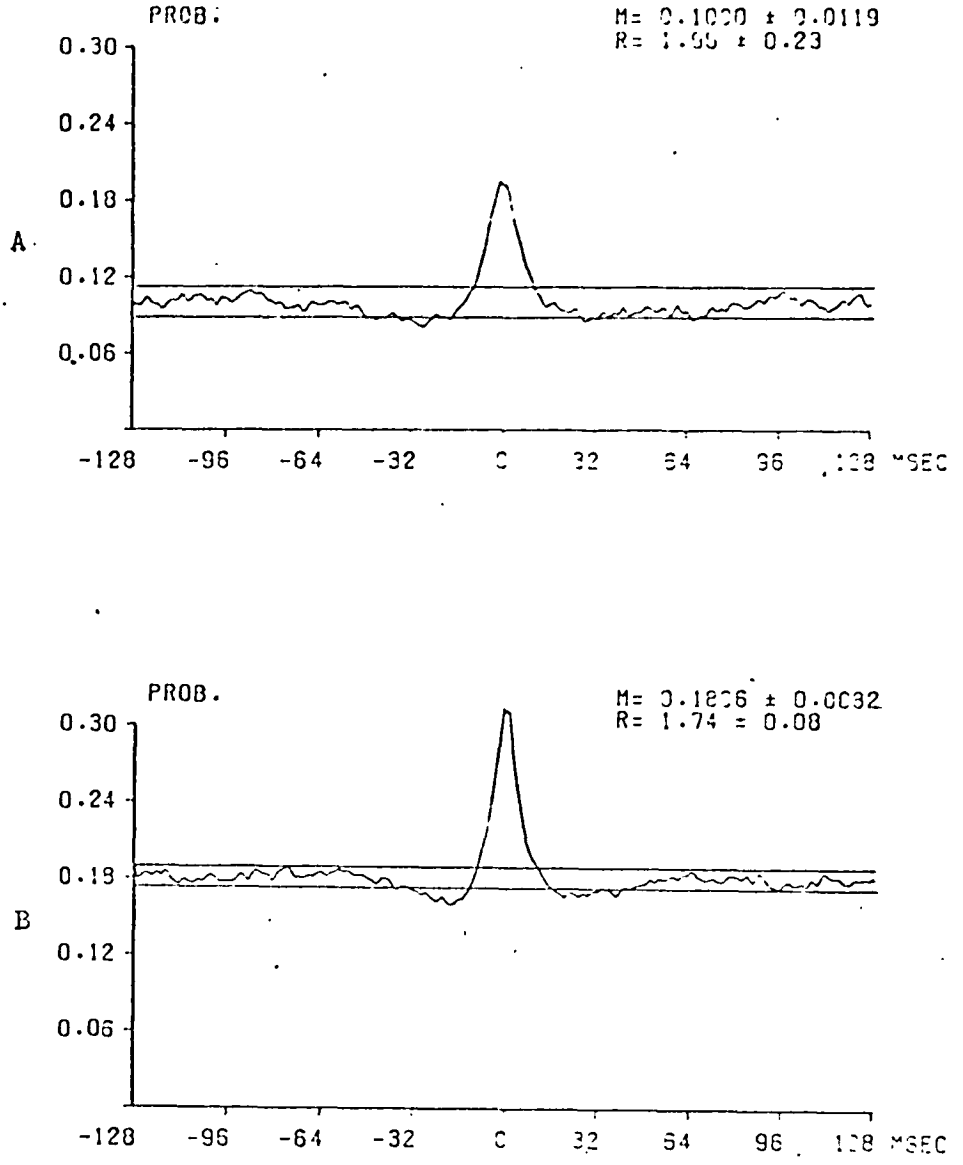

FIGURES 4.4.8:

The PPST Histogram results from a long term experiment (108 days, different cat) with hemisections at T6 and T10 and the dorsal roots at.T9 cut. (A) between intercostal segments T8/T9 with 5.6% CO_2, (B) T8/T9 and 8.6% CO_2.

the number of days following the acute lesions varies from zero up to 200 days; the only characteristic held in common being a well defined shape of the correlation peak. This briefly describes the state of experimental work currently under investigation. So far the results show some indication of a temporal trend in the value of R and the peak width but there is no clear cut evidence to statistically support this yet.

The possibility of gross changes in the trans-membrane mechanisms, or the cell time constant, contributing towards these phenomena have been ruled out by intracellular studies. On the other hand sprouting of the pre-synaptic pathways is unlikely to be a main cause as demonstrated by the strong features of the correlation peaks of some acute experiments. Until more experiments have been performed, and sufficient evidence gathered to allow a further hypothesis, the neuronal model cannot help in identifying the origins of these correlation characteristics. However, the present model with its realistic pre-synaptic excitation rates and trans-membrane mechanisms is adequate in accounting for the 'CONTROL' and 'HEMISECTION' PPST histogram results determined. It also demonstrates that changes in EPSP size alone cannot possibly explain the very wide peaks observed in the correlations derived from the ¾SECTION and TRANSECTION data, and indicates that even longer duration EPSPs could not be wholly responsible. Therefore, within the limits of the simulations presented some explanations have been achieved but also further research is necessary so that a complete description can be found.

4.5 INVESTIGATION OF COMMON CONNECTIVITY BY THE ACE POTENTIAL:

Given the assumption of common connectivity between intercostal alpha-motoneurones by branching in their pre-synaptic spinal stem pathways, the ACE Potential (examples of which are shown in Figure 4.5.1) must contain some information relating to the amount of shared input between pairs of motoneurones. In order that such a measure might be identified and reliably utilised, the neuronal pair model was used to investigate these possibilities. Kirkwood and Sears (1977) show theoretically that the ACE potential due to the common EPSPs released in neurones X and Y of Figure 4.2.1B, is a function of the EPSP shape and the PC Kernels (assumed) for the event Input-Output PDF. The description that follows investigates the ACE potential as a function of pre-synaptic structure and EPSP size.

Figures 4.5.2 and -3 display the ACE potentials determined from the neuronal pair simulation runs with the pre-synaptic common connectivity (COM) varied from 50 down to 5 percent of the total pre-synaptic input and can be compared with the physiological ACE, Figure 4.5.1.. Three sets of results are presented for different pre-synaptic input rates (I/P), 15.2KHz in the first figure, and 18KHz on the left and 14KHz on the right in the second. The ten ACE potentials all show a well defined rising edge from the baseline level beginning at times between 4 to 8 mSec prior to the trigger event (at zero time), to a distinct peak which occurs approximately 1.5mSec post-stimulus. Following the peak the potential falls away again, generally,

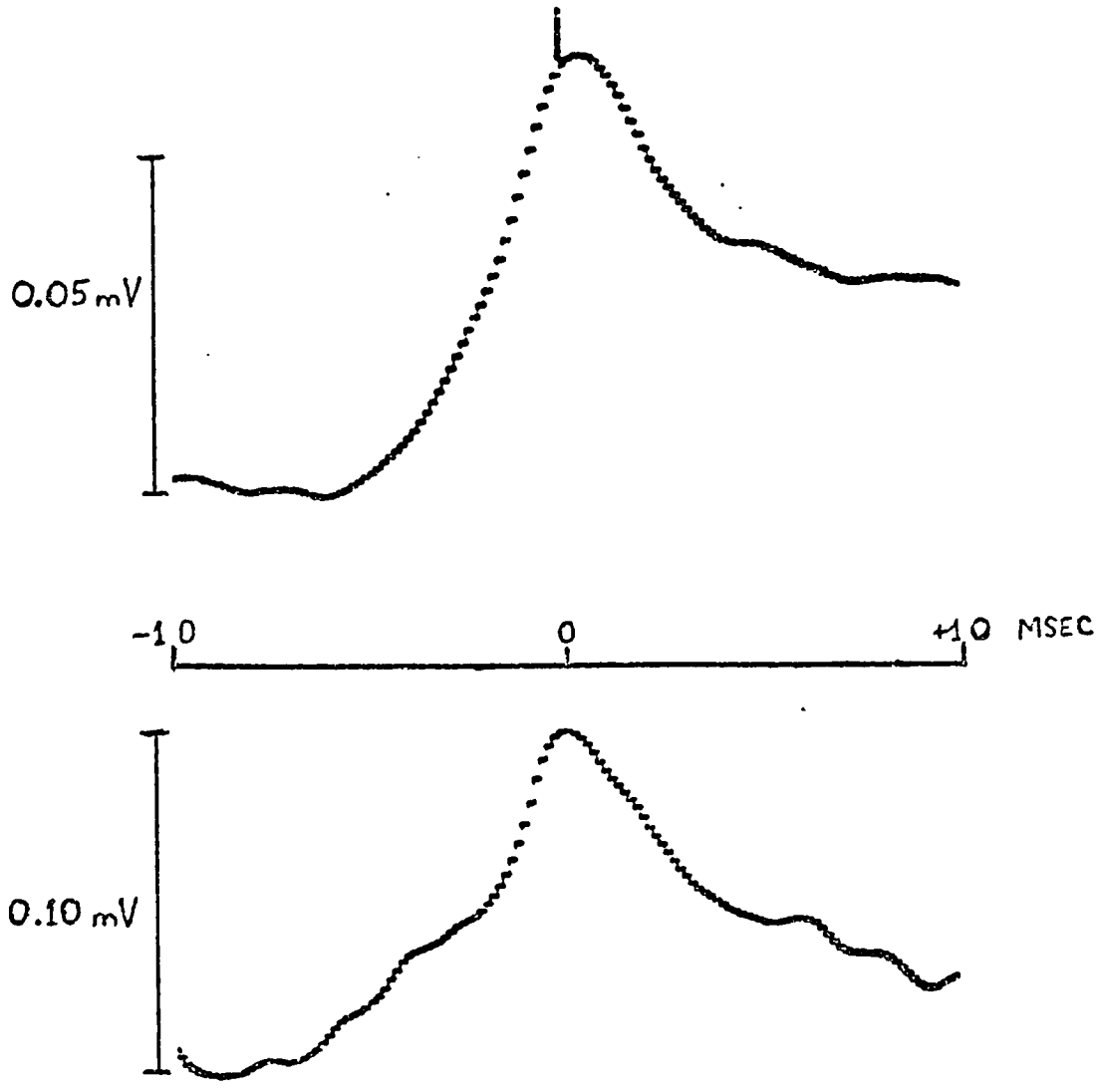

FIGURES 4.5.1:

Two typical ACE Potentials recorded in cat intercostal alpha-motoneurones.

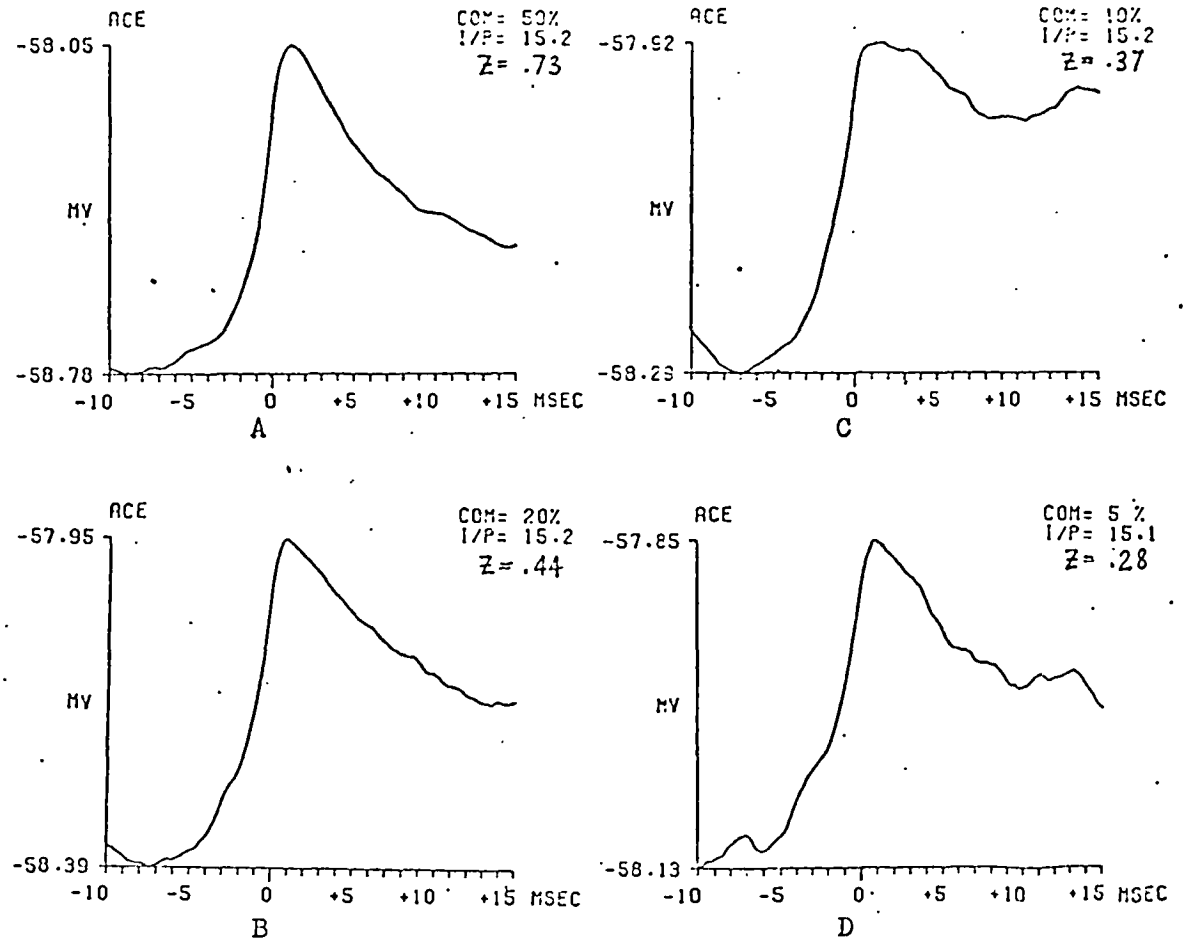

FIGURES 4.5.2:

The standard stationary simulation ACE Potentials with 0.1mV EPSP amplitudes and a total pre-synaptic rate of 15.2kHz. COM indicates the amount of common connectivity and Z the ACE potential amplitudes(mV).

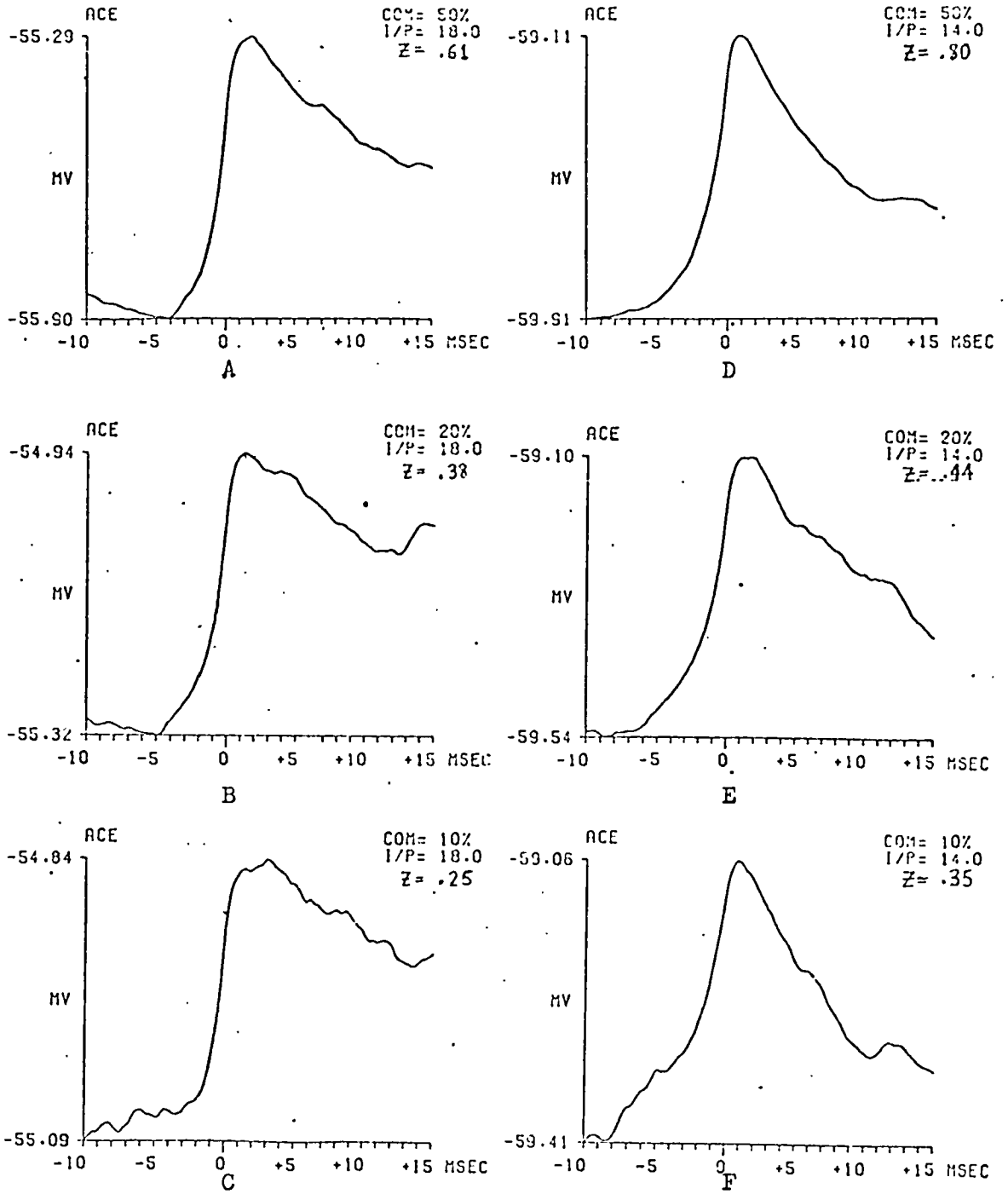

FIGURES 4.5.3:

The standard stationary simulation ACE Potentials, as in Figure 4.4.2 but with 18kHz (A-C) and 14kHz (D-F) total pre-synaptic rates (COM is the amount of common connectivity used, Z is the measured ACE potential amplitude).

in not such a well defined manner as the rising edge. The baseline level can be seen to be rate determined while the height of the ACE potential Ƶ can be shown to be related to the strength of the pre-synaptic common connectivity for these simulated results. From the values of Ƶ measured from the simulations the estimated ratios of shared inputs for actual common connectivity of 50:20:10 (and also for the 15.2KHz result :5) percent, determined by $Ƶ^2$ are 50: 18.2:12.8:5.9, 50:19.4:8.4 and 50:15.1:9.8 for the three pre-synaptic rates used respectively. Quantitatively, this should prove to be a very useful result, but of course it has only been shown for a single fixed shape and amplitude EPSP and in practice requires calibration if it is to be at all useful. Because the EPSP shape is not strictly described in terms of the parameters used by Kirkwood and Sears (1977), which suggest $\alpha' = 20\beta'$ approximately, it was considered necessary to reformulate their expression for the ACE Potential $x_2(\tau)$ and the output event cross-correlation function or CIF (Cross Intensity Function) $y_2(\tau)$. To do this the same model for the expression of the PC Kernel, that it may be described by proportions of EPSP shape and its derivative was made, and the expression for the simulated EPSP of $f(t) = K(e^{-\beta t} - e^{-\alpha t})$ mV used. Following the procedure described in the Appendix to the above paper, the expressions below are derived:-

For $\tau < 0$:

$$x_2(\tau) = \frac{ck^2 R_C}{2R_y} \frac{(\alpha-\beta)}{\alpha\beta(\alpha+\beta)} \left[\alpha(a-b\beta)e^{\beta\tau} - \beta(a-b\alpha)e^{\alpha\tau} \right] \text{ mV} \qquad \text{(ia)}$$

For $\tau > 0$:

$$x_2(\tau) = \frac{ck^2R_C}{2R_y} \frac{(\alpha-\beta)}{\alpha\beta(\alpha+\beta)} \left[\alpha(a+b\beta)e^{-\beta\tau} - \beta(a+b\alpha)e^{-\alpha\tau}\right] \text{ mV} \qquad \text{(ib)}$$

and for all τ:

$$y_2(\tau) = \frac{c^2K^2R_C}{2R_y} \frac{(\alpha-\beta)}{(\alpha+\beta)} \left[\alpha(a^2-b^2\beta^2)e^{-\beta|\tau|} - \beta(a^2-b^2\alpha^2)e^{-\alpha|\tau|}\right]$$

impulses/sec (ii)

where K = EPSP amplitude factor (mV)

$1/\alpha, 1/\beta$ = EPSP time constants as defined above

a,b = proportions of descriptive components of PC Kernel as modelled by Kirkwood and Sears, e.g.

$$g'(t) = c\left[af(t) + b\,\frac{df(t)}{dt}\right] \quad \begin{matrix}\text{impulses/sec} \\ \text{c assumed constant}\end{matrix} \qquad \text{(iii)}$$

R_C, R_y = the average pre-synaptic rates of release of common EPSPs in the neurones (X and Y) shown in Figure 4.2.1B and the mean firing rate of the stimulus neurone, Y respectively.

and $|\tau|$ = absolute value of τ.

Now from the PPST histogram the maximum value of $y_2(\tau)$ can be measured from the ratio of the total peak bin counts to the mean R, as $(R-1)\,R_x$. Finding the expression for the maximum of $y_2(\tau)$, which can be seen to occur at T = 0, and equating it with the PPST result gives an expression which estimates the average EPSP amplitude factor:

$$\text{e.g.} \quad K = \frac{R_x}{c(\alpha-\beta)} \left[\frac{2\alpha\beta(\alpha+\beta)\,(R-1)}{R_C(a^2+b^2\alpha\beta)}\right]^{\frac{1}{2}} \text{ mV} \qquad \text{(iv)}$$

By fitting the PC Kernel modelling equation (iii) to the simulation Common Input-Output PDF to determine a, b and using the known values of α, β, R_C, R_x, an estimate of K can be made for a simulation result of R. For a standard EPSP run with a pre-synaptic rate of 15.2kHz and 50% common connectivity, this estimate is 18 percent lower than the true value of 0.13674 mV.

The ACE potential magnitude Z can be found from the difference between the maximum and minimum values of $x_2(\tau)$ calculated for delays of τ closest to $\tau = 0$. These delays of τ_{min} and τ_{max} are found by equating the differentials of the expressions (ia) and (ib) to zero:

$$Z = \frac{ck^2R_C(\alpha-\beta)}{2R_y\alpha\beta(\alpha+\beta)}\left[\alpha(a+b\beta)e^{-\beta\tau_{max}} - \beta(a+b\alpha)e^{-\alpha\tau_{max}} + \alpha(a-b\beta)e^{\beta\tau_{min}} + \beta(a-b\alpha)e^{\alpha\tau_{min}}\right] \text{ mV} \qquad (v)$$

where:

$$\tau_{max} = \frac{1}{\alpha-\beta}\log_e\left[\frac{a+b\alpha}{a+b\beta}\right] \text{ sec and } \tau_{min} = \frac{1}{\alpha-\beta}\log_e\left[\frac{a-\alpha b}{a-b\alpha}\right] \text{ sec}$$

From this resulting expression (v) any experimentally measured ACE potential amplitude Z would seem to be proportional to K^2R_C/R_y, as is the peak value of $y_2(\tau)$, which from equation (ii) is given by:

$$CIF_{max} = \frac{C^2K^2R_C(\alpha-\beta)^2}{2R_y\alpha\beta(\alpha+\beta)}\left[a^2+b^2\alpha\beta\right] \text{ impulses/sec (at } \tau = 0) \qquad (vi)$$

However, looking now at the results from the neuronal simulation, only for the PPST histogram estimates of (R-1) shown in Figure 4.3.4B vary proportionally with the rate of common pre-synaptic drive R_C. From the simulation measures of Z above, it appears this variable is proportional to the square root of the amount of shared input. Kirkwood and Sears demonstrate the following, and the above formulae concur:

$$Z = \frac{cV^2R_C}{\beta R_y} p_{max} \qquad \text{and} \qquad R-1 = \frac{C^2V^2R_C}{\beta R_x R_y} q_{max}$$

where p_{max} and q_{max} are functions of α, β, a and b. These two expressions imply then, because all the other variables are held fixed for the simulations described above where Z was measured, that p_{max} must vary as $1/\sqrt{R_C}$ and q_{max} is constant; V is directly proportional to the EPSP amplitude factor K, and C is directly proportional to $\Delta Prob/\Delta t$, $\Delta Prob$ is the step in probability of the PC Kernel of the common Input-Output PDF, from the mean probability immediately preceding a common pre-synaptic event to the kernel probability in the first time bin of width Δt, following zero time from which the parameters a and b were determined - thus for any fixed total pre-synaptic rate, c remains constant. In turn, these conclusions suggest that

$$\alpha(a+b\beta)e^{-\beta\tau_{max}} - \beta(a+b\alpha)e^{-\alpha\tau_{max}}$$

is proportional to $1/\sqrt{R_C}$ (where τ_{max} is defined above for equation (v) and τ_{min} tends towards $-\infty$) while $a^2+b^2\alpha\beta$ is constant. Therefore the PC Kernel shape must change in such a manner that the resultant self convolution, by which the PPST histogram can be determined, maintains a constant peak value.

The next chapter, which specifically investigates the underlying processes contributing to the event Input-Output PDF of neuronal structures, should clarify this finding. Figure 4.5.4. demonstrates from the formulae above, three sets of results where A gives the standard EPSP shape used in the simulations ($\alpha = 2\beta = 2000$/sec), B shows the PC Kernels employed, C the resulting ACE potential forms and D the resulting PPST peaks. The best fit for the standard 15.2kHz, 50 percent common drive PC kernel observed by simulation was for a = 4b. Two other cases, a = 2b and a = b are presented: note the PC Kernel peak value is kept constant and only the shape is altered. These results display similar characteristics to the ACE and PPST forms measured from simulations with increasing R_C.

It is worth noting here that the analytical expression (v), with τ_{min} set to $-\infty$ and a, b are determined for the standard 50 percent (15.2KHz) PC Kernel , accurately predicts the magnitude of Z measured from the simulated ACE potentials shown in Figures 4.5.2A 4.5.2B, 4.5.2C and 4.5.2D; the value of Z in brackets is the estimate from equation (v). The examples demonstrated in Figure 4.5.3, only serve to reinforce the conclusion above: there is a relationship linking a, b and R_C. Figure 4.5.5 does however show that the above calculations are in error, which can be seen by the estimated values of Z given in brackets, for the variations of the EPSP amplitude factor K. In these examples the product of the EPSP amplitude and the total pre-synaptic rate was kept constant (1515mV/Sec) as were the values of α, β, a, b and common connectivity, and therefore indicates the PC Kernel also is dependent on other

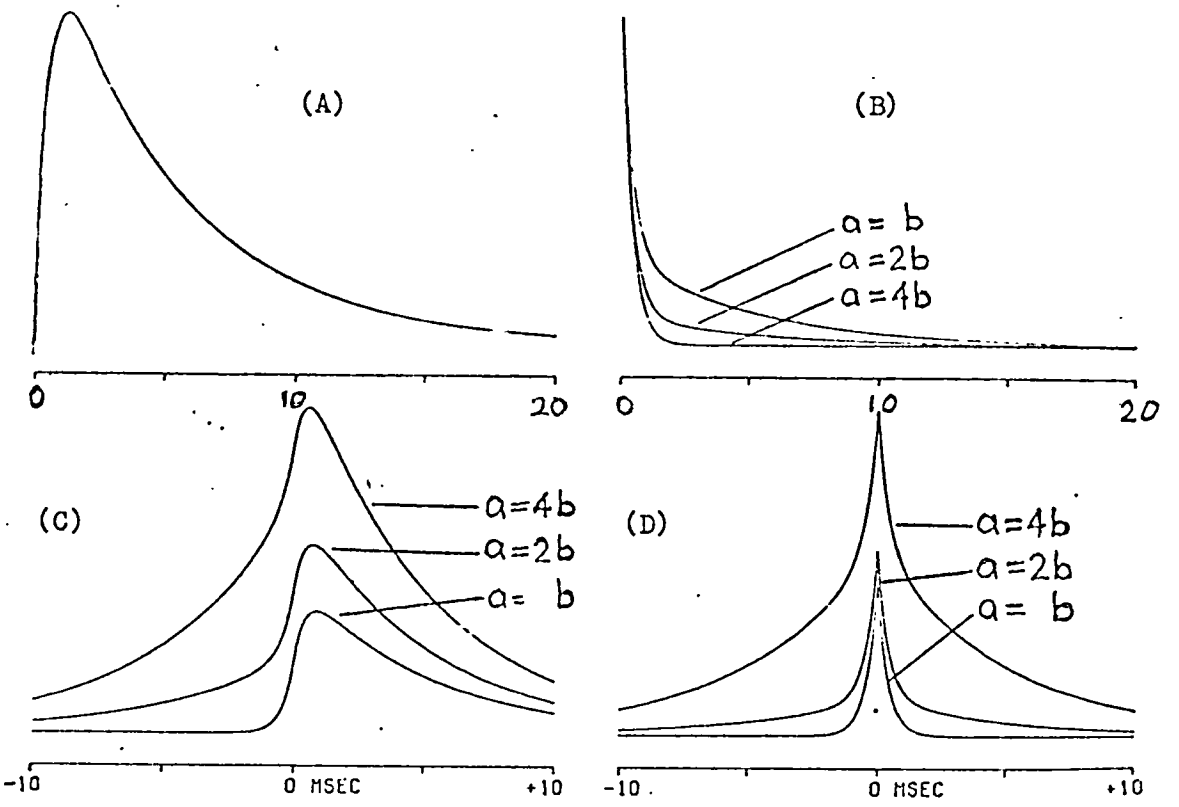

FIGURES 4.5.4:

Demonstrates the results from the analytical formulations of the text: (A) is the standard EPSP pattern, f(t);

(B) is the PC kernel, $g(t)$ where a=4b is the best fit case for 50% common, 15.2kHz simulation pc kernel recorded;

(C) is the ACE potential, $x_2(\tau)$ result;

(D) is the PPST kernel, $y_2(\tau)$ calculated.

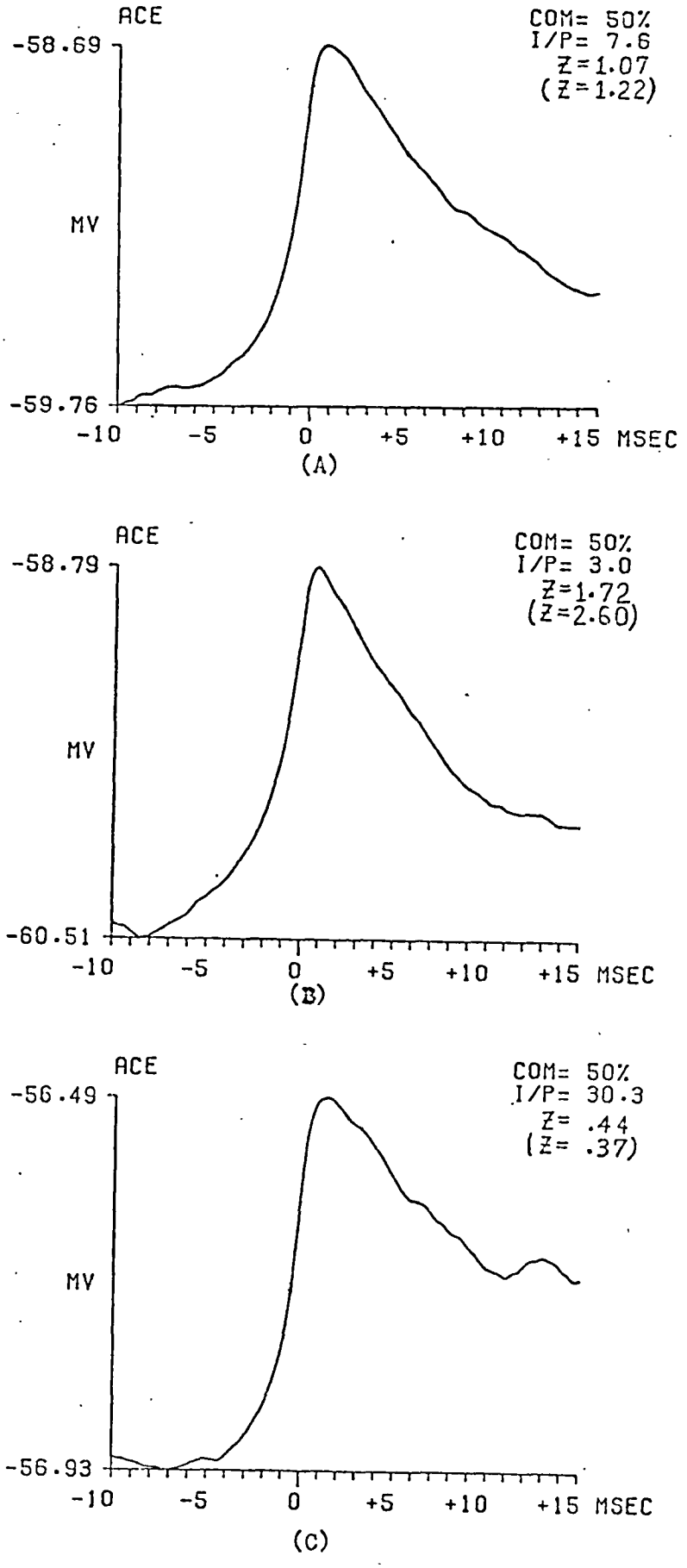

FIGURES 4.5.5:

The stationary simulation ACE Potentials for different EPSP amplitudes: (A) 0.2mV/7.6kHz, (B) 0.5mV/3.0kHz and (C) 0.05mV/30.3kHz. Values of Z in brackets are the estimated ACE potential amplitudes.

factors (such as EPSP amplitude) which is to be investigated in the next chapter.

To conclude this section, the simulation results shown in Figure 4.5.6, were produced by the model having 10,20 and 40 percent sinusoidal pre-synaptic rate modulation (about a mean of 15.2kHz) to examine the sensitivity of the ACE potential to the non-stationary situation. As observed, there is little variation in the ACE potential waveform and negligible change in Z for the case considered.

4.6 CONCLUSION

This chapter has demonstrated the application of two methods for testing the hypothesis of common pre-synaptic connectivity between neuronal groups. Both give strong evidence of common coupling in the pre-synaptic pathways. The neuronal pair network model has been extensively used to allow considerable interpretation of the physiological results determined. By simulation the useful measures of the applied techniques have been identified although simple quantitative measures have not been possible. This last result is directly related to the analytical expressions demonstrated in the section on the ACE potential. It is due to the inability to separate the factors of K^2R_C which is the primary determinant for the measures of CIF_{max} and Z. As demonstrated by Kirkwood and Sears, if one of these two factors can be measured independent of the other, the results determined for the physiology could then be calibrated and an absolute measure of common pre-synaptic connectivity be evaluated. Because no such separation appears possible, the model

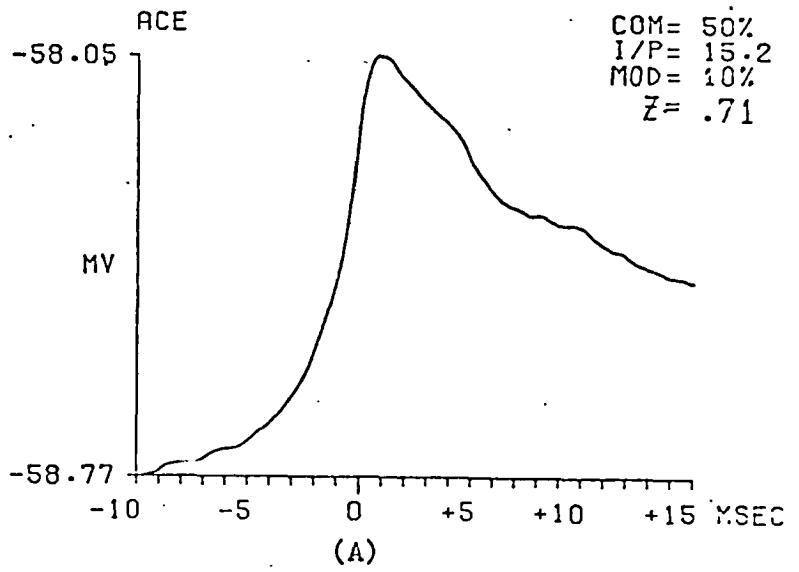

(A)

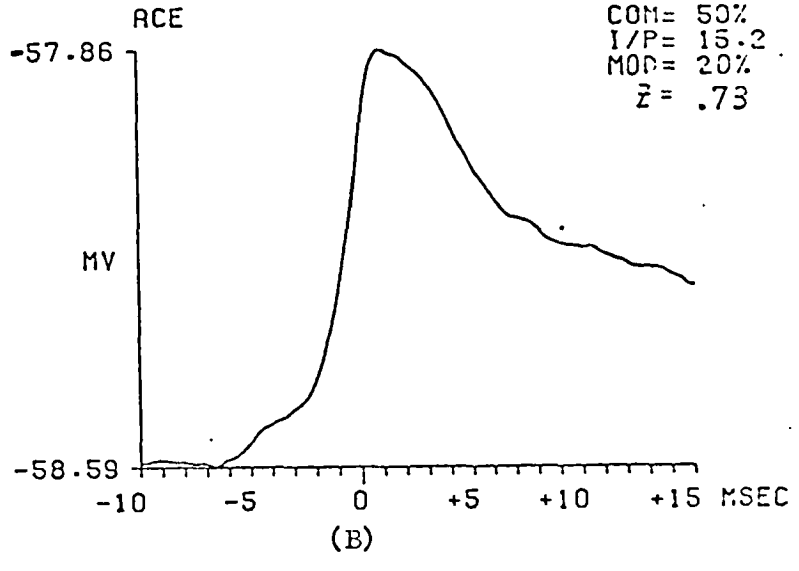

(B)

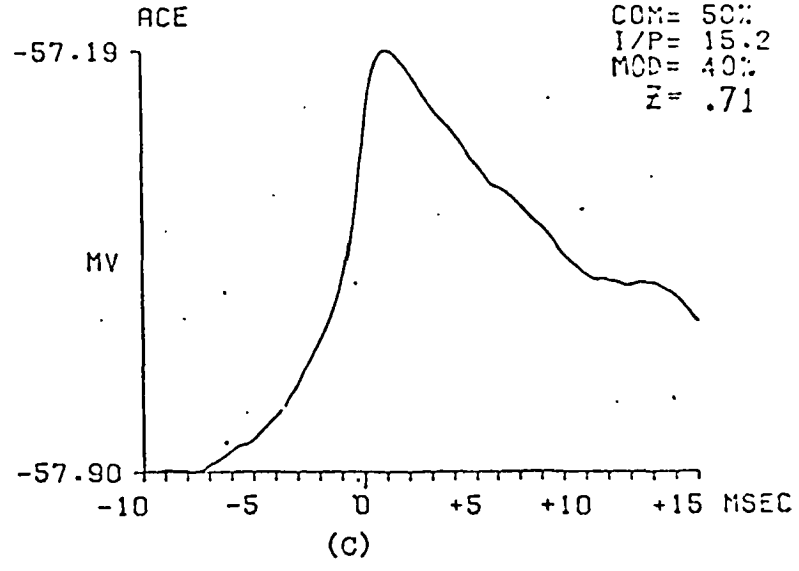

(C)

FIGURES 4.5.6:

Non-stationary simulation ACE Potential results. All runs are standard but with pre-synaptic sinusoidal modulation (MOD) about the mean rate of 15.2kHz as marked (50% common connectivity).

has been used to calibrate this measure. The accuracy in determining the amount of common coupling then relies strongly on the adequacy of the model in simulating the main properties of the pre-synaptic and trans-membrane mechanisms, which are important in the derivation of the PPST histogram and the ACE potential.

One common factor is the event Input-Output (pre-synaptic to discharge) PDF, or more specifically the PC Kernel. These probability density functions are a summary of the underlying mechanisms which are responsible for the raised probability for the generation of an axon discharge spike following a series of pre-synaptic events and in particular focusses on the last event of the sequence. The following chapter is therefore wholly concerned with a better understanding of factors important to and their relation in determining the PC Kernel.

5.0 INVESTIGATION OF THE UNDERLYING PROPERTIES OF THE EVENT INPUT-OUTPUT PDF.

5.1 THE SIMULATION PC KERNELS.

5.2 THE FORM OF THE PC KERNEL.

5.0 INVESTIGATION OF THE UNDERLYING PROPERTIES OF THE EVENT INPUT-OUTPUT PDF:

The importance of the event Input-Output probability density function as a fundamental operator for deriving information related to neuronal interconnection has been mentioned several times in the preceding chapter. This PDF conveys a great deal of information about the neuronal response to the pre-synaptic input and, of course, given the output about the input that produced it. It is therefore proposed here to investigate methods which will lead to at least some understanding of the origin of the PC Kernel and possibly also to a more complete interpretation of the processes underlying this Kernel.

5.1 THE SIMULATION PC KERNELS:

The event Input-Output cross-correlation function $n_{IO}(\tau)$ was briefly introduced in chapter three; some examples of its form for three different total pre-synaptic rates were shown. Later, in chapter four, the AC component (PC Kernel) of this function, derived between only common excitation events to a pair of neurones with shared pre-synaptic pathways and the discharge events, $n_{co}(\tau)$ was shown to be responsible for any synchronised correlation observed in the PPST histogram; this latter correlation was derived from the discharge event sequences of the two neurones.

Figure 5.1.1. presents the $n_{co}(\tau)$ results (for common input events only) from the three pre-synaptic

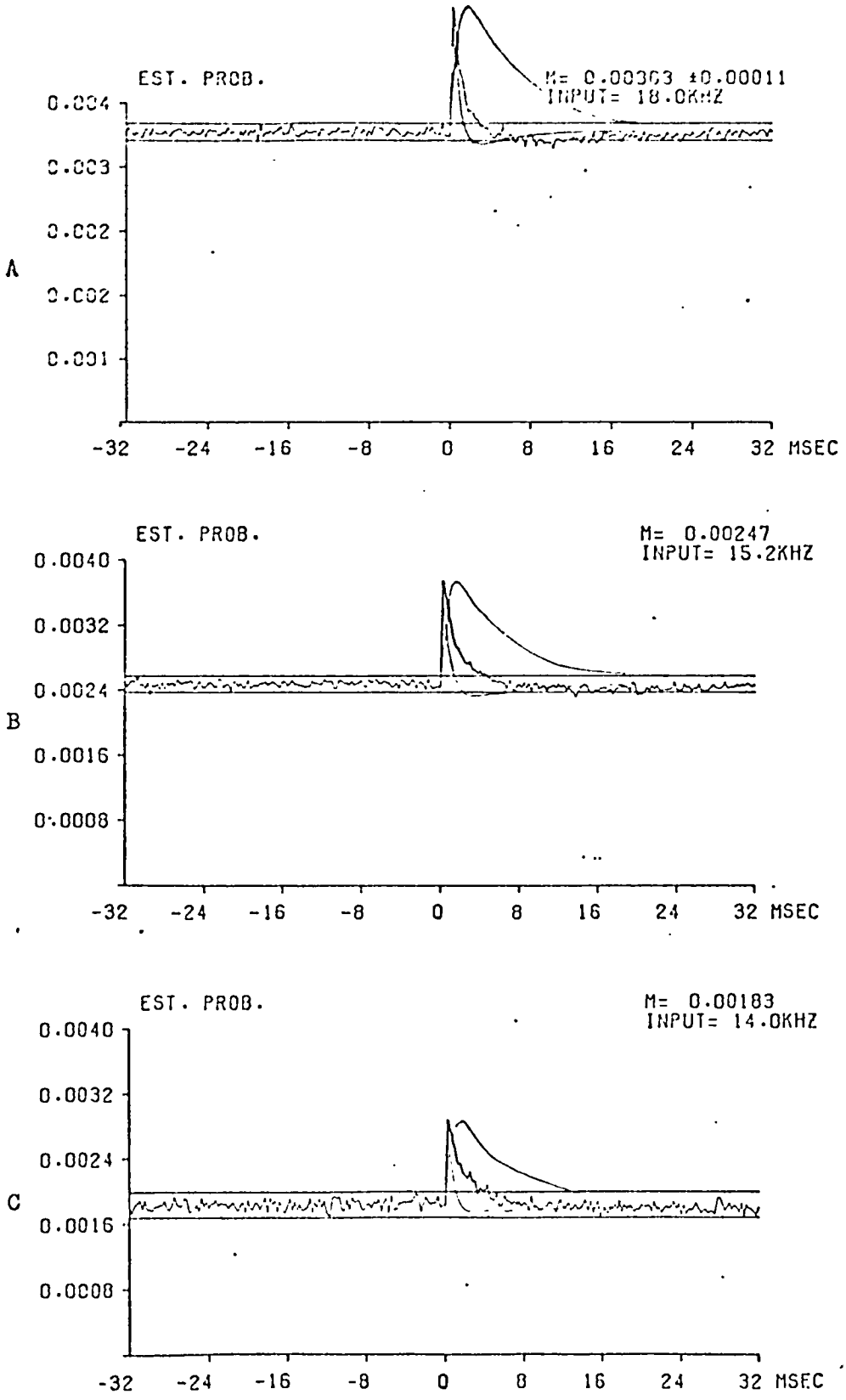

FIGURES 5.1.1:

The event Input-Output PDF results for common inputs only with 50% common connectivity and standard stationary simulations at the total pre-synaptic (INPUT) rates marked. Superimposed are the EPSP shape and its derivative.

rates (A)18, (B)15.2 and (C) 14KHz with 50 percent common connectivity. Superimposed on these are the EPSP form and its derivative. The mean probability level M is dependent on the resulting discharge rates (14.6, 10.0 and 7.29/Sec) which estimate M as 0.000365, 0.00250 and 0.00182 respectively for a 0.25mSec bin width.

Consider now the common event PC Kernels; the forms are very similar with a slight decrease in the base width of the peak with increasing rate, while the kernel height Δ Prob measured in the +0.25mSec bin is seen to vary directly with common pre-synaptic rate. For the three rates with 50 percent common connectivity demonstrated, ΔProb is 0.00158, 0.00129 and 0.00104 respectively. Further it was noted that for 20,10 and 5 percent common rates, of the 15.2KHz total pre-synaptic rate case, the values of M and ΔProb remained constant within the one percent confidence limit of the 50 percent common case (e.g. M = 0.00247, 0.00246, 0.00247; ΔProb = 0.00123, 0.00126, 0.00136 respectively). Also the Kernel form was not observed to alter much when compared with the superimposed forms. Now, because $n_{co}(\tau)$ is derived from only common input and discharge events, within the bounds of these consistencies Δ Prob is seen to be directly proportional to the common pre-synaptic rate R_C which was suggested above. This relationship was also observed for the other two rates considered above at different amounts of shared input.

Figure 5.1.2 demonstrates further examples of PC Kernels which now result from changes in EPSP amplitude

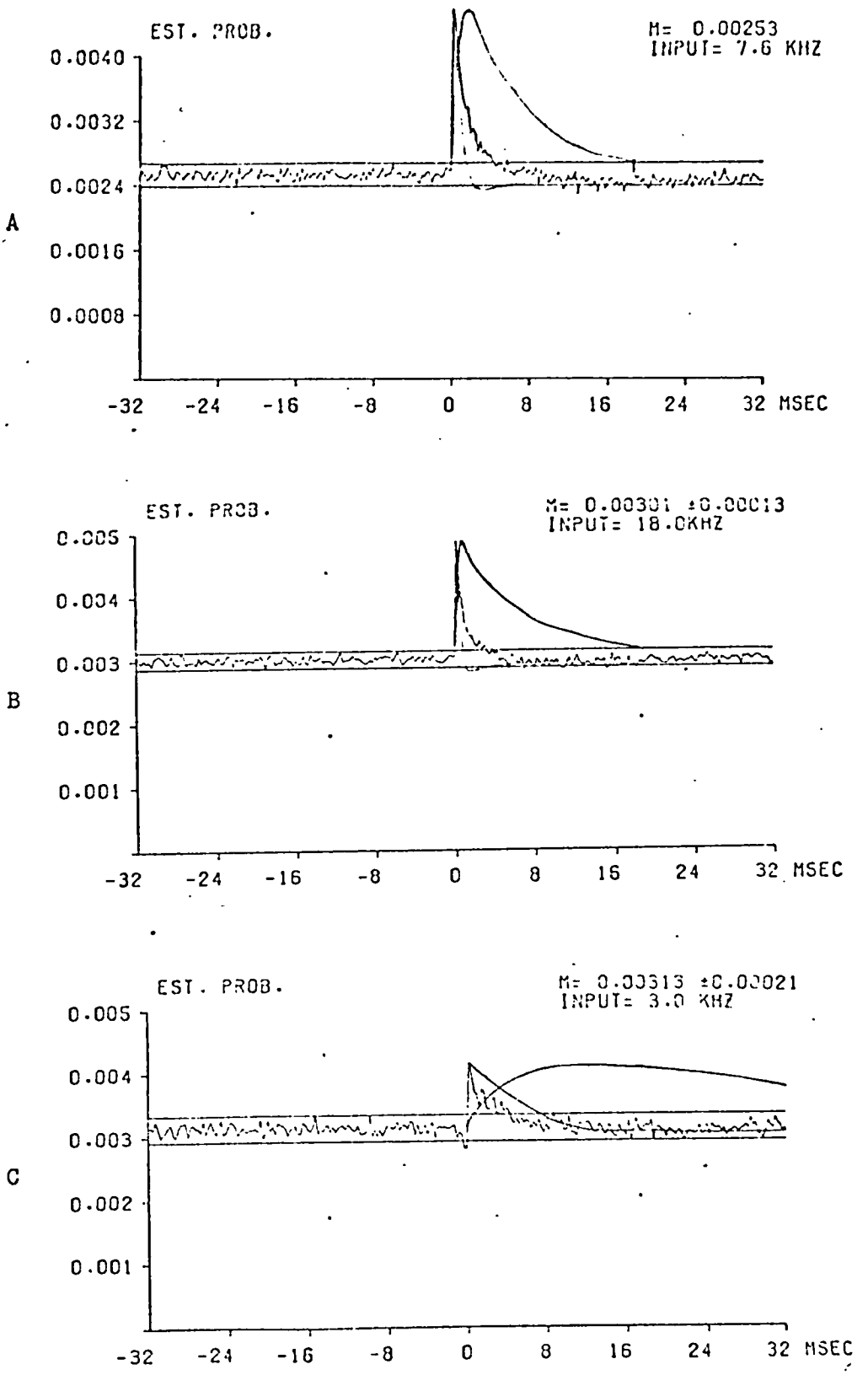

FIGURES 5.1.2:

The common event Input-Output PDF results from 50% common connectivity and non-standard stationary simulations. (A) 0.2mV EPSP /7.6kHZ otherwise standard, (B) 0.1mV EPSP with TRT=0.2 and TDK=6mSec, (C) 0.1mV EPSP with TRT=4 and TDK=48mSec. (Standard EPSP TCs are TRT=0.5 and TDK=6mSec.)

A(0.2mV, otherwise standard), and EPSP shape B(0.1mV, TRT = 0.2, TDK = 6mSec); C(0.1mV, TRT = 4, TDK = 48mSec). By comparison with their respective superimposed EPSP form and its derivative, together with the results of Figure 5.1.1, an interesting pattern is emerging. ΔProb for the results of Figure 5.1.2. is 0.00211, 0.00185 and 0.00103 respectively. Note that these last results are with 50 percent common connectivity and also the total pre-synaptic rates are (A)7.6, (B)18 and (C)3KHz.

In the case A although the input rate has been halved, ΔProb has increased by 64 percent with respect to the standard 15.2KHz and 0.1mV EPSP result which is about 3.3 times greater than the case had ΔProb been directly proportional to R_C and independent of EPSP amplitude. Further, on the basis of the model for the PC kernel used to derive the expressions for the ACE potential and PPST peak form, the resulting ΔProb measured for B should be at least 2.6 times that for the case of Figure 5.1.1A but it is only 1.15 times this. The factor 2.6 would arise because only the derivative term contributes at time zero and α(the EPSP rise-time constant)$^{-1}$ has been increased from 2000 to 5000 while β(the decay-time constant)$^{-1}$ remains fixed at 170. Even allowing for the 0.25mSec bin width an increase of 1.7 times would be expected. Finally from the result in C, the kernel is observed to lie below the derivative result of the EPSP which would suggest that the hypothesised linear relationship does not apply because the 'a' term of a.f(t) + b.df(t)/dt must

now be negative. Although, in this last case the EPSP might be considered to be grossly distorted, the modelled mechanisms have not been altered apart from the EPSP shape - the pre-synaptic rate beingreduced to keep the simulation within the standard operating state (approximately 12 discharges/sec). Hence it is questioned if the hypothesised relationship between EPSP shape and PC Kernel is anything other than an approximation that does reflect the underlying mechanisms usefully. In summary of the above findings the PC Kernel is observed to be related to R_C, the EPSP amplitude and the derivative of the EPSP shape.

It is proposed now to look closer at the kernel form and examine procedures by which it can be predicted. If the time reverse of the above $n_{co}(\tau)$ functions are considered, then these demonstrate the raised probability of the pre-synaptic events just prior to a discharge.

5.2 THE FORM OF THE PC KERNEL:

The form of the PC kernel shape has been related by various workers to the shape of the EPSP (Moore et al, 1970) or its derivative, but the matter is certainly in question though not subject to analytical investigation because of the difficulties found by Knox (1974). Two further possible approaches are available. The first utilises the intermediate functions available from the simulations in order to reduce the complexities of analysis somewhat; this is likely to be most convenient in numerical terms. The second is based on a transfer function analysis of shapes (EPSP to PC kernel) to check

if the proposals can be confirmed that relate the PC kernel to some linear form of the EPSP and its derivative. Some attempt at both approaches has been made here.

From the work discussed above, in which some properties of the MP of the motoneurone were investigated, two valuable statistics have been measured: the MP probability density function MPDF and the average MP end-trajectory. The first measure is a non-conditional function while the second is conditional on a discharge event. By selecting any time prior to the reference discharge occurrence along the MP end-trajectory, the probability of finding the MP at that time related potential may be may be determined from the MPDF. These intermediate functions maybe helpful in exploring the PC Kernel.

With a knowledge of the probabilistic properties of the pre-synaptic event generating process and the EPSP amplitude and form, then an estimate may be made of the subsequent combinations of the numbers of events coming forward in equal width time bins between the time selected along the MP end-trajectory and the time of the discharge. These bin-event combinations, together with the EPSP pattern, must produce just sufficient MP rise to allow a threshold crossing (discharge) at the latency chosen. By calculating the specific probabilities of occurrence from the estimated input event combinations and scaling their summation by the probability of finding the MP at the initial level selected, the PDF should be calculable and should coincide with the PC kernel of the input process considered.

For example, if the standard 15.2KHz case is considered, then the total input process is known to be poisson; the EPSP shape and amplitude are defined, and the MPDF and MP end-trajectory have been measured from the simulation. Considering a bin width of 0.25mSec, then the mean level of the MP (below the threshold) is approximately 0.132 mV; the probability of finding the MP between this level and the threshold is $P_{MP}(0.25) = 0.00534$. The simplifying assumption is now made that all the 0.1mV EPSPs released within this first bin (and the others considered later), occur at the centre of the relevant bin (for the first at a latency of -0.125mSec from the threshold crossing); consequently each EPSP will have risen 0.0274mV at the point of discharge. This suggests that at least 4.8 EPSPs contribute toward depolarising the MP to the threshold level and for a Poisson event process, with the expected total input interval of 0.066mSec and for 0.25mSec time bins, the probability of discharge, $P_D(1) = P_{MP}(1).p_{\geq 4.8}(0.25) = 0.00176$. However, because this is a conditional process (i.e. the MP must just cross the threshold after the half bin width) the probability of discharge is $P_{MP}(1)P_{4.8}(0.25) = 0.00086$. The actual measure PC Kernel probability is 0.00088, which demonstrates that this simple constructional procedure, or some elaboration of it, might be useful.

Proceeding in a similar manner with the second bin removed from the time of discharge, the mean MP is 0. 274mV below the threshold ($P_{MP}(0.5) = 0.00088$) and the EPSPs released at its centre will have risen 0.0639mV which indicate at least 4.3 pre-synaptic events must occur in

that bin. Therefore contributions only from these events in the second bin, conditional to a discharge at time zero, give a probability of $P_{MP}(0.5).P_{4.3}(0.25) = 0.00037$ which is evidently too small (c.f. measured 0.00078). Now consider combinations of events in both pre-discharge bins with the limit of 4.3 in the second as has just been predicted as the maximum. Working down from this number in unit steps it can be shown that, allowing for EPSPs in the first bin to contribute 0.0274mV and in the second 0.0639mV as used above, the only possible combinations are $P_{3.3}(0.25).P_{3}(0.25)$, $P_{2.3}(0.25).P_{5}(0.25)$ and $P_{1.3}(0.25).P_{7}(.25)$. Together, with the $P_{4.3}(0.25).P_{0}(0.25)$ result, produce the total bin probability of discharge. $P_D(2) = 0.00072$. This too is a good estimate of the measured 0.00078 value, considering the simplifying assumptions used.

However, with the next estimate ($P_D(3) = 0.00037$ c.f. Measured = 0.00060) the assumptions are evidently showing their limitations and the whole procedure used then becomes very complicated, involving no less than seventeen combinations. For these reasons, such a simplified approach cannot be justifiably pursued. It is also foreseen that further complications would arise in the calculations going beyond the fifth bin. This is because the decaying phase of some of the EPSPs must then be taken into account (i.e. time to the standard EPSP peak is 1.335mSec).

On the other hand by the direct use of simulation, this investigation into the pre-synaptic event mechanics underlying the form and amplitude of the Input-Output PDF

can be taken further. A series of simulations were run with the model modified so that the statistics of the events in the final ten (0.25mSec) time bins could be recorded. These results, given in Table 5.2.1, are akin to the average MP end-trajectory. Consider the 15.2KHz findings; the average bin count is increasing (clearly demonstrated by the ratio of the counts determinded divided by the expected number, assuming a Poisson process), while the variance shows no strong trend. These results suggest that the input process is no longer Poisson (i.e. mean = variance for event process).

Remembering that the situation under consideration is conditional on a discharge immediately following the last bin, then the contributing sequences must be chosen by what is an inherently a trend-selective process. This is further evidenced by the fact that, over 100 discharges, a minimum of two events are observed in the last bin (mean = 5.4, variance = 3.8); in the last two bins six events minimum (mean = 10.8); in the last three bins ten minimum (mean = 15.9); in the last four bins fifteen minimum (mean = 20.7); and in the last five bins twenty minimum (mean = 25.5, variance = 3.4). From this information a better estimation of the PC kernel can now be made, but more importantly the minimal bin counts and the variation of the counts around the mean demonstrate the high degree of selectivity of the process involved. Similar characteristics were found for the 14 and 18KHz similations considered.

TABLE 5.2.1:

The Mean 0.25 mSec Bin Counts and Variance in Counts Prior to a Discharge-

Relative Time of Bin before Discharge(mSec):	Counts and Variance for Pre-synaptic Rate:		
	14 kHz	15.2 kHz	18 kHz
0.25	5.1 (3.6)	5.4 (3.8)	6.1 (4.0)
0.50	5.1 (3.7)	5.4 (4.4)	6.1 (4.9)
0.75	4.9 (4.4)	5.1 (5.0)	5.7 (4.8)
1.00	4.7 (4.5)	4.8 (4.3)	5.3 (4.4)
1.25	4.5 (4.2)	4.8 (4.1)	5.2 (4.8)
1.50	4.3 (3.6)	4.6 (4.0)	5.0 (4.7)
1.75	4.2 (4.0)	4.1 (3.1)	4.8 (4.5)
2.00	4.0 (3.9)	4.1 (4.2)	4.7 (4.3)
2.25	4.1 (3.9)	4.2 (3.9)	4.7 (4.2)
2.50	3.9 (4.0)	4.1 (4.4)	4.7 (4.5)
Expected Bin Count for Poisson Process:	3.5 (3.5)	3.8 (3.8)	4.5 (4.5)

N.B. Numbers in Brackets are the Variance of Counts.

Results are from sequences of 500 Discharges.

Consider now an alternative approach to the task of elucidating more about the underlying mechanisms contributing to the event Input-Output PDF. The hypothesis has been assumed above (also by Kirkwood and Sears, 1977) that the PC kernel can be viewed as the weighted sum of the EPSP shape and its time differential. The complex ratio of the spectra of the actual PC form and the EPSP shape offers a convenient method for a closer examination of their possible relations; the result can be turned into an equivalent impulse response by an inverse Fourier transform (the technique is demonstrated in connection with the detection of trends in cardiac signals by Sayers, 1976). This impulse response (IR) can be regarded as that of the linear system that convolves the EPSP into the PC kernel, and so describes their relationship. Figure 5.2.1 shows the initial time related signals (superimposed) in A, the complex real (B) and imaginary (C) parts of their spectral ratio, the amplitude (D) and phase (E) spectra from the complex division and the inverse Fourier transformed IR result (F).

If the relation is as hypothesised then, noise disregarded, the IR would comprise a Dirac pulse added to which is a biphasic pattern (representing the derivative component). In practice these are generally observed but only in the very broadest terms; to optimize the effect it might have been necessary to adjust the relative time shift between the PC kernel and the EPSP, but little if any shift is actually required. The IR is naturally

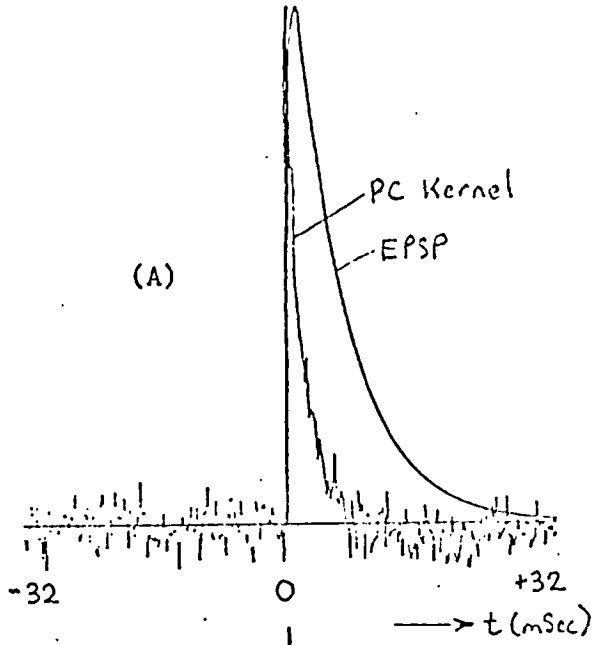

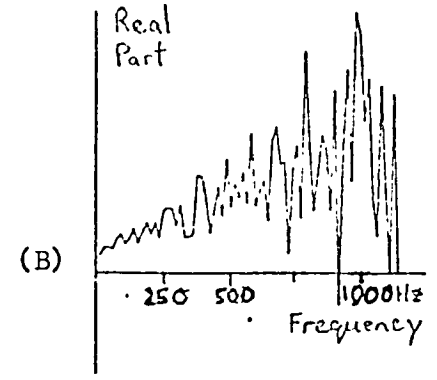

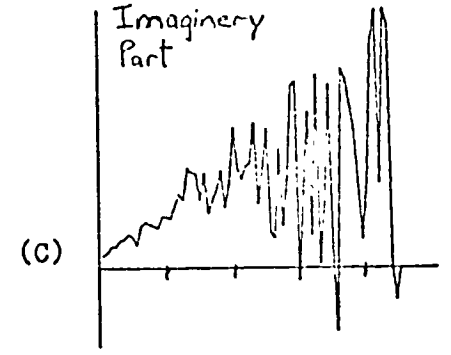

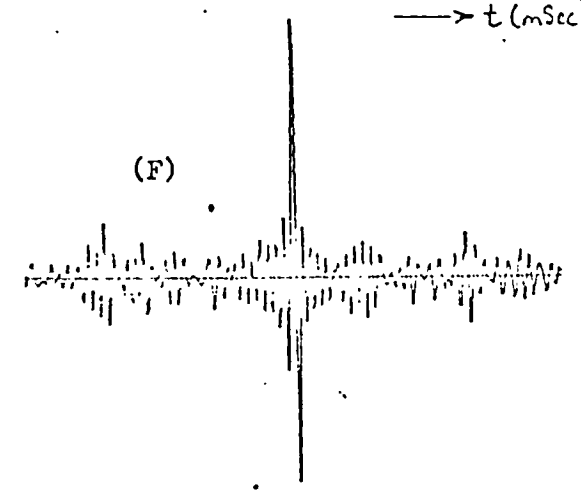

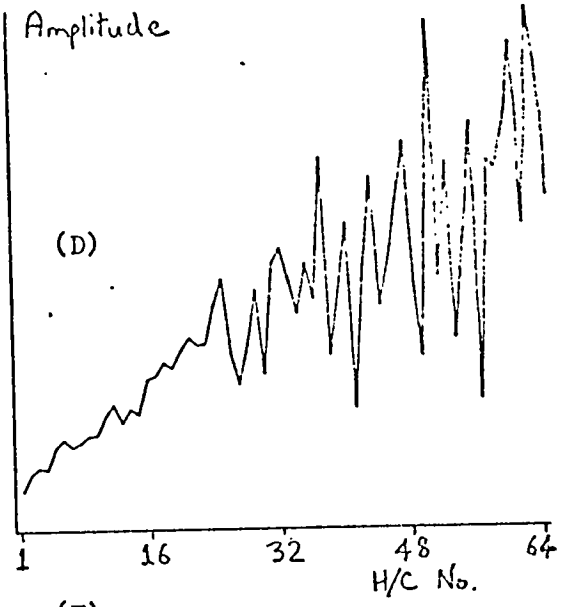

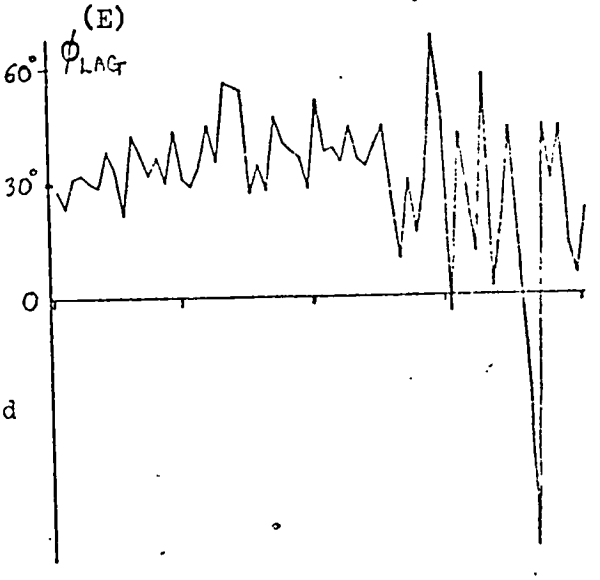

FIGURES 5.2.1:

The Impulse Response and its spectra.

(A) The initial time relation of the EPSP and PC forms.

(B) and (C) The complex parts of the spectral ratio PC:EPSP.

(D) and (E) The amplitude and phase spectra from B and C.

(F) The inverse Fourier transformed Impulse Response result.

smoothed out by the limited spectral range employed, and degraded by noise, but the main features are interesting and warrant closer attention.

The amplitude of the complex spectral ratio (PC to EPSP) rises proportionally with frequency from a non-zero value while the phase stays roughly constant at minus $30\text{-}40^{o}$ over the important harmonics. It can be concluded that (in terms of the presumed relation of EPSP = f(t) and PC kernel as af + bf') the requirement that amplitude rises with frequency non-linearly while phase alters linearly with frequency, is not met. Accordingly the pattern of the IR reflects only a broad correspondence with the expectations (as would be anticipated from the fact that the relation was suggested at all), but not to any convincing extent.

On the otherhand the amplitude and phase results of the complex ratio would not appear to reflect any common natural system transfer relationship. Thus, while the simple relationship already employed do_{Λ}^{es} seem to be unsupported, some further work would be needed in order to clarify the matter but it is not pursued here. Nevertheless, the approach taken is likely to be worth following up since it does produce explicit, even thought challenging, results for the EPSP-PC relationship.

6.0 CONCLUSIONS

6.1 SUMMARY AND DISCUSSION OF THE RESEARCH.

6.2 PROPOSALS FOR FUTURE WORK.

6.0 CONCLUSIONS:

6.1 SUMMARY AND DISCUSSION OF THE RESEARCH:

Recent research into the nervous control of intercostal muscles has generated many interesting findings and prompted a number of hypotheses to explain the results observed. In particular the PPST Histogram of Sears and Stagg (1976), determined between pairs of multiunit spike trains recorded from the same and neighbouring segmental levels, exhibited significantly strong and narrow peaks that suggest the existence of branching in the spinal pre-synaptic pathways to intercostal alpha-motoneurones.

Due to difficulties of direct neuro-anatomical investigation and the need to achieve an adequate account of, and explanation for, the properties of the various neuronal signals recorded in the intercostal system, a neuronal model was considered appropriate. Because there was no previous report of a model which fitted even the general properties of mammalian motoneurones, it was necessary to develop and assess a realistic model of one before pursing the task of clarifying some of the origins of the intercostal motoneuronal characteristics observed.

This model integrates high rates of very small EPSPs, accommodates a non-stationary breathing rhythm, and allows the investigation of common pre-synaptic connectivity. The principles of the digital simulation adopted allow for a realistic EPSP shape of graded

amplitude to be summed to the instantaneous membrane potential (MP) with each pre-synaptic event. Refractoriness also influences the MP, which is set to a hyperpolarised level immediately after each of the discharges which are initiated when the membrane is sufficiently depolarised to cross a threshold level. Because such a model is potentially very costly to run, its careful optimisation is vital. In the present case this has been achieved by programming in assembler language and utilising look-up table techniques in place of time consuming algorithms.

In order to assess the validity of this simulation of the intercostal alpha-motoneurone, a variety of statistical signal and ensemble-analysis techniques have been employed which enabled a thorough comparison with its neurophysiological counterpart. In the course of assessment and application, it was shown that the model produces results in good accordance with the experimental observations. To select two matters in which the model has clarified experimental observations and demonstrate how they are to be interpreted, the relation between the PPST histogram features and shared inputs may be cited. It was found by investigation with the model that the strength of correlation, given by (R-1), which is the ratio of the excess peak value to the mean level, varied directly with the percentage of common connectivity. Secondly, it was shown that the PPST peak shape originates from the self-convolution of the event Input-Output PDF

which also accounts for the peak amplitude.

The model thus also offers the prospect of further insight into functional neurophysiological behaviour by the study of those intermediate processes in the model which are not accessable at all in the experimental preparation. The property of the fundamental event Input-Output PDF, for example, was first encountered at this preliminary stage and its importance to the rest of the investigation became very apparent. Even the limitations within the present model, such as the lack of interaction between neighbouring synapses, which can greatly reduce the effectiveness of the EPSP contribution to the MP, have allowed some positive evaluation of the alpha-motoneurone and the trans-membrane processes.

Having once established that the model of the synaptic and trans-membrane processes was adequate, within the bounds of practical limitations, the hypothesis of shared inputs was then simulated. This was achieved by simulating a pair of motoneurones receiving excitation from both a common pre-synaptic source and independent sources. By adjustment of the ratio of common-to-total drive, the strength of correlation measured from the PPST histogram (determined from the two discharge event sequences from the motoneurones) was quantified. For the experiments on the cat (CONTROL-1 and -2) it would appear that there might be at least 10 percent of common pre-synaptic connectivity. This is observed to remain fairly constant for the PPST histograms determined between segmental levels T_5/T_6, T_6/T_7 and T_7/T_8 at both normal and high levels of

CO_2. With regard to the study of lesioned animals, the simulations demonstrate the usefulness of the model by allowing some hypothetical interpretation of what might be happening in the HEMISECTION studies, and suggest that for further lesions our understanding of the spinal inter-neuronal pre-synaptic pathways is incomplete.

Also in Chapter Four more evidence for the hypothesised common pre-synaptic connectivity is investigated by simulation. The recent discovery of the ACE (average common excitation) potential was taken into account, and its claim to support the existence of branching in the pre-synaptic pathways was shown to be reasonable. It is unfortunate that neither the correlation strength factor (R-1) for the PPST histogram nor the ACE potential amplitude appear to allow a direct measure of the amount of shared input. This is supported by the theoretical calculations derived for both which indicates that only if a reasonable estimate for the average common EPSP size and shape were available could the measures be calibrated to achieve some quantification of shared input. Even under these circumstances the event Input-Output PDF (Primary Correlation) kernel must be assumed, but as demonstrated by the simulations, this is not the most critical factor (in fact minimal for the PPST case).

The role of the event Input-Output PDF has been shown to be fundamental to all measures of common connectivity in the pre-synaptic pathways. It has also been demonstrated that if this important function were more readily available, a better insight into the synaptic and trans-membrane processes of the neuronal structures should be possible. By investigation

of the factors which influence the form and magnitude of this probability density function, some guiding points as to its interpretation have been established. In the pursuit of identifying these defining mechanisms it was established that the model of the PC Kernel assumed by Kirkwood and Sears (1977) was in no way complete. There is evidence though, from the investigations in Chapter Five, that the derivative of the EPSP shape may contribute to the general form of PC Kernel as demonstrated in any artificial situation by Knox (1974) but this is far from a complete explanation. A more detailed study is required before a quantitative understanding of the underlying processes which influence this PDF can be achieved.

The work described in this thesis has demonstrated the successful application of modelling techniques, combined with a number of methods for statistical and signal analysis, in enhancing knowledge about the nervous control of respiration. In the investigation of common pre-synaptic connectivity between the intercostal alpha-motoneurones, several important and associated aspects have also been pursued. These secondary studies have in no way detracted from the main goal, but rather have allowed some progress towards a better insight into the operation of the complete system. They also point the way for further work.

6.2 PROPOSALS FOR FUTURE WORK:

Within the scope of the present model developed and used, a number of aspects of the intercostal motoneural role in the nervous regulation of breathing were examined.

The successful pursuit of the initial goals have in turn pointed to further work.

If the model employed could be practically implemented with the additional features which could account for the non-linear summation of the EPSPs and account for some of the effects generated by dendritic EPSPs, a more detailed investigation of shared inputs would be worthwhile. This model might prove to be instrumental in explaining the very wide PPST histogram peaks observed for some lesioned animals.

The fundamental importance of the event Input-Output PDF, in accounting for the results observed from the investigations described in this thesis, has been clearly demonstrated. Future studies might examine the feasibility of self-deconvolution of the PPST histogram to arrive at an estimate of this PDF for the neurophysiological results. Such an approach, when combined with a more detailed study of the mechanisms which dominate in generating this function, should allow further insight into the synaptic and trans-membrane processes of the motoneurones concerned. On a more general scale, this last approach could be applied to the eludication of systems in which synchronisation is known to occur and in which only a limited access to the intermediate and driving processes is available.

Finally, to allow further elucidation of the intercostal motoneuronal behaviour and connectivity, more animal experimental investigations are necessary. It is worth

remarking that this has become evident mainly in the application of the modelling techniques described in this thesis; consequential action is already being taken.

APPENDIX

Neural spike acquisition interface: Before the construction of this interface, all data acquisition was carried out off-line from F.M. multichannel tape recordings as is described by Stagg (1973) and Sears and Stagg (1976). Their software technique requires effectively a total of three passes of the recorded neuronographic multiunit sequences: the first is to digitise the analogue recordings using the Laboratory's IBM 1800 computer; the next is to allow a reduction of the resulting very long digitised version, coding the spike events in terms of the interval to the next peak from the last recorded, the amplitude at the peak and the channel identification of the particular occurrence while simultaneously determining the multiunit peak amplitude distributions for each channel; and finally a third pass of the reduced data sequence in which selective unit processing is done.

The complete process and the recording of compressed data information described above is reduced to a single pass or, if a computer were available, could be achieved directly on-line with the experiment by the hardware acquisition interface which has been developed and will now be described. Figure 7.1.1. demonstrates a block diagram representation of the interface. Each channel has an independently controllable, spike amplitude discriminating window circuit which can be set to select the required single or multiunit sequence to be processed.

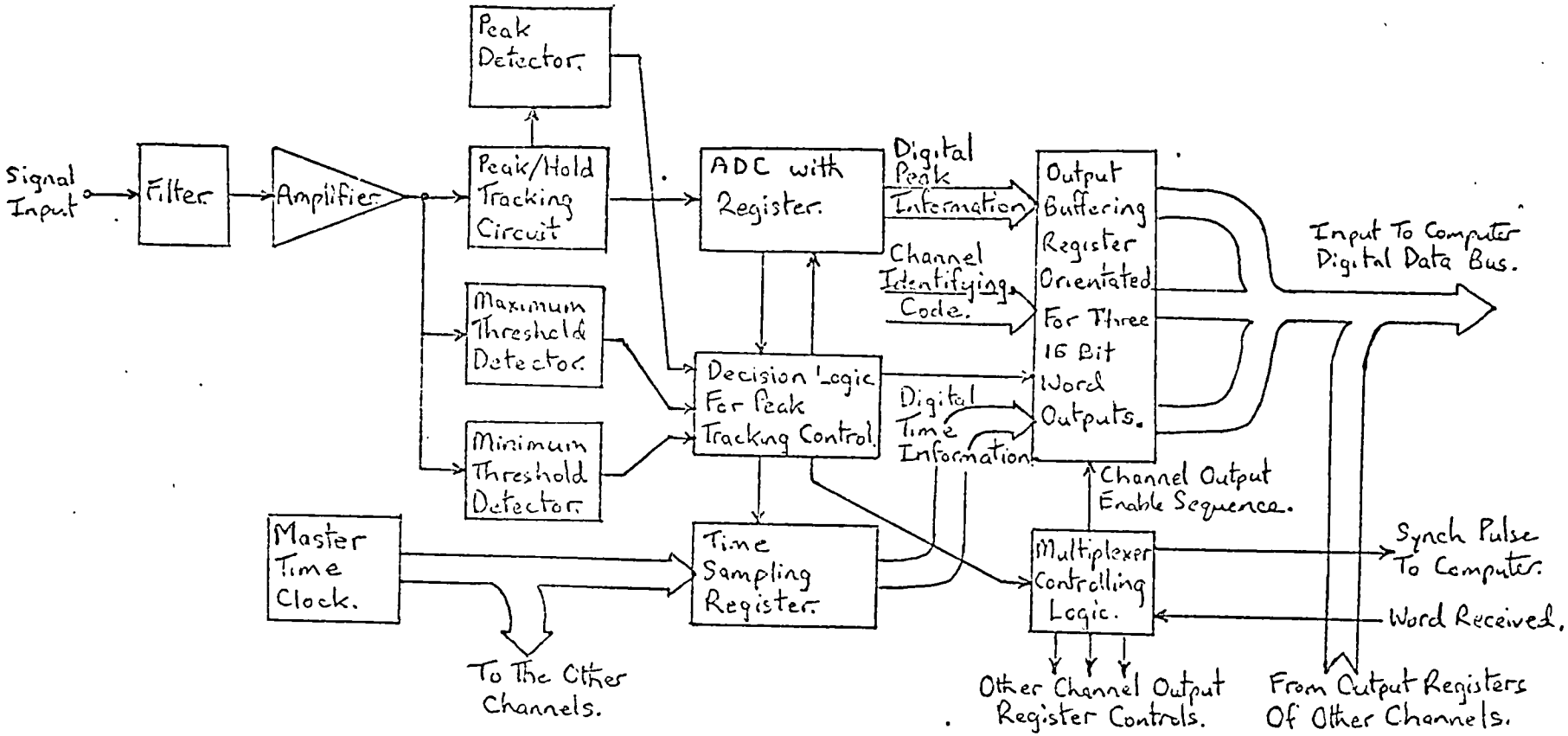

FIGURE 7.1.1:

The block diagram for the data acquisition interface unit showing only one channel.

After amplification, two level detectors and some logic circuitry decide whether each spike amplitude is to be recorded and processed or not (i.e. the amplitude falls within the discriminating voltage window set). The flow chart shown in Figure 7.1.2. demonstrates the logic descisions concerned. Once an acceptable event has occurred the ADC (analogue-to-digital convertor) is enabled and the amplitude of that spike, which is held in the peak detect-and-hold circuitry is digitised. At the completion of an AD conversion, after completing the checking loop given in Figure 7.1.3A, the channel concerned sets a channel READY Flag which is eventually recognised by the multiplexed 'Channel READY Flag' scanning circuitry and a data transfer is set up to the computer via the computer's DMA (Direct Memory Access) Digital Input (parallel bus) lines. Figure 7.1.3B demonstrates the logic followed by the main control circuitry.

Within the acquisition interface's main control circuitry is a Master Clock, which works with a time resolution of 10μSec so that whenever a spike peak is detected the absolute time of occurrence is recorded in a time latch associated with the channel concerned. Two 16 bit words are used to store this referenced time of the peak and another coded 16 bit word records the 12 bit digitised peak amplitude and the 4 bit identification for the channel. The channel transfer to the computer memory can be either by three 16 bit words or, for a 12 bit word machine, by four 12 bit

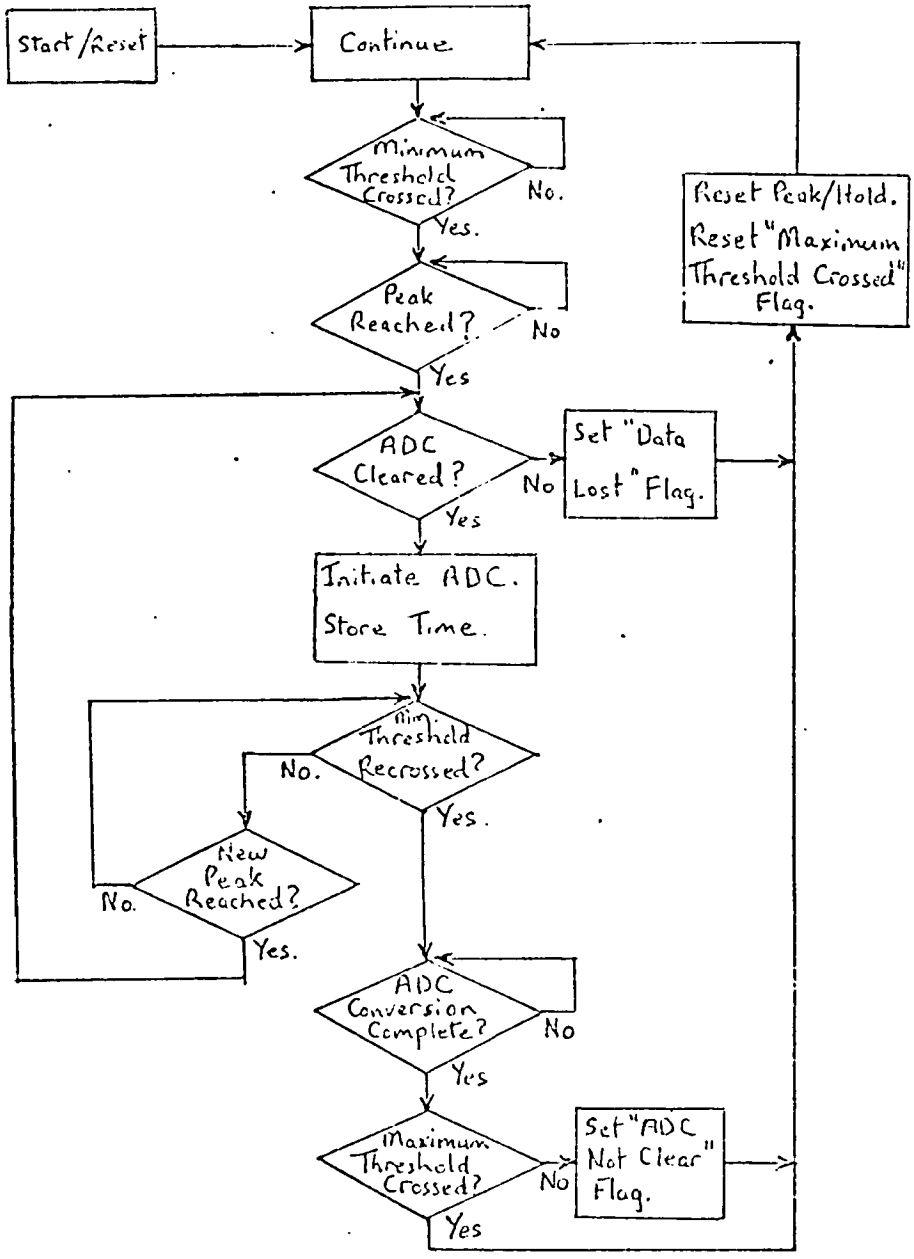

FIGURE 7.1.2:

The flow chart for the peak tracking and decision making logic.

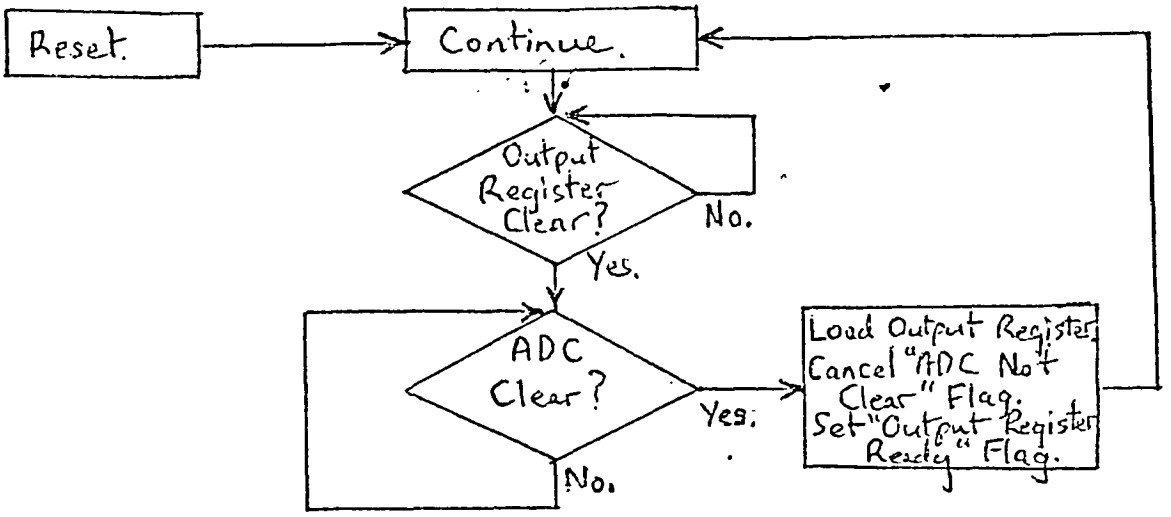

(A) The Output Register updating decision pathways of each aquisition channel.

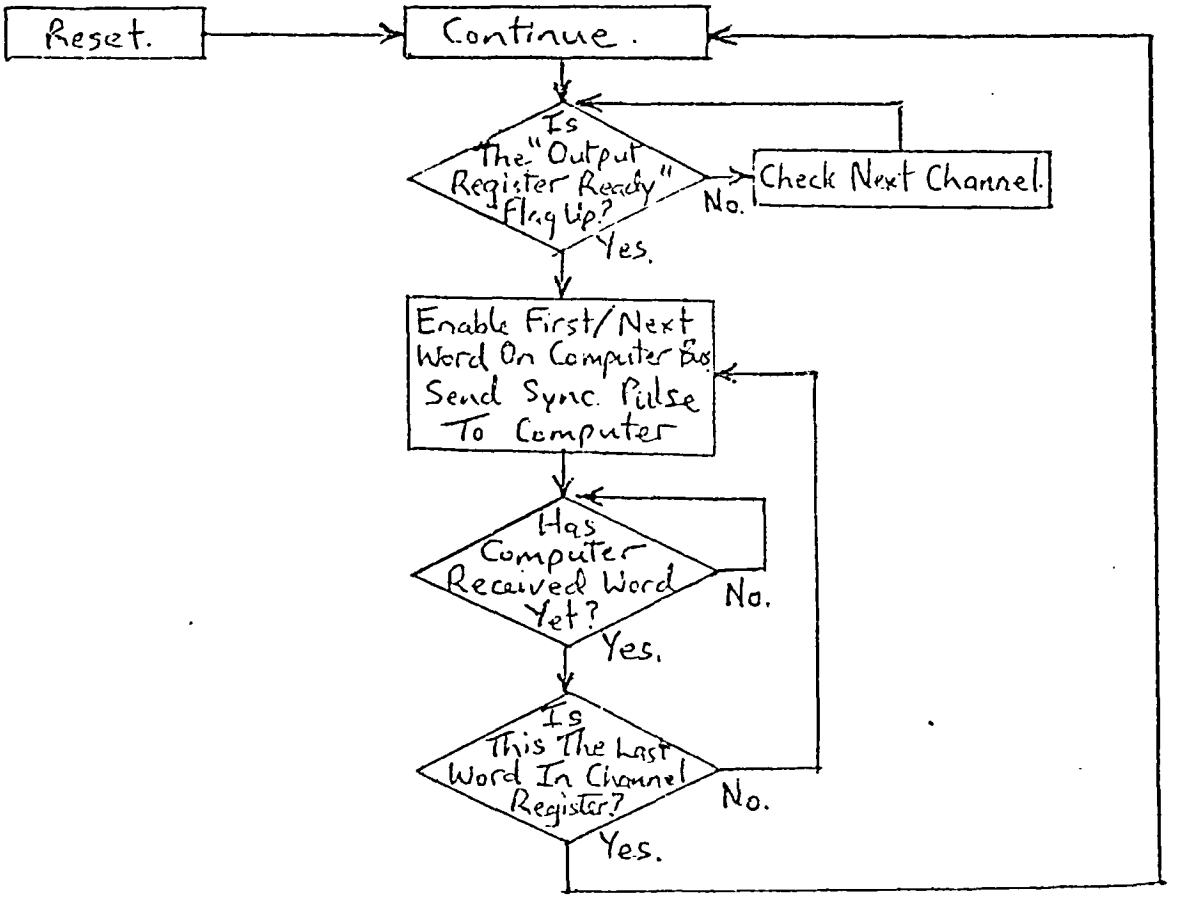

(B) The output multiplexing decision logic of the interface control circuitry.

FIGURES 7.1.3:

words. Simplicity in channel transfer multiplexing, and in the selectable word length required, was made possible by a 16 line data bus and extensive usage of Tri-state TTL bus buffering. Each word transfer is synchronised by the computer's 'DMA READY Flag' which generally (IBM 1800 used at present) is held 'low' while a data word is being accepted and set 'high' at the completion; the DMA External Sync. line is used by the interface to indicate when the next word transfer is ready on the Digital Input bus (i.e. suitably buffered extension of the interface's data bus). This method allows a very fast direct transfer of data into the computer memory, independent of the CPU (Computer Processing Unit), thereby leaving the CPU free to carry on with other processing. By using two crossed linked DMA tables (only a maximum of 255 words can be stored in a single DMA table) an arrangement whereby, while one table is being filled, the other (having already been filled) can be written up onto disc or digital magnetic tape and this reciprocating process can be employed to accumulate a long record of selected neuronographic data. It was necessary to write the controlling software in assembler language to ensure the timing is correct between the interface and the computer, and that, should on-line processing be required it is fast enough to avoid the loss of any information.

For the present no direct on-line processing is done and the controlling programme, ACQRE only

writes the acquired data onto digital magnetic tape and the general disc drive data area after coding in the standard format for processing by the Stagg (1973) programmes. Any subsequent processing is then very fast because of the compressed form of the coded data (i.e. Interval from last recording, the spikes amplitude and channel). A preliminary programme, PUNIT is used with the interface to obtain an indication of the multi-unit peak amplitude distributions to allow the spike acquisition discriminating windows to be set up, but this generally only requires approximately one minute of the data length to allow a reasonably well defined distribution.

It can be seen that the hardware acquisition interface is a trade-off of expense for the time before the results are known. The ADC represents more than 50 percent of the cost of one channel and as this application requires only an economy 12 bit general purpose device, the construction of the neural spike acquisition interface was completely justified economically and by its efficiency of processing. A manual is being prepared for this interface which will give instructions on its usage (together with the controlling programmes written), and a more detailed description of the circuitry involved.

REFERENCES

1. BARRETT, J.N. (1975)
Motoneuron dendrites: role in synaptic integration
Federation Proceedings, Vol.34, 1398-1407

2. BRONK, D.W. and FERGUSON, L.K. (1934)
The nervous control of intercostal respiration
American Journal of Physiology, Vol.110, 700-707

3. CALVIN, W.H. and SCHWINDT, P.C. (1972)
Steps in production of motoneuron spikes during rhythmic firing.
Journal of Neurophysiology, Vol.35, 297-310

4. CALVIN, W.H. and STEVENS, C.F. (1968)
Synaptic noise and other sources of randomness in motoneuron interspike intervals
Journal of Neurophysiology, Vol.31, 574-587

5. CLAMMAN, H.P. (1969)
Statistical analysis of motor unit firing patterns in a human skeletal muscle
Biophysical Journal, Vol. 9, 1233-1251

6. ECCLES, J.C. (1966)
The physiology of nerve cells
The John Hopkins Press, Baltimore (5th Printing)

7. EKHOLM, A. and HYVÄRINEN, J. (1970)
A pseudo-Markov model for a series of neuronal spike events
Biophysical Journal, Vol.10, 773-796

8. FRIZE, M. (1970)
The significance of neural spike sequence patterns in the respiratory control system
M.Phil. Thesis, London.

9. GEISLER, C.D. and GOLDBERG, J.M. (1966)
A stochastic model of the repetitive activity of neurons
Biophysical Journal, Vol.6, 53-69

10. GERSTEIN, G.L. and MANDELBROT, B. (1964)
Random walk models for the spike activity of a single neurone
Biophysical Journal, Vol.4, 41-68

11. GERSTEIN, G.L. and PERKEL, D.H. (1972)
Mutual temporal relationships among neuronal spike trains
Biophysical Journal,Vol.12, 453-473

12. HARMON, L.D. and LEWIS, E.R. (1966)
Neural modelling
Physiological Reviews, Vol.46, 515-591

13. IANSEK, R. and REDMAN, S.J. (1973)
The amplitude, time course and charge of unitary excitatory post-synaptic potentials evoked in spinal motoneurone dendrites
Journal of Physiology, Vol.234, 665-688

14. JACK, J.J.B., MILLER,S., PORTER, R., and REDMAN, S.J. (1971)
The time course of minimal excitatory post-synaptic potentials evoked in spinal motoneurones by group Ia afferent fibres
Journal of Physiology, Vol.215, 353-380

15. JACK, J.J.B. and REDMAN, S.J. (1971)
An electrical description of the motoneurone and its application to the analysis of synaptic potentials
Journal of Physiology, Vol.215, 321-352

16. KATZ, B. (1966)
Nerve, muscle and synapse
McGraw-Hill Book Co., New York.

17. KERNELL, D., and SJÖHOLM, H. (1972)
Motoneurone models based on voltage clamp equations for peripheral nerve.
Acta Physiologica Scandinavica, Vol.86, 546-562

18. KIRKWOOD, P.A., and SEARS, T.A. (1974)
Mono-synaptic excitation of motoneurones from secondary endings on muscle spindles.
Nature, Vol.252, 243.

19. KIRKWOOD, P.A., and SEARS, T.A. (1976)
The average common excitation (ACE) potential and its significance.
Journal of Physiology, Vol.259, 36-37P.

20. KIRKWOOD, P.A. and SEARS, T.A. (1977)
The synaptic connections to intercostal motoneurones as revealed by the average common excitation (ACE) potential.
(To be published).

21. KNOX, C.K. (1974)
Cross-correlation functions for a neuronal model
Biophysical Journal, Vol.14, 567-582.

22. LEVITAN, H., SEGUNDO, J.P., MOORE, G.P. and PERKEL, D.H. (1966)
Statistical analysis of membrane potential fluctuations.
Biophysical Journal, Vol.8, 1256-1274.

23. MATTHEWS, P.B.C. (1972)
Mammalian muscle receptors and their central actions.
Edward Arnold Ltd., London.

24. MENDELL, L.M. and HENNEMAN, E. (1971)
Terminals of single Ia fibres: location, density and distribution within a pool of 300 homonymous motoneurones
Journal of Neurophysiology, Vol.34, 171-187

25. MOORE, G.P., SEGUNDO, J.P., PERKEL, D.H. and LEVITAN, H. (1970)
Statistical signs of synaptic interaction in neurones.
Biophysical Journal, Vol.10, 876-900

26. PERKEL, D.H. (1964)
A digital-computer model of nerve cell functioning
RAND Corp., Memorandum RM-4132-NIH (June),
San Monica, California, (51 pages).

27. PERKEL, D.H., GERSTEIN, G.L. and MOORE, G.P. (1967a)
Neuronal spike trains and stochastic point processes
I. The single spike train
Biophysical Journal, Vol.7, 391-418

28. PERKEL, D.H., GERSTEIN, G.L. and MOORE, G.P. (1967b)
Neuronal spike trains and stochastic point processes
II. Simultaneous spike trains
Biophysical Journal, Vol.7, 419-440

29. SAYERS, B. McA. (1970)
Inferring significance from biological signals
In: Biomedical engineering systems
Clynes, M. and Milsum, J.H.(eds), McGraw-Hill,
New York, (pp84-165).

30. SAYERS, B. McA. (1976)
Spatial and temporal analysis of cardiac signals
In: Medical data processing
Laudet, M., Anderson, J. and Begon, F.(eds),
Taylor and Francis Ltd., London, (pp 567-580).

31. SCHWINDT, P.C., and CALVIN, W.H. (1972)
Membrane potential trajectories between spikes
underlying motoneuron firing rates.
Journal of Neurophysiology, Vol.35, 311-325

32. SEARS, T.A. (1964a)
Efferent discharges in alpha and fusimotor
fibres of intercostal nerves of the cat
Journal of Physiology, Vol.174, 295-315

33. SEARS,,T.A. (1964b)
Investigations of respiratory motoneurones
of the thoracic spinal cord.
In: Progress in brain research: Physiology
of spinal neurons.
Eccles, J.C., and Schadé, J.P. (eds) Vol.12,
Elsevier Publishing Co., Amsterdam, (pp259-274)

34. SEARS, T.A., and STAGG, D.T. (1976)
Short term synchronization of intercostal
motoneurone activity.
Journal of Physiology, Vol.263, 357-381.

35. SEGUNDO, J.P., PERKEL, D.H., WYMAN, H., HEDSTAD, H. and MOORE, G.P. (1968)
Input-Output relations in computer-simulated nerve cells.
Kybernetik, Vol.4, No.5, 157-171

36. STAGG, D.T. (1970)
The control of mammalian muscle spindles studied by analysis of neuroelectric signals.
PhD. Thesis, Institute of Neurology, London.

37. STAGG, D.T. (1973)
Aquisition and analysis of multi-unit nerve spike sequences.
Analysis/Application Report, Engineering in Medicine Laboratory, Imperial College, London, (19 pages).

38. STAUFFER, E.K., WATT, D.G.D., TAYLOR, A., REINKING, R.M. and STUART, D.G. (1976)
Analysis of muscle receptor connections by spike-triggered averaging. 2. Spindle group II afferents.
Journal of Neurophysiology, Vol.39, 1393-1402

39. STEIN, R.B. (1965)
A theoretical anlysis of neuronal variability
Biophysical Journal, Vol.5, 173-194

40. TAYLOR, A. (1960)
The contribution of the intercostal muscles to the effort of respiration in man.
Journal of Physiology, Vol.151, 390-402

41. TEN HOOPEN, M. (1966)
Impulse sequences of thalamic neurones - an attempted theoretical interpretation.
Brain Research, Vol.3, 123-140(Research Report).

42. VIERNSTEIN, L.J. and GROSSMAN, R.G. (1961)
Neural discharge patterns in the transmission of sensory information.
In: 4th London symposium of information theory
Cherry, C.(edr), Butterworth and Co., London,
(pp252-269).

43. WALLOE, L., JANSEN, J.K.S., and NYGAARD, K. (1969)
A computer simulated model of a second order sensory neurone.
Kybernetik, Vol.6, No.4, 130-145.